Numerical modelling of flow through packed beds of uniform spheres

Abraham Christoffel Naudè Preller
B.Eng. (Mechanical)
Student Number: 20281048

Dissertation submitted in partial fulfilment of the requirements for the degree
Master of Engineering in Mechanical Engineering at the Potchefstroom Campus of
the North-West University.

Supervisor: Prof. C.G. du Toit

Potchefstroom

2011

ABSTRACT

This study addressed the numerical modelling of flow and diffusion in packed beds of mono-sized spheres. Comprehensive research was conducted in order to implement various numerical approaches in explicit[1] and implicit[2] simulations of flow through packed beds of uniform spheres.

It was noted from literature that the characterization of a packed bed using porosity as the only geometrical parameter is inadequate (Van Antwerpen, 2009) and is still under much deliberation due to the lack of understanding of different flow phenomena through packed beds. Explicit simulations are not only able to give insight into this lack of understanding in fluid mechanics, but can also be used to develop different flow correlations that can be implemented in implicit type simulations.

The investigation into the modelling approach using STAR-CCM+®, presented a sound modelling methodology, capable of producing accurate numerical results. A new contact treatment was developed in this study that is able to model all the aspects of the contact geometry without compromising the computational resources. This study also showed, for the first time, that the LES (large eddy simulation) turbulence model was the only model capable of accurately predicting the pressure drop for low Reynolds numbers in the transition regime. The adopted modelling approach was partly validated in an extensive mesh independency test that showed an excellent agreement between the simulation and the KTA (1981) and Eisfeld and Schnitzlein (2001) correlations' predicted pressure drop values, deviating by between 0.54% and 3.45% respectively.

This study also showed that explicit simulations are able to accurately model enhanced diffusion due to turbulent mixing, through packed beds. In the tortuosity study it was found that the tortuosity calculations were independent of the Reynolds number, and that the newly developed tortuosity tests were in good agreement with techniques used by Kim en Chen (2006), deviating by between 2.65% and 0.64%.

The results from the TMD (thermal mixing degree) tests showed that there appears to be no explicit link between the porosity and mixing abilities of the packed beds tested, but this could be attributed to relatively small bed sizes used and the positioning and size of the warm inlet. A multi-velocity test showed that the TMD criterion is also independent of the Reynolds number. It was concluded that the results from the TMD tests indicated that more elaborate packed beds were needed to derive applicable conclusions from these type of mixing tests.

---

[1] Explicit refers to a simulation that physically models the flow relative to each sphere's geometrical position.

[2] Implicit refers to the modelling of the presences of the spheres by means of correlations and functions.

The explicit BETS (braiding effect test section) simulation results confirmed the seemingly irregular temperature trends that were observed in the experimental data, deviating by between 5.44% and 2.29%. From the detail computational fluid dynamics (CFD) results it was possible to attribute these irregularities to the positioning of the thermocouples in high temperature gradient areas. The validation results obtained in the effective thermal conductivity study were in good agreement with the results of Kgame (2011) when the same fitting techniques were used, deviating by 5.1%. The results also showed that this fitting technique is highly sensitive for values of the square of the Pearson product moment correlation coefficient (RSQ) parameter and that the exclusion of the symmetry planes improved the RSQ results. It was concluded that the introduction of the new combined coefficient (CC) parameter is more suited for this type of fitting technique than using only the RSQ parameter.

Keywords: Numerical modelling, packed beds, spheres, explicit, implicit, contact treatment, turbulence model, enhanced diffusion, mesh independency, tortuosity, TMD, BETS, effective thermal conductivity.

OPSOMMING

Die studie handel oor die numeriese modellering van vloei en diffusie deur gepakte beddens met uniforme grootte sfere. Ten einde verskeie numeriese benaderings in eksplisiete[3] en implisiete[4] simulasies te implementeer, is omvattende navorsing gedoen.

Vanuit literatuur was dit duidelik dat die karakterisering van 'n gepakte bed in terme van porositeit as enigste geometriese parameter, verder uitgebrei moet word weens die feit dat dit onvoldoende is (Van Antwerpen, 2009). Oor die korrekte karakterisering word steeds wyd bespiegel weens die gebrek aan insig in verskillende vloeiverskynsels wat voorkom in gepakte beddens. Eksplisiete simulasies is nie net in staat om insig te verskaf ten opsigte van hierdie gebrek aan begrip in vloeimeganika nie, maar kan ook gebruik word om verskillende vloeikorrelasies, wat in die implisiete tipe simulasies geïmplementeer kan word, te ontwikkel.

Die gebruik van STAR-CCM+® (VERSION 6.02.011) in die ondersoek na die numeriese modellering het as grondslag gedien vir die ontwikkeling van 'n betroubare modelleringsmetodologie, wat in staat is om akkurate numeriese resultate te lewer. 'n Nuwe kontakhanteringstegniek is ontwikkel in die studie wat dit moontlik maak om alle aspekte van die kontak-geometrie numeries voor te stel sonder benadeling van die numeriese berekeningspoed. Die studie het ook (vir die eerste keer) bewys dat die LES ("large eddy simulation") turbulensie model in staat is om die drukval oor 'n gepakte bed in die oorgangsvloei regime, by lae Reynoldsgetalle, akkuraat te voorspel. Die aanvaarde numeriese benadering is gedeeltelik gevalideer in 'n uitgebreide rooster onafhanklikheidstudie. Die validasie resultate afwyking was binne 0.54% en 3.45% van die KTA (1981) en Eisfeld en Schnitzlein (2001) korrelasies se voorspelde drukval waardes.

Hierdie studie het ook getoon dat eksplisiete simulasies in staat is om diffusie na aanleiding van turbulente vermenging, deur gepakte beddens akkuraat te modelleer. Die kronkelingstoetse wat uitgevoer is het bevestig dat die kronkelingberekeninge onafhanklik van die Reynolds getal is. Die resultate van die voorgestelde kronkelingberekeningstegniek wat gebruik is in die studie stem goed ooreen met vorige werk wat gedoen is deur Kim en Chen (2006), met gemiddelde afwykings tussen 2.65% en 0.64%.

Die resultate van die TMD ("thermal mixing degree") toetse het getoon dat daar geen duidelike skakel blyk te wees tussen die porositeit en vermengingsvermoëns van die gepakte beddens nie, maar dit kan toegeskryf word aan die relatief klein bedgroottes en die posisionering en grootte van

---

[3] Eksplisiet verwys na 'n simulasie wat fisies die vloei relatief tot elke sfeer se geometriese posisie modelleer.

[4] Implisiet verwys na die modellering van die teenwoordigheid van die sfere deur middel van korrelasies en funksies.

die warm inlaat. 'n Multi-snelheid toets het getoon dat die TMD maatstaf ook onafhanklik van die Reynolds getal is. Die resultate van die TMD toetse het aangedui dat meer omvattende gepakte beddens nodig sou wees om toepaslike gevolgtrekkings uit hierdie tipe vermengingstoetse af te lei.

Die eksplisiete BETS ("braiding effect test section") simulasie resultate toon dieselfde onreëlmatige temperatuur tendense wat in die eksperimentele data waargeneem is en 'n gemiddelde afwyking van 2,29% is ondervind tussen die simulasie en eksperimentele temperatuur profiele. Met die detail CFD ("computational fluid dynamics") resultate was dit moontlik om hierdie onreëlmatige temperatuur tendense toe te skryf aan die posisionering van die termokoppels in hoë temperatuurgradiënt gebiede. Die valideringsresultate wat verkry is in die effektiewe termiese geleidingsvermoë studie toon 'n goeie ooreenkoms met die resultate van Kgame (2011) wanneer dieselfde passingstegnieke gebruik word, wat dan 'n afwyking van 5,1% lewer. Die resultate het ook getoon dat hierdie passingstegniek baie sensitief is vir die waardes van die RSQ ("square of the Pearson product moment") parameter en dat die uitsluiting van die simmetriese vlakke, die resultate verbeter. Daar is tot die gevolgtrekking gekom dat die gebruik van die nuwe gekombineerde koëffisient parameter meer gepas is as om slegs die RSQ parameter vir dié tipe passings te gebruik.

Kernwoorde: Numeriese modellering, gepakte beddens, sfere, eksplisiet, implisiet, kontak hantering, turbulensie model, termiese diffusie, rooster onafhanklikheid, kronkeling, TMD, BETS, effektiewe termiese geleiding.

ACKNOWLEDGEMENTS

Firstly, I want to express my gratitude to my study supervisor, Professor Jat du Toit, for his intellectual guidance, patience and advice on many points of detail. I want to thank the NWU and THRIP for their financial support, it is sincerely appreciated.

I would like to thank my family for their understanding and moral support the past two years.

Lastly I want to thank God for blessing me with this opportunity and giving me the strength to finish.

TABLE OF CONTENTS

INTRODUCTION

LITERATURE STUDY

MODELLING APPROACH

ENHANCED MIXING

SUMMARY AND CONCLUSION

LIST OF FIGURES

LIST OF TABLES

NOMENCLATURE

Latin – Lowercase

Symbol	*Description*	*Unit*
d	Diameter	m
d_c	Cell diameter - surface triangulation size	m
d_{cont}	Contact diameter	m
d_p	Particle diameter	m
f_w	Wall damping function	-
k_{er}	Effective radial thermal conductivity	W/m-K
k_g	Gas natural conductivity coefficient	W/m-K
k_{lm}	Radial thermal conductivity	W/m-K
k_p	Proportionality constant	-
k	Cell face value	-
n	Number of paired planes	-
p	Pitch	m
t	Time	s
u	Mean Velocity component	m/s
u	Velocity in a Cartesian coordinate system	m/s
v	Velocity in a Cartesian coordinate system	m/s
v_o	Superficial velocity	m/s
w	Velocity in a Cartesian co-ordinate system	m/s
x	Cartesian coordinate position	m
y	Cartesian coordinate position	m
z	Cartesian coordinate position	m

Latin – Uppercase

A	Constant in friction factor	-
A_0	Constant in the κ-ε model	-
A_s	Constant in the Realizable κ-ε model	-

B_w	Empirical porosity effect	-
C_μ	Constant in the κ-ε model	-
C	Constant in the Realizable κ-ε model	-
D	Diameter	m
D_B	Diameter of the bed	m
D_H	Hydraulic diameter	m
$D_{(n)}$	Deviation between parameters	-
E	Natural base for exponential function	-
H	Packing Height	m
Nu	Nusselt number	-
M	Dimensionless hydraulic diameter of the walls	-
P	Fluid pressure	Pa
$P_{(n)}$	Average pressure drop over a plane section	-
Re	Reynolds number	-
Re_m	Modified Reynolds number	-
Re_p	Particle Reynolds number	-
S	The rate of deformation	-
L	bed length	m
L_{CT}	Cell target size	m
L_{CM}	Minimum cell size	m
T	Temperature	°C
T_{ND}	Non-dimensional temperature value	-
$T_{braiding}$	Braiding temperature profile	°C
$T_{hot\ inlet}$	Temperature at the hot inlet	°C
$T_{cold\ inlet}$	Temperature at the cold inlet	°C
T_{inlet}	Temperature at the inlet section	°C
T_{outlet}	Temperature at the outlet section	°C
ΔT_{inlet}	Difference between the minimum and maximum temperatures at the inlet	°C
ΔT_{out}	Difference between the minimum and maximum temperatures at the outlet	°C
y^+	Dimensionless cell distance from the wall	-
V_{void}	Void volume in packed bed	m^3
V_{Total}	Total volume of the packed bed	m^3

Greek

Δ	Difference	-
ρ	Density	kg/m^3
ν	Viscosity	Kg/m-s
σ	Constant in the κ-ε model	-
τ	Reynolds stresses tensor	Pa
μ_f	Fluid viscosity	Kg/m-s
μ_T	Dimensionless eddy (turbulent) viscosity	-
μ_{eff}	Effective viscosity	Kg/m-s
δ	Kronecker delta	-
ω	Vorticity	-
ℓ	Length scale in the κ-ω model	-
κ	Turbulent kinetic energy	J
ε	Viscous dissipation	-
ε_p	Porosity	-
β	Is a closure constant in the κ-ω model	-
Π	Transport of Reynolds stresses due to turbulent pressure	-
Ω	Transport of Reynolds stresses due to rotation	-
ϕ	Particles shape factor	-
ζ	Tortuosity factor	-
ξ	Tortuosity	-
λ	Dimensionless diffusion coefficient	-
ψ	Friction factor	
ν	Fluid viscosity	kg/m^3

Subscripts

ij	Tensor matrix format

Superscripts

*	Dimensionless variable
'	Fluctuating component
˜	Dynamic

Mathematical

→	Vector
Bold	Vector
‾	Average

Abbreviations

BCC	Body-centred cubic
BETS	Braiding effect test section
CAD	Computer aided design
CAE	Computer aided engineering
CC	Combined coefficient
CCP	Cubic close packing
CFD	Computational fluid dynamics
CT	Contact treatment test
div	Derivative
FCC	Face-centred cubic
grad	Gradient
HCP	Hexagonal close packing
HMD	Homogenisation mixing degree
HTTU	High temperature test unit
KTA	Kern Technisches Ausschuss
LES	Large eddy simulation
MD	Mesh independency test
MV	Multiple velocity test
PBMR	Pebble bed modular reactor
RBP	Random bulk packing
RMSD	Root mean square deviation
RSM	Reynolds stress equation model
RSQ	Square of the Pearson product moment correlation coefficient
SC	Simple cubic
SGS	Sub-grid scale
SST	Shear-stress transport
SV	Single velocity test
HTR-10	10MW high temperature gas-cooled reactor test module
TM	Thin mesh contact treatment test

TMD	Temperature mixing degree
TS	Two sphere test
VB	Visual Basic

1

INTRODUCTION

1.1. BACKGROUND TO THE STUDY

Recent years have seen an important trend in industrial optimization of overall production processes and efficiencies due to continued global economic pressure. In the chemical, metallurgical and nuclear industries, packed pebble beds are used in catalytic, chromatographic and nuclear reactors but can also be applied in ion exchangers, heat exchangers and absorbers. In order to optimize packed bed applications, further research is needed to fully characterize different flow phenomena through these packed beds. In each packed bed application the pressure drop, flow and temperature distribution differs with bed and packing structure. The thermal performance and safety evaluation of a packed bed reactor require extensive knowledge of these parameters.

Different theoretical models and various numerical correlations exist that describe the flow through packed beds, but these are generally bound by experimental variables and are thus dependent on the specific bed (Subagyo *et al.*, 1997:1376). Each of these models was derived using different parameters and measuring techniques. Van Antwerpen (2009) concluded that characterizing a packed bed structure using only porosity is inadequate. In order to understand and predict flow through packed beds it is necessary to determine and implement appropriate variables into the different flow correlations used in implicit modelling. The first fundamental step towards a better understanding of the effect of a packed bed structure on flow and flow phenomena, is to study its mixing ability.

The seemingly endless growth in computer processor and storage technologies ensures that computational fluid dynamics (CFD) is one of the fastest growing tools used in computer aided engineering design (CAE). CFD is mainly used to optimize existing processes and energy requirements, cycle design and the development of new processes and products. This type of detail modelling is essential in the design of fixed-bed reactors, seeing that the ever increasing performance requirements of such equipment demand that the proposed model not only include spatial distribution of different flow parameters but also the temperature and velocity profiles for the reactor (Guardo *et al.,* 2005:1733).

Explicit simulations are not only able to provide insight into the fluid mechanics of flow through packed beds, but can also be used to develop different flow correlations that can be implemented into implicit type simulations. Although various studies have been done (Tobis, 2000; Nijemeisland & Dixon, 2001; Calis *et al.,* 2001, Guardo *et al.,* 2005; Lee *et al.,* 2007; McLaughlin *et al.,* 2008) on the numerical implementation of flow through packed beds using commercial CFD codes, it is evident that some residing shortcomings (e.g. contact handling) still need to be addressed.

Finally, this investigation has been done using different modelling approaches to validate the numerical setup, which was used to address some of the shortcomings associated with the modelling of flow through packed bed geometries. This study was also concerned with the development of explicit simulations and techniques required to extract and compare different mixing parameters.

1.2. RESEARCH PROBLEM STATEMENT

Different opinions are found in literature on the velocity distribution, experimental variables and the influence of confining walls on the pressure drop in a packed bed. It was also noted that the characterization of a packed bed using porosity as the only geometrical parameter is inadequate (Van Antwerpen, 2009).

The characterization of packed beds is still greatly debated due to the lack of understanding of the fluid mechanics through packed beds. This is mainly caused by the technical difficulty of measuring flow parameters inside packed beds, but can potentially be resolved through detailed modelling. Large scale CFD modelling of flow through packed beds generally uses implicit type simulations, due to the large computational resources required to explicitly model each particle. Therefore it is essential to re-evaluate the accuracy and the applicability of the flow correlations used to implicitly model different flow phenomena in packed beds. A proper understanding of the fluid mechanics inside a packed bed is vital in the development of these flow correlations.

This led to the proposal of establishing a numerical laboratory and methodology that can accurately predict the fluid mechanics through structured and unstructured packed beds that will enable researchers to gain important insight into the flow dynamics inside packed beds.

1.3. OBJECTIVES OF THIS STUDY

The purpose of this study is to establish the numerical modelling methodology needed to obtain highly accurate explicit simulation results. This study will focus on:

- The numerical approach required to address the treatment of the contact between spheres, the resolution of the computational mesh, and the modelling of turbulence.
- The development of explicit simulations and techniques necessary to extract and compare different mixing parameters.

The numerical methodology will be validated throughout the study by comparing the simulated results with different pressure drop correlations and by comparing the mixing parameters obtained in this study to previous work. The aim of the study is not to derive flow correlation or to implement correlations into any form of implicit simulation.

The numerical simulation models were to be generated for structured and random packed beds by using a computer software package known as STAR-CCM+®.

1.4. CHAPTER OUTLINE

Following this introductory chapter, Chapter 2 presents a literature survey regarding packing structures, factors influencing flow parameters, enhanced mixing parameters and aspects regarding explicit modelling. Furthermore, several aspects regarding the treatment of the contact between spheres, the resolution of the computational mesh, and the modelling of turbulence are investigated in terms of work that has previously been done.

Chapter 3 focuses on the modelling approach needed to explicitly simulate flow through packed beds and the aspects influencing the accuracy of the results. Key issues regarding the contact treatment, mesh density and turbulence models are addressed.

Chapter 4 discusses the implementation of enhanced mixing simulations and techniques necessary to extract and compare different mixing parameters. These tests will include tortuosity, thermal mixing degree and braiding test simulations.

Chapter 5 summarises the study and provides concluding remarks and recommendations for future work.

2

LITERATURE STUDY

2.1. INTRODUCTION

The flow of a fluid through a packed bed of spheres is of importance in various industries as mentioned previously. This study aims to exploit the abilities of the rapidly developing numerical modelling of flow known as computational fluid dynamics (CFD), to model flow phenomena occurring in spherical packed beds. The characterization of packed beds is still greatly debated due to the lack in understanding of the fluid mechanics through packed beds. This is mainly caused by the technical difficulty of measuring flow parameters inside packed beds, but can potentially be resolved through detailed modelling. In order to be able to accurately model flow through different packing structures of spheres it is necessary to thoroughly understand the different types of structures, flow regimes, flow phenomena and CFD constraints.

In this study explicit modelling will refer to a simulation that physically models the flow relative to each sphere's geometrical position whereas implicit modelling will refer to the modelling of spheres by means of correlations and functions that are able to approximate the porosity or any other geometrical parameter.

This chapter and the study as a whole will focus on the development of a methodology to model flow through packed beds by focussing on:

- The numerical approach required to address the treatment of the contact between spheres, the resolution of the computational mesh, and the modelling of turbulence.
- The development of explicit simulations and techniques necessary to extract and compare different mixing parameters.

2.2. PACKING STRUCTURES

The focus of this study was limited to only three types of packing structures namely, body-centred cubic (BCC), face-centred cubic (FCC) and random packings. The FCC structure is known as a close packing which has the densest structure of all packings (Ashby & Jones, 2002). A close packing has numerous stacking configurations of which the hexagonal close packing (HCP) and the cubic close packing (CCP) will be used in this study.

Figure 2.1 shows the SC (simple cubic) and the BCC crystal structures. The SC structure consists of four spheres, equally spaced in a cube as shown. The BCC structure is also formed in a cube-like structure with a single sphere situated at the centre of the lattice and eight evenly spaced spheres surrounding it, forming the corners of the unit structure (Ashby & Jones, 2002). The spheres in the BCC structure are only in contact along the diagonal of the unit cell.

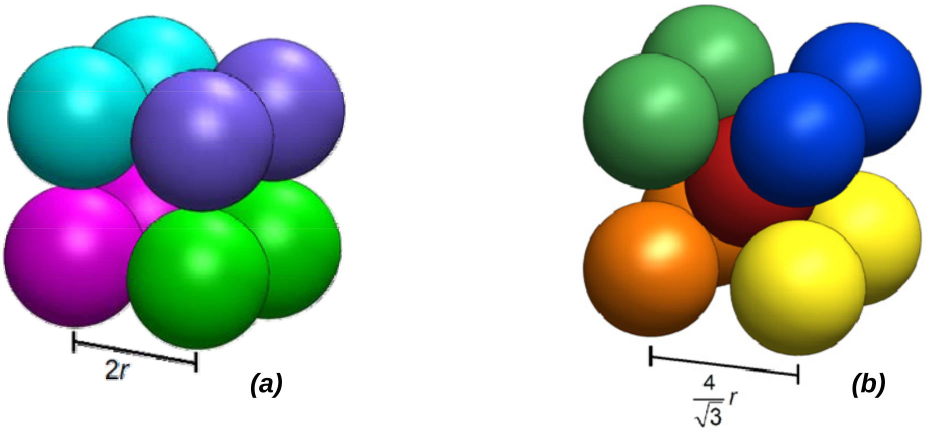

Figure 2.1: SC (a) and BCC (b) crystal structure.

A close packing structure consists of different arrangements of close packed layers. These layers are formed by a centre sphere with six contacting neighbour spheres. The HCP structure is stacked with close packing layers that alternate between sites A and B (A-B-A), whilst the CCP structure is stacked on sites A, B and C (A-B-C-A) as displayed in Figure 2.2 (Ashby & Jones, 2002).

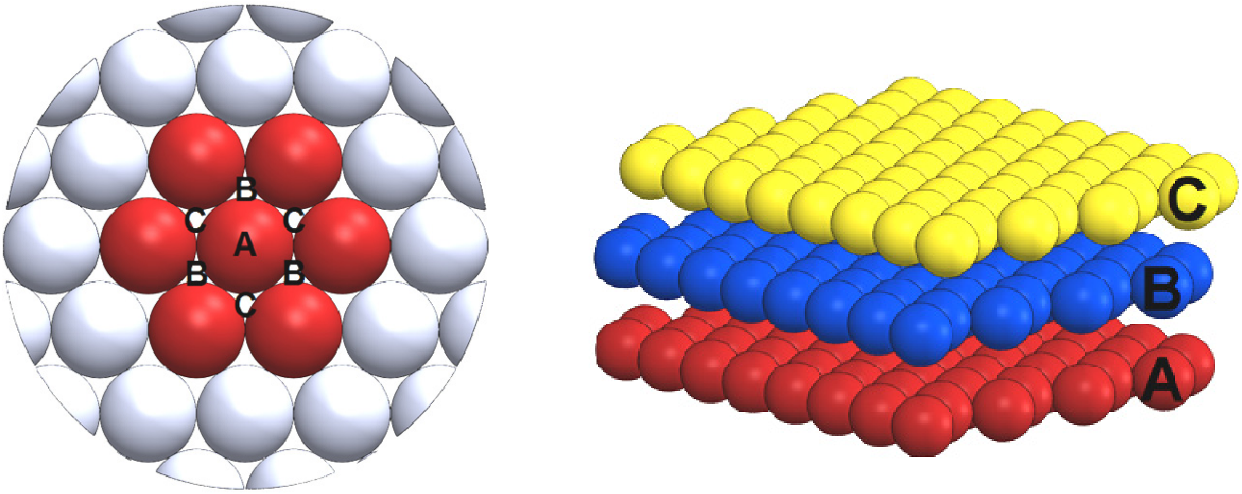

Figure 2.2: FCC structure with HCP and CCP packing configurations and sites.

In this study, the same definition for porosity will be used as defined by Liu *et al* (1999:438), who stated that porosity is the ratio between the unoccupied spaces (voids) and the total volume. Porosity is therefore a geometrical parameter that gives an indication of the effectiveness of the packing or structure. A dense packing similar to the FCC structure will have a porosity that is less than a BCC structure implying that the BCC structure is packed less efficiently:

$$\varepsilon_p = \frac{V_{void}}{V_{Total}} \tag{2.1}$$

where ε_p is the porosity, V_{void} is the volume of the void and V_{Total} is the total volume of the packing.

The coordination number is also a geometrical parameter that is used to express the average number of spheres that are in contact with each other. All the different geometrical properties for the two types of structured packings are presented in Table 2.1.

Table 2.1: BCC and FCC unit cell geometrical properties.

Crystal structure	***Porosity***	***Spheres per unit cell***	***Coordination number***
SC	0.48	1	6
BCC	0.32	2	8
FCC	0.26	4	12

Although FCC packed beds have the same geometrical parameters, the flow through HCP and CCP packings will differ due to the different flow paths that are available to the fluid. The main reason for choosing to analyse two FCC structured packings in this study was to investigate different flow phenomena of different structures that had the same porosity, to confirm that the porosity as geometrical parameter is inadequate to characterize a packed bed's structure.

In this study, the fluid domain for randomly packed beds will be divided into three regions, namely the wall, near-wall and the bulk region:

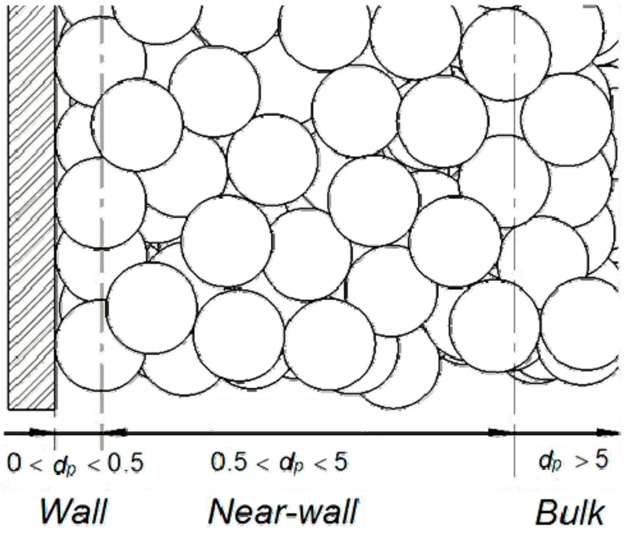

***Figure 2.3:* The different packed bed regions defined in this study, with d_p the particle diameter.**

It is necessary to divide a randomly packed bed into these three regions since its structure varies from the wall to the bulk region. This variation in structure means that the porosity parameter also differs in all three regions. Van Antwerpen (2009) noted that when different regions in randomly packed beds were compared to the porosities in structured packings, the SC and BCC structures correlated best to the bulk region and the FCC in the near-wall region. He concluded that although the different porosities in a randomly packed bed can be quantified by structured packings, the coordination and coordination flux numbers significantly deviate from those of a randomly packed bed. For that reason, characterizing a porous structure using porosity alone is not sufficient.

2.3. THE STATISTICAL NATURE OF FLOW THROUGH PACKED BEDS

The geometrical complexity of a structured or unstructured packing causes fluctuating flow and vortices. This instability is a very important variable in the characterization and prediction of flow and flow phenomena inside packed beds. This fluctuation or statistical nature of experimental data is of no particular significance to this study, but for the sake of completeness it is briefly mentioned in this literature study.

Bey and Eigenberger (1996:1365) measured velocity profiles for randomly packed beds of different spheres by using a monolith to support the structure and preserve the flow profile. They noted that due to the statistical nature of packed beds, the scatter in the bulk region is much more prominent than at the wall region as displayed in Figure 2.4. This is most likely due to the lack in structure at the tube centre, which suggests that the average velocity profile should be obtained over several repackings (Bey and Eigenberger, 1996:1366). Their results also showed that the maximum velocity peaks deviated with about 15% after several repackings.

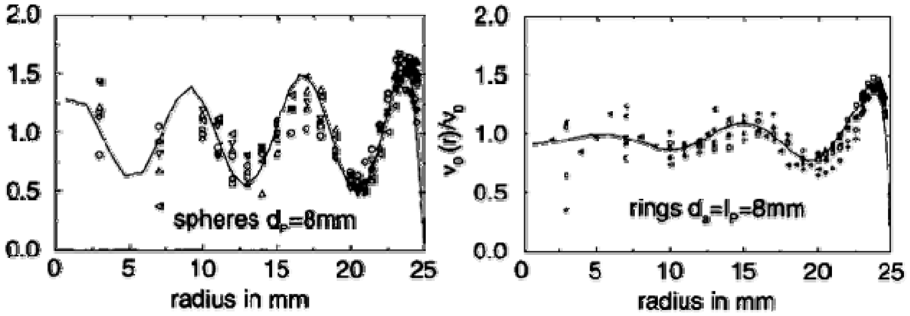

Figure 2.4: Comparison between the velocity profiles after the bed was repacked with a mean velocity of v_o = 0.5 m/s, (Bey and Eigenberger, 1996:1366).

This result is in line with the results obtained by Subagyo *et al.* (1997:1379) who did a similar experiment validate their theoretical models and carried out their experiments in a cylinder with three random packings of glass spheres, ranging between 15.7 mm < d_p < 34.33 mm, with d_p the particle diameter. The results showed reasonable agreement between the repackings, with a 12% absolute deviation between the mean velocities.

2.4. FACTORS INFLUENCING FLOW PARAMETERS

All the flow parameters associated with randomly and structured packed beds are dictated by the velocity distribution through the fluid domain. Numerous factors influence the velocity distribution through a packed bed of which the most important factors are:

- the packing's geometrical parameters of which porosity is most commonly used in correlations;
- the Reynolds number;
- the axial length of the bed; and
- the ratio between the particle and vessel diameter.

As mentioned previously, the best known geometrical parameter that is used to help predict the velocity profile is the porosity distribution through a packed bed. The porosity distribution of a randomly packed bed differs from that of other porous mediums since the porosity distribution is not homogeneous due to the effects of the wall. The wall tends to structure the packing and the effect on flow can be detected five sphere diameters from the wall into the bulk region as can be observed in Figure 2.5.

From literature it was found that all the friction factors that are used in pressure drop correlations including the Ergun (1952:92), KTA (Kern Technisches Ausschuss - Safety Standards of the Nuclear Safety Standards Commission, KTA 3102.3 - 1981) and Eisfeld and Schnitzlein (2001) type friction factors only use porosity as geometrical parameter. One of the objectives of this study is to identify and analyse other candidate geometrical parameters that can be used in these types of correlations.

The porosity distributions for cylindrical as well as annular randomly packed beds are well documented. Du Toit (2008:3073) confirmed that radial porosity distribution correlations derived from cylindrical packed beds may also be used for an annular packed bed. Van Antwerpen (2009:14) concluded that the oscillatory correlation for the variation of porosity in the radial direction proposed by De Klerk (2003:2022) is the most accurate correlation for an annular packed bed as displayed in Figure 2.5.

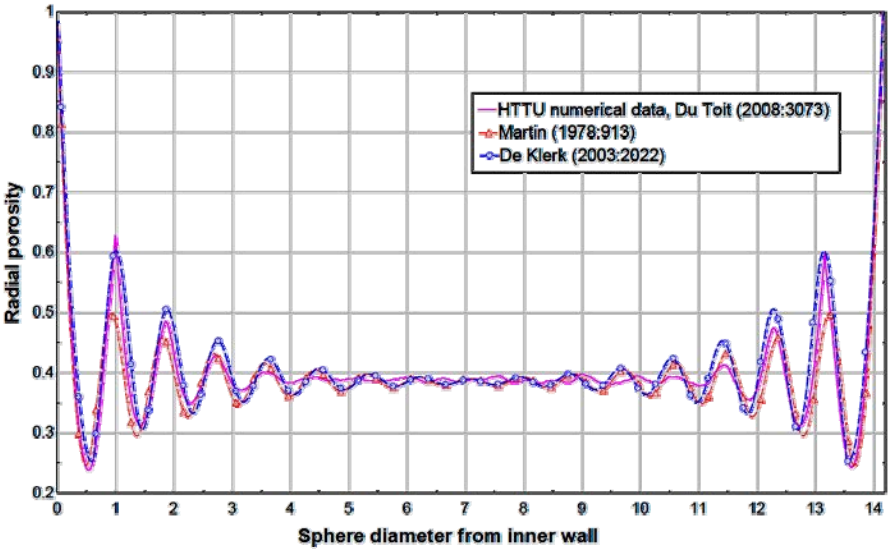

Figure 2.5: Comparison between oscillatory correlations and numerical results for the High Temperature Test Facility (HTTU) (Van Antwerpen, 2009:14).

Two types of Reynolds numbers will be used in this study, namely a Reynolds number based on the hydraulic diameter of the flow domain and a Reynolds number based on the diameter of the particle known as the particle Reynolds number. The generic form is given by:

$$\mathrm{Re} = \frac{\rho v_0 D_H}{\mu_f} \tag{2.2}$$

where ρ is the fluid density, V_0 the superficial velocity, μ_f the fluid viscosity and D_H the hydraulic diameter or the particle diameter depending on the type of Reynolds number used.

Bey and Eigenberger (1996:1365) measured and modelled velocity profiles in cylindrical packings of spheres, rings and cylinders in order to use the results to contribute to heat transfer parameters in packed beds. The outlet velocities of air flow were measured between 0.5 m/s < v_o < 1.5 m/s. Bey and Eigenberger (1996:1367) found that there is no observable dependency of the flow profile on particle Reynolds numbers between 74.2 < Re_p < 969.8. Bey and Eigenberger (1996:1369) used the extended Brinkman equation to describe the flow distribution in their model.

Similarly Giese *et al.* (1998) measured the velocity profile for low particle Reynolds numbers in a packed cylinder with differently shaped objects. They measured the velocity profile for particle Reynolds numbers between 4 < Re_p < 532 and found that the flow profile reflects the oscillation of the porosity distribution for the whole cross section and that the flow profile is constant for 77 < Re_p < 532 if the flow is fully developed.

Price (1968:10) measured the flow profiles over a large number of packed beds. He used four different flow rates over a 229 mm diameter bed with 12.7 mm diameter steel spheres with particle Reynolds numbers between $1470 < Re_p < 4350$. From the results he concluded that the normalized velocity distribution was independent of the Reynolds number for the range tested.

Subagyo *et al*. (1997:1383) validated his new theoretical model for flow in packed beds by measuring velocity inside, as well as downstream of packed beds. From their findings Subagyo *et al.* concluded that the velocity distribution is dependent on the Reynolds number for $Re_p < 500$ and that Reynolds number dependence for the velocity distribution at higher Reynolds numbers is insignificant as shown in Figure 2.6, where N_{RE} is the dimensionless Reynolds number and u_m/u_M dimensionless velocity.

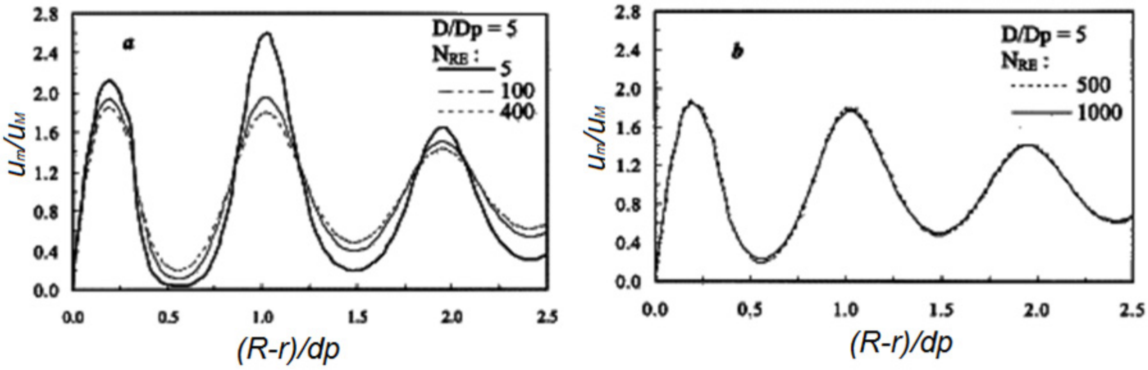

Figure 2.6: The dependency of the velocity distribution on the particle Reynolds number inside packed beds for low (a) and high (b) ranges (Subagyo et al., 1997:1383)

Hlushkou and Tallarek (2006:75) analysed flow regimes in packed beds of spherical particles. In their study they defined three flow regimes and concluded that the transitions in porous media is not sharp, but develops gradually throughout the different flow regimes. The three flow regimes are displayed in Figure 2.7: creeping flow ($0 < Re_p < 100$), viscous-inertial flow ($30 < Re_p < 500$) and inertial flow ($Re_p > 500$).

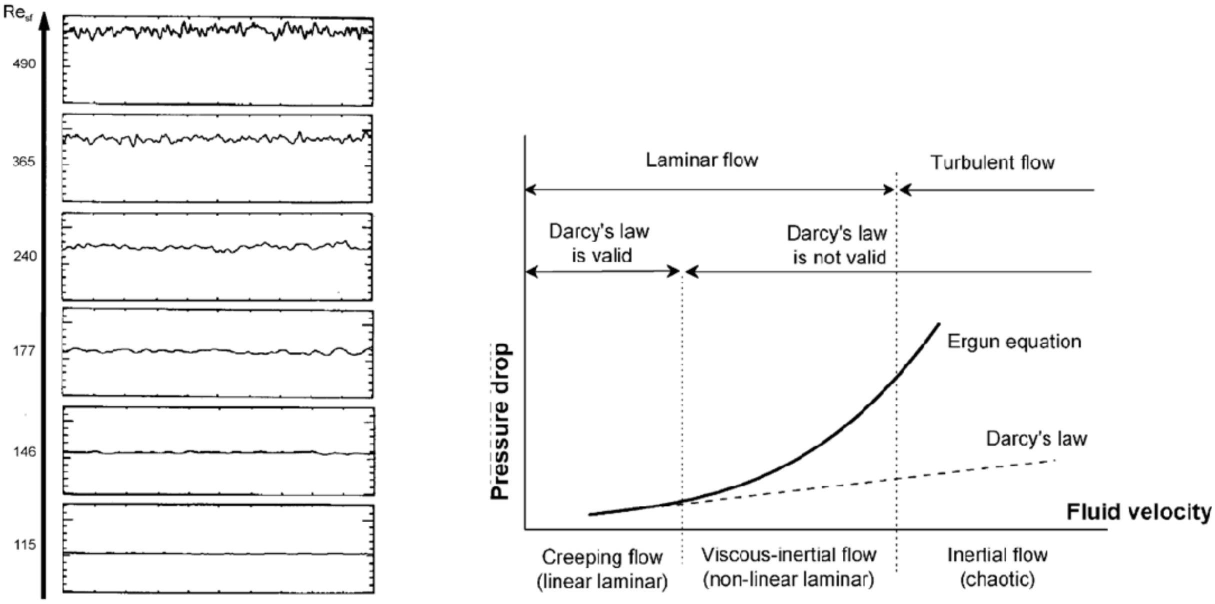

Figure 2.7: (a) Recordings of the velocity instability measured by electrochemical probes at different superficial Reynolds numbers in a fixed bed of glass spheres and (b) the characterization of different hydrodynamic regimes (Hlushkou & Tallarek, 2006:75).

From the preceding literature it is evident that the velocity profile is dependent on the Reynolds number up to the point where the inertial forces becomes dominant, at approximately Re > 500. This explains why Price (1968:10) stated that the velocity profile was independent of the Reynolds number in his study. This gradual development of the flow regime might also be the reason why Giese *et al.* (1998) and Bey and Eigenberger (1996:1367) noted that there is no observable dependency of the flow profile on particle Reynolds numbers $Re_p > 74.2$ and $Re_p > 77$.

Bey and Eigenberger (1996:1367) studied the effect of particle size on velocity profiles for bed to particle ratios of $3.57 < D_B/d_p < 11$. Their results showed that different sphere packings have no to very little influence on the mean velocity bypass behaviour. A similar study was conducted by Price (1968:13). He compared the influence of D_B/d_p by measuring the velocity profile over packed beds with 6.35 mm, 12.7 mm and 25.4 mm spheres and a bed depth of 228.6 mm. Price (1968:13) concluded that for a bed-to-particle diameter ratio between $12 < D_B/d_p < 48$, no to slight systematic effects can be observed near the wall.

Price (1968:11), studied the influence of bed length on the velocity distribution by comparing the velocity measurements for three different bed lengths, namely $L/d_p = 9$, $L/d_p = 18$ and $L/d_p = 36$. From the results, Price (1968:11) concluded that for bed lengths between the range of $9 < L/d_p < 36$, the normalized velocity distribution is independent of the bed length. This result from Price agrees well with the findings of Schwartz and Smith (1953:1212) and Morales *et al.* (1951:230). They conducted similar tests for bed lengths of $16 < L/d_p < 46$ and $6 < L/d_p < 46$ and both found no significant effect of bed depth on the velocity distribution.

Zou and Yu (1995:1505) studied the effect of sphere-to-cylinder diameter ratio (d_p / D_B) and the ratio between the sphere diameter to packing height (d_p/H) on the porosity distribution in a random packing. Their results showed that the bulk porosity started to increase when $d_p/H > 0.05$. A variation in bulk porosity of $0.398 < \varepsilon_p < 0.72$ was observed when d_p/H was varied between 0.01 and 0.6.

2.5. PRESSURE DROP CORRELATIONS

Establishing pressure drop correlations for porous media has been an ongoing development for many years. The most important correlations for flow through a packed bed of uniform spheres is those of Ergun (1952) and Carman-type friction factors. The original Ergun (1952) friction factor can be formulated as follows (Van der Walt and Du Toit, 2006):

$$\Psi = \frac{\Delta P}{\rho v_0{}^2} . \frac{d_p}{L} = \frac{150}{\mathrm{Re}_p} . \frac{(1-\overline{\varepsilon_p})^2}{(\overline{\varepsilon_p})^3} + 1.75 \frac{(1-\overline{\varepsilon_p})}{(\overline{\varepsilon_p})^3} \tag{2.3}$$

$$\mathrm{Re}_m = \frac{\mathrm{Re}_p}{\left(1-\overline{\varepsilon_p}\right)} \tag{2.4}$$

where $\overline{\varepsilon_p}$ is the average porosity of the packing, Ψ is the friction coefficient, ΔP is the pressure drop, L is the length of the bed and Re_m is the modified Reynolds number.

The Ergun (1952) correlation is valid for a porosity range of $0.36 < \overline{\varepsilon_p} < 0.4$ and a modified Reynolds number range of $1 < \mathrm{Re}_m < 2500$ (Ergun, 1952:93). It has to be noted that most of the development of this correlation was focused on $\mathrm{Re}_m < 1000$, therefore the application for flow with a modified Reynolds numbers higher than 1000 is debatable.

The development of high temperature modular based nuclear reactors required a more extensive pressure drop correlation for licensing and safety reasons. Hence extensive research done in Germany played an important role in the development of the Carman-type pressure drop correlation known as the KTA (1981) equation. This equation is valid for a packed bed of spherical particles with a modified Reynolds number of up to 50000 (Van der Walt & Du Toit, 2006). Although this correlation was empirically derived for a cylindrical packed bed, Van der Walt and Du Toit (2006) confirmed that can also be used in an annular packed bed. The KTA (1981) friction factor can be calculated as follows:

$$\Psi = \frac{\Delta P}{\rho {v_0}^2} . \frac{d_p}{L} = \frac{160}{\mathrm{Re}_p} . \frac{(1-\overline{\varepsilon_p})^2}{(\overline{\varepsilon_p})^3} + \frac{3}{(\mathrm{Re}_p)^{0.1}} . \frac{(1-\overline{\varepsilon_p})^{1.1}}{(\overline{\varepsilon_p})^3} \tag{2.5}$$

Eisfeld and Schnitzlein (2001:4327) analysed more than 2300 data points from literature and found that external boundaries lead to an increase in losses in the creep flow regime and decrease in the turbulent flow regime compared to an identical infinite bed. They also noted that Reichelt's correlation that incorporates the wall effect into the Ergun (1952) equation, is the most promising correlation. After a statistical analysis on Reichelts correlation, Eisfeld and Schnitzlein (2001:4327) proposed the following improved correlation (Van der Walt & Du Toit, 2006):

$$\Psi = \frac{\Delta P}{\rho {v_0}^2} . \frac{d_p}{L} = \frac{154}{\mathrm{Re}_p} . \frac{(1-\overline{\varepsilon_p})^2}{(\overline{\varepsilon_p})^3} . M^2 + \frac{M}{B_w} . \frac{(1-\overline{\varepsilon_p})^{1.1}}{(\overline{\varepsilon_p})^3} \tag{2.6}$$

$$B_w = \left[1.15 \left(\frac{d_p}{D_B} \right)^2 + 0.87 \right]^2 \tag{2.7}$$

$$M = 1 + \frac{4 d_p}{6 D_B (1-\varepsilon)} \tag{2.8}$$

where B_w describes the empirical porosity effect of the walls and M accounts for the hydraulic diameter of the walls. This correlation is valid for $0.01 < \mathrm{Re}_p < 17635$, a mean porosity of $0.33 < \overline{\varepsilon_p} < 0.882$ and a tube-to-particle diameter ratio of $1.624 < D_B / d_p < 250$.

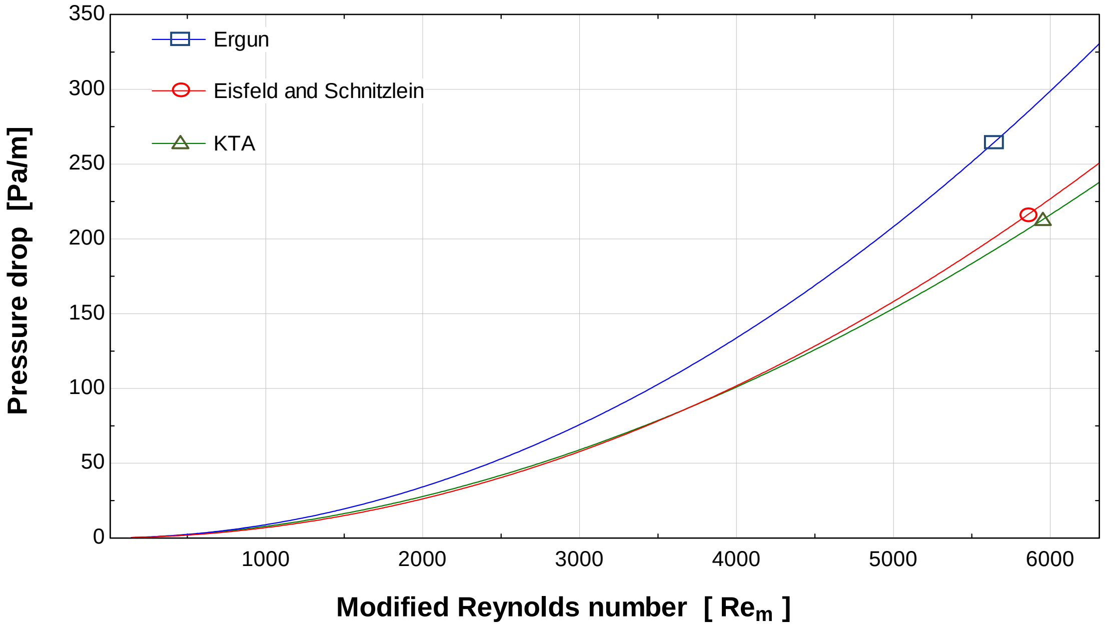

***Figure 2.8:* Comparison between Ergun (1952), Eisfeld and Schnitzlein (2001) and the KTA (1981) pressure drop correlations for $Re_m > 6000$.**

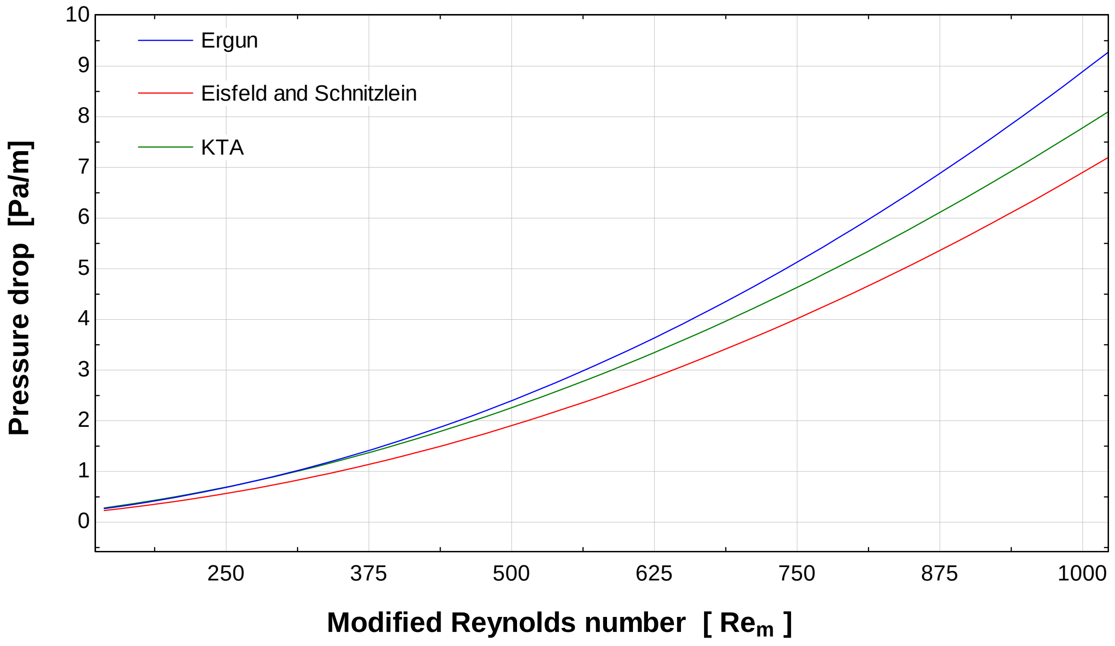

***Figure 2.9:* Comparison between Ergun (1952), Eisfeld and Schnitzlein (2001) and the KTA (1981) pressure drop correlations for $Re_m < 1100$.**

Figure 2.8 and Figure 2.9 compares the different pressure drop correlations. The Eisfeld and Schnitzlein (2001) correlation was calculated using the infinite bed assumption. The results shows that for low Reynolds numbers all of the correlations is in reasonable agreement with each other, as shown in Figure 2.9. The Ergun (1952) correlation starts to deviate dramatically from both Eisfeld and Schnitzlein (2001) and the KTA (1981) correlations for a modified Reynolds number larger than

1000, which is expected, and can be seen in Figure 2.8. From Figure 2.8 it is also evident that the KTA (1981) and Eisfeld and Schnitzlein's (2001) correlations are in close agreement with each other, with a deviation of 4.7% at $R_m = 6000$.

It can thus be concluded that the KTA (1981) and Eisfeld and Schnitzlein's (2001) correlations would be the best choice for both low and high Reynolds number flows.

2.6. ENHANCED MIXING

Flow through conservative domains, i.e. pipes and ducts, experience much less radial flow variation than in packed beds. This radial flow variation is the result of highly uneven, or complex alternating flow paths which induce turbulence at much lower Reynolds numbers than in conservative domains. This type of mixing (laminar or turbulent) causes mass to be dispersed (momentum) relative to the flow direction which leads to the enhanced mixing phenomena which is frequently referred to in literature as dispersion or a braiding effect (Van Antwerpen, 2007).

2.6.1. Thermal diffusion

Although the transport mechanism for heat dispersion through a packed bed is convection, it is easier to model the braiding effect as an enhanced diffusion, which can easily be accounted for by increasing the effective conductivity of the fluid (Van Antwerpen, 2007). The pebble bed effective radial thermal conductivity is given by (Kgame, 2011):

$$k_{er} = k_g + k_{lm} \tag{2.9}$$

where k_{er} is the effective radial thermal conductivity, k_g is the gas thermal conductivity coefficient and k_{lm} is the thermal conductivity caused by the radial (lateral) mixing.

Kgame (2011) studied the braiding effect by calculating the effective radial thermal conductivity coefficient (k_{er}) in a BCC structured packed bed with a warm and a cold inlet. He derived braiding temperature profiles at the bottom and top part of the structured packing by using experimental data, which he used to help him calculate the k_{er} in his CFD simulations. His experimental setup named BETS (braiding effect test section) can be seen in Figure 2.10.

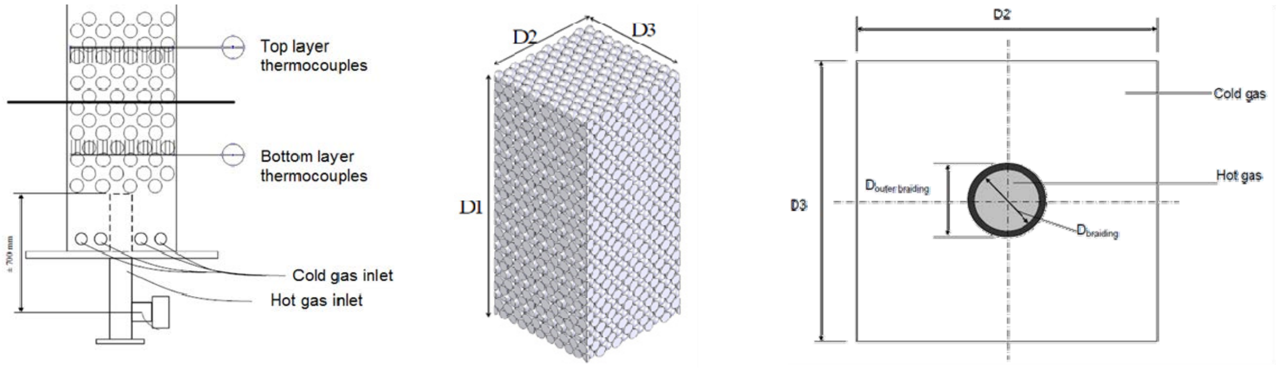

Figure 2.10: The schematic diagram of the BETS test section (Kgame, 2011).

Table 2.2 shows the geometry of the BETS experiment. Two Braiding temperature profiles were extracted from the test section, both 247 mm from the top and bottom of the packed bed.

Table 2.2: BETS geometry description Kgame (2011).

Description	**Value**
Porosity	0.352
D1 [mm]	741.1
D2 [mm]	300
D3 [mm]	300
$D_{braiding}$ ***[mm]***	77
$D_{outer\ braiding}$ ***[mm]***	79.58
Pebble diameter [mm]	28.575

Kgame (2011) used a non-dimensional temperature value to calculate the braiding temperature profiles to compensate for the different inlet temperatures which were kept at ambient temperature. The braiding temperature can be calculated as follows:

$$T_{ND} = \frac{(T - T_{cold\ inlet})}{(T_{hot\ inlet} - T_{cold\ inlet})} x100 \tag{2.10}$$

where T_{ND} is the non-dimensional temperature value, T is the measured temperature and $T_{hot\ inlet}$ and $T_{cold\ inlet}$ are the temperatures at the two inlets as can be seen in Figure 2.10.

Kgame (2011), then further derived a normalised braiding temperature profile by using the non-dimensional temperature values from equation (2.10) and the average inlet gas temperatures over four test runs:

$$T_{braiding} = \frac{\overline{T}_{ND}}{100} x(\overline{T}_{hot\ inlet} - \overline{T}_{cold\ inlet}) + \overline{T}_{cold\ inlet} \tag{2.11}$$

where $\overline{T}$ are the average temperatures and $T_{braiding}$ the normalized braiding temperature profile.

He calculated k_{er} by simulating an eighth of the BETS test section, using a commercial CFD code, Flow++[4]. The boundary conditions were setup to represent the BETS test section without the presence of the spheres. This was done to exclude the effect of the pressure drop on the fluid dispersion, with the intention that the fluid conductivity solely accounts for the turbulent mixing. The CFD domain and grid are shown in Figure 2.11.

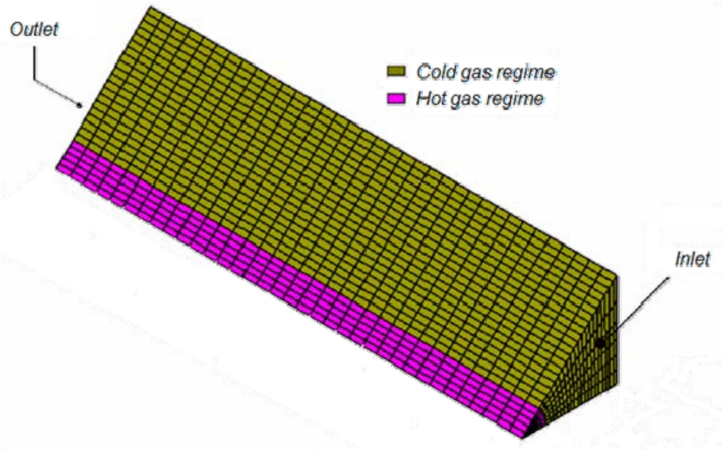

Figure 2.11: Three-dimensional CFD grid for the 1/8 portion of the BETS structure (Kgame, 2011).

The k_{er} was calculated by guessing a value for the fluid's molecular conductivity and solving for a steady-state solution. This was done iteratively in order to optimize the simulation's temperature profile to fit the normalized experimental temperature profile. Kgame (2011) used the square of the Pearson product moment correlation coefficient (RSQ) for his optimization. The RSQ compares two sets of data and tells us how closely the shape of the comparison compares to unity.

By using RSQ as the only parameter for the calculation of k_{er}, one runs the risk of a potentially inaccurate solution since the correlation coefficient does not take the residuals between the data points into account. Therefore it would be recommended to combine the RSQ parameter with a residual parameter i.e. root mean square deviation (RMSD).

Yao et al. (2002:236) studied the effect of thermal mixing by experimentally analyzing different mixer modules for the hot gas chamber of the 10 MW high temperature gas-cooled reactor test module (HTR-10). In his study he defined a dimensionless thermal mixing degree (TMD) which is a unique criterion for characterising a temperature mixing process. He applied the physical meaning of a dimensionless temperature difference to describe the degree of mixing efficiency between a hot and cold gas:

$$TMD = 1 - \frac{\Delta T_{out}}{\Delta T_{in}} \tag{2.12}$$

Where ΔT_{in} and ΔT_{out} are the differences between the minimum and maximum temperatures at the inlet and outlet sections. This means that if 100% efficient mixing took place, the TMD will have a value of one.

Yao *et al.* (2002:236) also defined a more elaborate mixing degree called the dimensionless thermal homogenisation mixing degree (HMD). This was in an attempt to capture the total effect of the momentum and energy exchange in the thermal mixing process. When the results of the two models were compared it was decided that on the basis of similarity, the more conservative TMD models are directly applicable to the reactor conditions.

2.6.2. Tortuosity

Tortuosity is a geometrical parameter that can be used to characterize the packing structure in fixed beds (Lanfrey *et al.*, 2010:1891). Kim and Chen (2006:131) defined tortuosity as the ratio of the average incremental length to the straight length a solute should travel through a porous medium.

Lanfrey *et al.* (2010) developed a theoretical tortuosity model for randomly packed beds. They found that tortuosity is proportional to the packing structure factor, which is explicitly defined by voidage and particle sphericity. They considered the bulk region of an isentropic fixed bed, with randomly packed particles and constant porosity. Lanfrey *et al.* (2010:1892), derived a model for tortuosity by using particle sphericity and bed porosity, as defined in equation (2.13).

$$T = k_p \left(3\frac{\sqrt{\pi}}{4} \right)^{4/3} \frac{(1-\varepsilon)^{4/3}}{\varepsilon\phi^2} \tag{2.13}$$

where k_p is a proportionality constant and ϕ is the particles shape factor which will be equal to 1 for a sphere.

To close the model for the parameter k_p an appropriate constant for scaling the tortuosity model is needed. Lanfrey *et al.* (2010:1893) considered an SC structure and assumed that the value of k_p is generally valid to obtain an average flow length, which was used to derive a new equation (2.14) for tortuosity:

$$T = 1.23\frac{(1-\varepsilon)^{4/3}}{\varepsilon\phi^2} \tag{2.14}$$

Since Lanfrey *et al.*'s (2010:1893) k_p parameter was scaled for an SC unit cell, it is most likely to over-predict the tortuosity for denser packings. Therefore it would be more accurate to expand the proportionality constant for different types of packings.

Kim and Chen (2006:129) investigated the diffusive tortuosity through different structures using a Pearsonian random walk simulation of solute tracers. Their simulation results were given in the form of a tortuosity factor but can be related to pure tortuosity as follows:

$$\zeta = \xi^2 \tag{2.15}$$

$$\lambda = \frac{1}{\zeta} \tag{2.16}$$

where ζ is the tortuosity factor, ξ is pure tortuosity and λ is a dimensionless diffusion coefficient.

Kim and Chen (2006:137) concluded that FCC and SC structures with periodic voids restrained the tracer solutes for much longer in the local voids than structures such as BCC, and consequently their diffusion path is longer as shown in Figure 2.12.

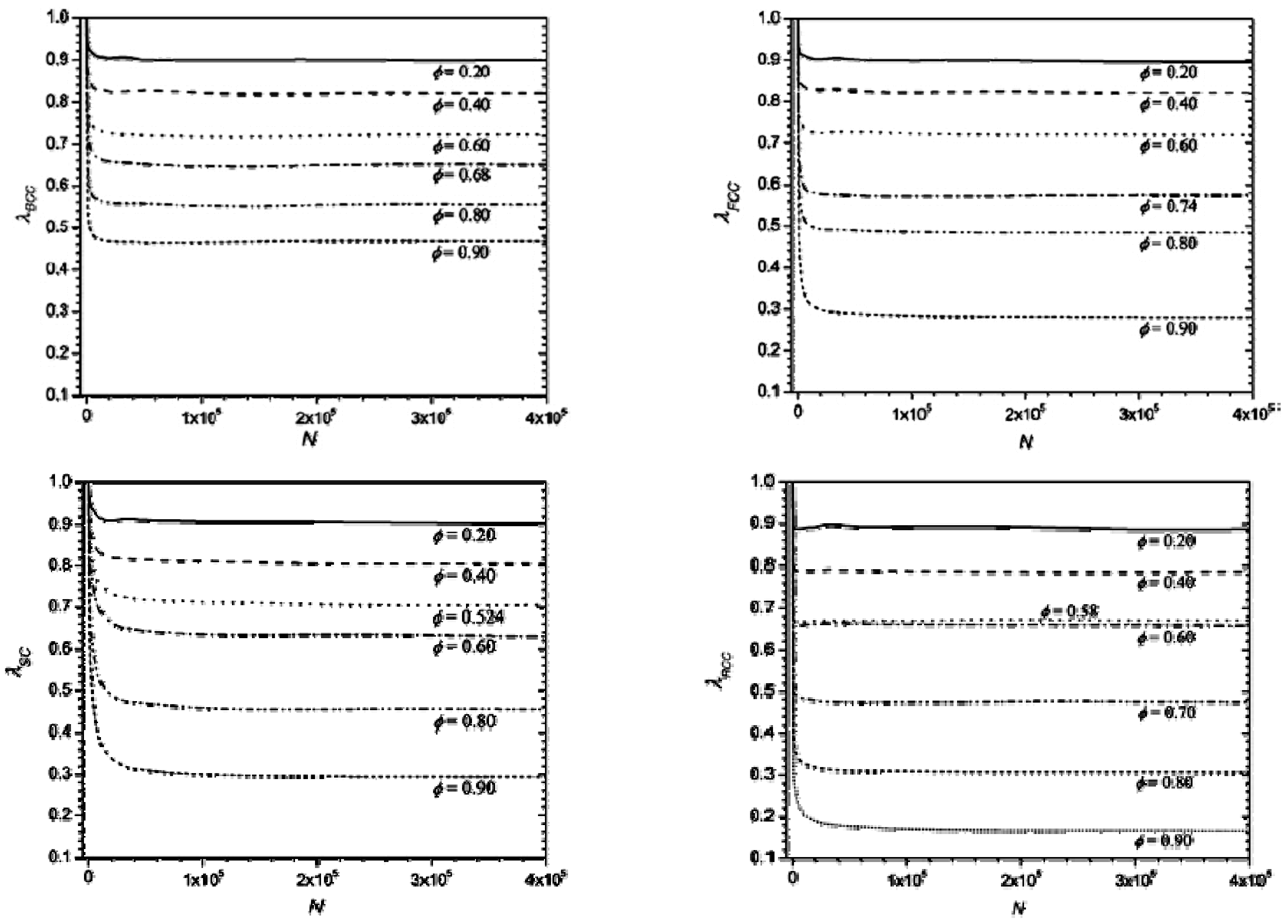

***Figure 2.12:* Dimensionless diffusion coefficient (λ) for different void fractions (ϕ) as a function of time step N for (a) BCC, (b) FCC, (c) SC and (d) random packing (Kim & Chen, 2006:134).**

The tortuosity for the different packed beds can be calculated by using equations (2.15) and (2.16) and the dimensionless diffusion coefficient from Kim and Chen's (2006:135) results. Table 2.3 shows the porosity and tortuosity for the packed beds used in Kim and Chen's (2006) study.

***Table 2.3:* Tortuosity results for different packing structures (Kim & Chen, 2006).**

Crystal structure	***Porosity***	***Tortuosity***
FCC	0.2595	1.32
BCC	0.32	1.24
Random	0.42	1.23
SC	0.476	1.19

The results show that tortuosity is dependent on the porosity of the packed bed since the tortuosity values increase with a decrease in porosity. This is expected since the porosity of a packed bed is proportional to the volume available for flow paths.

Table 2.4 compares the tortuosity results of Kim and Chen (2006) and Lanfrey *et al.* (2010). The deviation observed between the different tortuosity results also suggests (as previously stated) that the k parameter scaled for an SC unit cell over-predicts the tortuosity for denser FCC and BCC packings.

Table 2.4: Tortuosity comparison between the theoretical and simulation results.

Crystal structure	*Kim and Chen (2006)*	*Lanfrey et al. (2010)*	*Deviation [%]*
FCC	1.32	3.175	58.42
BCC	1.24	2.298	53.96
Random	1.23	1.417	13.20
SC	1.19	1.092	8.97

2.7. EXPLICIT PACKED BED SIMULATIONS

2.7.1. Turbulence modelling

Turbulence is a natural phenomenon that occurs when high velocity gradients are present in fluids. Turbulence typically causes disorder in the flow field and is characterized by irregular and highly diffusive flow, with three dimensional eddy fluctuations (CD-ADAPCO, 2010). These random fluctuations can be successfully modelled by time-averaging the flow variables to separate the fluctuations from the mean quantities (Chung, 2002:679). This averaging of flow variables deduces new unknown variables which have to be accounted for by adding additional equations to the governing equations. This process is known as turbulence modelling and enables us to model the effects of large and small scale eddies. This is done to avoid the mesh refinement that is necessary for direct numerical simulations.

2.7.1.1. Reynolds-average Navier-Stokes (RANS)

The physical basis of turbulent fluctuations can be examined by considering a two-dimensional control volume:

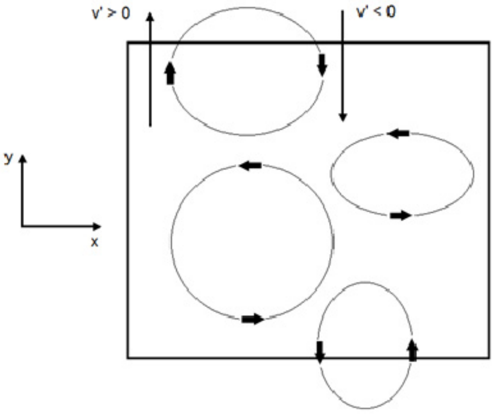

__Figure 2.13: Control volume for two-dimensional shear flow.__

In the control volume (Figure 2.13), the mean velocity is in the y-direction and the shear flow parallel to the x-axis. Strong mixing is created by the eddy motion as fluid is transported across the boundaries. These recirculating fluid motions transport fluid parcels which will carry momentum and energy in and out of the control volume (Versteeg & Malalasekera, 2007). The fluid layers will experience additional turbulent shear stresses due to momentum exchange. These shear stresses are caused by the net convective transport of momentum due to eddies, which cause slower moving layers to be accelerated and faster moving fluid layers to decelerate. The additional shear stresses are also known as Reynolds stresses.

If we consider the time-averaged Navier-Stokes and instantaneous continuity equations with the velocity vector $\mathbf{u}$(*u,v,w*) that uses a Cartesian co-ordinate system for the x, y and z components, it can be shown that:

$$div(\mathbf{u}) = 0 \tag{2.17}$$

$$\frac{\partial u}{\partial t} + div(u\mathbf{u}) = -\frac{1}{\rho}\frac{\partial p}{\partial x} + \nu div(grad(u)) \tag{2.18}$$

$$\frac{\partial v}{\partial t} + div(v\mathbf{u}) = -\frac{1}{\rho}\frac{\partial p}{\partial y} + \nu div(grad(v)) \tag{2.19}$$

$$\frac{\partial w}{\partial t} + div(w\mathbf{u}) = -\frac{1}{\rho}\frac{\partial p}{\partial z} + \nu div(grad(w)) \tag{2.20}$$

where ρ and ν is the fluid density and kinematic viscosity and p the fluid pressure.

Every turbulent flow is governed by the above set of equations (Versteeg & *Malalasekera*, 2007:64). In order to determine the effects of fluctuations on the mean flow, Reynolds decomposition have to be applied to the above equations and the flow variables replaced by the sum of the mean and fluctuating components. After some algebra the Reynolds-averaged Navier-Stokes equations for the U velocity component can be obtained as can be seen in equation (2.21) (Versteeg & *Malalasekera*, 2007:64):

$$\frac{\partial U}{\partial t} + div(U\mathbf{U}) = -\frac{1}{\rho}\frac{\partial P}{\partial x} + \nu div(grad(U)) + \frac{1}{\rho}\left[\frac{\partial(-\rho\overline{u'^2})}{\partial x} + \frac{\partial(-\rho\overline{u'v'})}{\partial y} + \frac{\partial(-\rho\overline{u'w'})}{\partial z}\right] \tag{2.21}$$

where the variables in capital letters represent a mean quantity and the letters with an accent represent the time averaged fluctuating components. The same can be written for V & W velocities.

From equation (2.21) it is evident that three additional stresses are present. The stresses are called Reynolds stresses. The first term is a normal stress while the last two terms are shear stresses.

2.7.1.2. Standard κ-ε model

A turbulence model needs transport equations to be able to monitor change and transfer turbulent quantities. The standard κ-ε model uses two transport equations, one for viscous dissipation (ε) and one for turbulent kinetic energy (κ). Launder and Spalding (1974) based this model on the change of the turbulent quantities due to viscous dissipation and turbulent kinetic energy. Large scale turbulence is represented by both κ and ε in a length scale ℓ (Versteeg & *Malalasekera*, 2007:75).

$$\ell = \frac{\kappa^{3/2}}{\varepsilon} \tag{2.22}$$

In equation (2.22) the large eddy scale ℓ is defined by 'n small eddy variable ε. This can be justified when the flow does not change rapidly, because then the rate at which small dissipating eddies transfer energy across the energy continuum is matched by the rate at which large eddies extract energy from the mean flow (Versteeg & *Malalasekera*, 2007:75).

The transport equations for ε and κ in the standard model are given as follows:

$$\mu_t = \rho C_\mu \frac{\kappa^2}{\varepsilon} \tag{2.23}$$

$$\frac{\partial(\rho\kappa)}{\partial t} + div(\rho\kappa\mathbf{U}) = div\left[\frac{\mu_t}{\sigma_\kappa} grad(\kappa)\right] + 2\mu_t S_{ij}.S_{ij} - \rho\varepsilon \tag{2.24}$$

$$\frac{\partial(\rho\varepsilon)}{\partial t} + div(\rho\varepsilon\mathbf{U}) = div\left[\left(\frac{\mu_t}{\sigma_\varepsilon} + \mu\right) grad(\varepsilon)\right] + C_{1\varepsilon}\frac{\varepsilon}{\kappa} 2\mu_t S_{ij} \cdot S_{ij} - C_{2\varepsilon}\rho\frac{\varepsilon^2}{\kappa} \tag{2.25}$$

where μ_t is the dimensionless eddy viscosity with C_μ a dimensionless constant, S_{ij} is the rate of deformation in tensor form, C_ε and σ_ε are constants that are obtained from experimental data (Chung, 2002:680).

To best way to understand the mechanics of the two transport equations (2.24) and (2.25), is to put them into words (Versteeg & *Malalasekera*, 2007:75):

Table 2.5: The meaning of the terms in κ and ε transport equation.

Rate of change of ε or κ	+	Convective transport of ε or κ	=	Transport of ε or κ by diffusion	+	Rate of production of ε or κ	-	Rate of destruction of ε or κ

The Reynolds stresses are computed by using the Boussinesq relationship (Boussinesq, 1877) as cited by Versteeg & *Malalasekera* (2007:67):

$$\tau_{ij} = 2\mu_t S_{ij} - \frac{2}{3}\rho\kappa\delta_{ij} \tag{2.26}$$

where δ_{ij} is the Kronecker delta ($\delta_{ij} = 1$ if $i = j$ and $\delta_{ij} = 0$ if $i \neq j$).

The κ-ε model provides a good compromise between robustness, computational cost and accuracy. This turbulence model is generally well suited to industrial-type applications because it is very well established and widely validated. The κ-ε model is most frequently used with low-speed incompressible flows and isotropic turbulence (Chung, 2002:680). The disadvantage of this model is that it performs poorly in cases with unconfined and curved boundary flow that has large strain stresses, rotating flow and flow driven by normal Reynolds stresses (Versteeg & *Malalasekera*, 2007:80).

2.7.1.3. Realizable κ-ε model

Another successful development in the κ-ε model is the realizable model, which was developed by Shih *et al*. (1994:227). Shih *et al* (1994:228) made the assumption that the generation and destruction terms in the original dissipation rate equation are proportional to the production and dissipation of turbulent kinetic energy per large eddy turnover time, κ / ε.

Shih *et al.* (1994:231) then modified equation (2.25) to be independent of Reynolds stresses making it more robust, especially when using poor initial conditions. The Realizable κ-ε model's dissipation rate can be defined as:

$$\frac{\delta\varepsilon}{\delta t} + \varepsilon_i v_i = v\varepsilon_{ii} - (\nu' v'_i)_i - C_{1\varepsilon} S_{ij}\varepsilon - C_{2\varepsilon}\frac{\varepsilon^2}{\kappa + \sqrt{\nu\varepsilon}} \tag{2.27}$$

where ν' and v' are the time averaged fluctuation of the viscous dissipation rate and velocity and v the velocity. The subscripts t, i and j are the derivatives of the variables.

Shih *et al.* (1994:231) also developed a new eddy viscosity formulation which is defined as:

$$\mu_T = C_\mu \frac{k^2}{\varepsilon} \tag{2.28}$$

$$C_\mu = \frac{1}{A_0 + A_s U^* \frac{\kappa}{\varepsilon}} \tag{2.29}$$

$$A_s = \sqrt{6}\cos\left(\frac{1}{3}\text{arc }\cos\left(\sqrt{6}\frac{S_{ij}S_{jk}S_{ki}}{\sqrt{S_{ij}S_{ij}}}\right)\right) \tag{2.30}$$

where U^* is the dimensionless velocity and A_0 a constant.

In the new eddy viscosity formulation, the variable C_μ is no longer a constant as in the standard model, thus ensuring realizability and containment of the effects of mean rotation on turbulence stresses (Shih *et al.*, 1994:238).

The new Realizable κ-ε model performed better in almost all the tests conducted and enhanced stability in turbulent flow computations, especially with the use of second order closure schemes (Shih *et al.*, 1994:238).

2.7.1.4. Two-layer approach

The two-layer approach was originally developed by Rodi (1991), and allows the κ-ε model to be applied in the viscous sub-layer by separating the computation into two layers. Wall functions are applied to the first layer near the wall for turbulent viscosity μ_T and the turbulent dissipation rate ε. The specified value of ε is blended with the results obtained far from the wall by solving the transport equation, while the turbulent kinetic energy is solved for the entire flow field.

Although the values of ε and μ_T are explicitly specified, the method is no less empirical than the damping function approach and is more often than not, better or just as good (CD-ADAPCO, 2010). The two-layer formulation is an alternative to the low Reynolds number approach and will thus work with either low Reynolds number type of meshes with the dimensionless wall distance $y^+ \approx 1$ or with wall-function type meshes where $y^+ \geq 30$.

2.7.1.5. Standard κ-ω model

The κ-ω model is an alternative to the κ-ε model and is also a two-equation model. The two transport equations are solved for the turbulent kinetic energy κ and turbulence vorticity or frequency, $\omega = \varepsilon / \kappa$.

The original idea of the κ-ε model was that the turbulence relate to vorticity (ω). If this variable is used, the Reynolds stresses will remain the same as in equation (2.26), the length scale will become $\ell = \rho\kappa / \omega$ and the eddy viscosity (Chung, 2002:688):

$$\mu_T = \rho\frac{\kappa}{\omega} \tag{2.31}$$

The transport equations as proposed by Wilcox (1988) may be written as:

$$\frac{\partial(\rho\kappa)}{\partial t} + div(\rho\kappa\mathbf{U}) = div\left[\left(\frac{\mu_t}{\sigma_\kappa} + \nu\right)grad(\kappa)\right] + P_\kappa - \beta^*\rho\kappa\omega \tag{2.32}$$

$$\frac{\partial(\rho\omega)}{\partial t} + div(\rho\omega\mathbf{U}) = div\left[\left(\frac{\mu_t}{\sigma_\varepsilon} + \mu\right)grad(\omega)\right] + \gamma_1\left(2\rho S_{ij}.S_{ij} - \frac{2}{3}\rho\omega\frac{\partial U_i}{\partial x_i}\delta_{ij}\right) - \beta\rho\omega^2 \tag{2.33}$$

where β is a closure constant (Chung, 2002:679).

The mechanics of the two transport equations (2.32) and (2.33) is the same as shown in Table 2.5 if ω replaces ε.

The advantage of the κ-ω model over the κ-ε model is the improved performance for boundary layer calculations under complex pressure gradients. The κ-ε model may be applied throughout the boundary layer without modification or computation of wall distance.

The biggest disadvantage of this turbulence model is its sensitivity to the values of ω in the boundary layer computations in free stream flow. This causes extreme sensitivity to the inlet boundary conditions (CD-ADAPCO, 2010). This type of problem does not occur in the κ-ε model.

2.7.1.6. SST (shear-stress transport) κ-ω model

The sensitivity of the standard κ-ω model to free-stream/inlet conditions was addressed by Menter (1994) who transformed the ε transport equation in the standard κ-ε model into the ω transport equation by the means of variable substitution. This adapted the κ-ω model to give identical results to the κ-ε model (CD-ADAPCO, 2010). This new equation is thus based on the κ-ω model, but adds a non-conservative cross-diffusion term that includes the dot product $\Delta\kappa \cdot \Delta\omega$. Menter (1994) recommended that a blending function approach be used to effectively modify the κ-ω model in the far-field by using a cross-diffusion term and using the unmodified κ-ω model in the near-wall region. The basic transport equation for ω is defined as follows:

$$\begin{aligned}\frac{\partial(\rho\omega)}{\partial t} + div(\rho\omega\mathbf{U}) = div\left[\left(\frac{\mu_t}{\sigma_\varepsilon}+\mu\right)grad(\omega)\right] + \gamma_1\left(2\rho S_{ij}.S_{ij} - \frac{2}{3}\rho\omega\frac{\partial U_i}{\partial x_i}\delta_{ij}\right) \\ -\beta_1\rho\omega^2 + 2\frac{\rho}{\sigma_\omega\omega}\frac{\partial\kappa}{\partial x_k}\frac{\partial\omega}{\partial x_k}\end{aligned} \qquad (2.34)$$

where the extra source term on the right-hand side of the equation is known as the cross-diffusion term, which arises during the transformation of the diffusion term in the ε-equation.

To understand the mechanics of the SST transport equation (2.34), it is best to put into words:

Table 2.6: The meaning of the terms in the SST κ-ω transport equation.

Rate of change of ω	+	Convective transport of ω	=	Transport of ω by diffusion	+	Rate of production of ω	-	Rate of destruction of ω	+	The rate of cross-diffusion

2.7.1.7. Reynolds stress equation model (RSM)

In the κ-ε model the Reynolds stresses are poorly represented by equation (2.26). This causes the κ-ε model to inadequately predict flows with large centrifugal forces and complex strain fields (Versteeg & *Malalasekera*, 2007:80). The Reynolds stress equation model (RSM) on the other hand uses the exact Reynolds stress transport equation that accounts for the directional effect of the Reynolds stress field. The kinematic Reynolds stress is defined by (Versteeg & *Malalasekera*, 2007:81):

$$\tau_{ij} = \frac{-\tau_{ij}}{\rho} = \mu_i^{'} \mu_j^{'} \tag{2.35}$$

The exact Reynolds stress transport equation then takes on the following form:

$$\frac{\partial \tau_{ij}}{\partial t} + C_{ij} = P_{ij} + D_{ij} - \varepsilon_{ij} + \Pi_{ij} + \Omega_{ij} \tag{2.36}$$

The meaning of each term in equation (2.36):

Table 2.7: The meaning of the exact Reynolds stress transport equation (Versteeg & Malalasekera, 2007:81).

Rate of change of τ_{ij}	+	Transport of τ_{ij} by convection	=	Rate of production of τ_{ij}	+	Transport of τ_{ij} by diffusion	-	Rate of dissipation of τ_{ij}	+	Transport of τ_{ij} due to fluctuating pressure	+	Transport of τ_{ij} due to rotation

The terms in equation (2.36) are partial differential equations that transport each of the six Reynolds stresses. In the Reynolds stress transport equations the production (P_{ij}), convection (C_{ij}) and rotation terms (Ω_{ij}) may be modelled in their exact form (Versteeg & *Malalasekera*, 2007:81). The dissipation rate (ε_{ij}) in equation (2.36) is applied by assuming isotropy of the small dissipative eddies and the normal Reynolds stresses prescribed to be affected in equal measure. The most important but equally difficult to model, is the pressure-strain term (Π_{ij}) in equation (2.36). The function of this term is to decrease anisotropy of the Reynolds stresses in the fluid region and to increase anisotropy of normal Reynolds stresses in the near-wall regions. The diffusion D_{ij} is modelled by assuming that the gradients of the Reynolds stresses are proportional to the rate of transport of Reynolds stresses due to diffusion (Versteeg & *Malalasekera*, 2007:81):

$$D_{ij} = div\left(\frac{v_t}{\sigma_\kappa} grad(R_{ij})\right) \tag{2.37}$$

where v_t is equal to the Realizable κ-ε eddy viscosity in equation (2.28).

Although the RSM is the simplest model able to describe all the mean flow properties and Reynolds stresses, it is still a very complex turbulence model. One of the major drawbacks of the RSM is that it can sporadically experience convergence problems due to numerical coupling of the turbulence stress field and the mean velocity. Once consensus on the numerical solution strategy is reached and as computing resources increases, this type of turbulence model will certainly be widely used in the industry (Versteeg & *Malalasekera*, 2007:84).

2.7.1.8. Spalart-Allmaras turbulence model

In the Spalart-Allmaras turbulence model the turbulence viscosity is solved by means of a single transport equation (Spalart & Allmaras, 1992:439) which is in contrast to previous one-equation models that solved the transport for turbulent kinetic energy. The Spalart-Allmaras transport equation is defined as follows (Versteeg & *Malalasekera*, 2007:90):

$$\frac{\partial(\rho\tilde{v})}{\partial t} + div(\rho\tilde{v}\boldsymbol{U}) = \frac{1}{\sigma_v} div\left[(\mu + \rho\tilde{v}) grad(\tilde{v}) + C_{b2}\rho \frac{\partial\tilde{v}}{\partial x_k}\frac{\partial\tilde{v}}{\partial x_k}\right] + C_{b1}\rho\tilde{v}\tilde{\Omega} - C_{w1}\rho\left(\frac{\tilde{v}}{\kappa y}\right)^2 f_w \tag{2.38}$$

where $\tilde{v}$ is the kinematic eddy viscosity, f_w is the wall damping function and the different C variables are empirical constant.

The physical meaning of each of the terms is given in Table 2.8:

Table 2.8: The meaning of the Spalart-Allmaras transport equation, (Versteeg & Malalasekera, 2007:81).

Rate of change of viscosity parameter $\tilde{v}$	+	Transport of $\tilde{v}$ by convection	=	Transport of $\tilde{v}$ by turbulent diffusion	+	Rate of production of $\tilde{v}$	-	Rate of dissipation of $\tilde{v}$

This model was developed for the aerospace industry with the intention of solving external flow with an unstructured mesh. The model's constants were fitted, derived and adjusted for external aerodynamic flows with adverse pressure gradients. Moreover, it is expected to deliver the best results for attached boundary layers and flow with calm separation such as the flow past a fuselage (CD-ADAPCO, 2010). Wilcox (1998) modified this model by adding free-shear flow to the diffusion rate. These modifications obtained reasonable results for mixing layers and radial jet flow but did not seem to improve the model's performance for complex recirculation and natural convection problems.

Thus Spalart-Allmaras models for RANS equations are not suited to accommodate flows that are dominated by free-shear layers, flows where complex recirculation occurs (particularly with heat transfer) or natural convection (CD-ADAPCO, 2010).

2.7.1.9. Large eddy simulation

Great advancements in turbulence modelling have been made in recent years, but despite all the studies it remains difficult to model geometrically and physically complex flow fields. This can be attributed to the difference between behaviour in small and large eddies. Large eddies extract energy from the mean flow and are more anisotropic while small eddies have a universal behaviour and are nearly isotropic.

An alternative to RANS modelling is large eddy simulations (LES) which use more refined meshes than the RANS systems (CD-ADAPCO, 2010).

Large eddy simulation (LES) is an essentially transient technique and is resolved by modelling small scale eddies and calculating large eddies, thus placing the performance and requirements of LES in-between the direct numerical simulations (DNS) and Reynolds-average Navier-Stokes (RANS). The modelling of the small scale eddies in LES is simpler than in RANS because it is coupled with a dissipation range of isotropic turbulence (Chung, 2002:696).

In LES the equations are obtained by means of filtering rather than averaging as in RANS equations. These filtered equations appear to be identical to the RANS equations except that the turbulent stress tensor τ_{ij} represents the sub-grid scale stresses (CD-ADAPCO, 2010). The Boussinesq approximation is used for the turbulent stress tensor and is defined in equation (2.26).

Smagorinsky (1963) proposed that the Boussinesq hypothesis will be able to accurately model the effects of the unresolved small eddies since they are almost isotropic. In the sub-grid scale (SGS) model of Smagorinsky (1963), the local SGS stresses τ_{ij} are taken to be proportional to the rate of strain of the resolved flow $\overline{S}_{ij}$ (Versteeg & *Malalasekera*, 2007:102):

$$\overline{S}_{ij} = \frac{1}{2}\left(\frac{\partial \overline{u}_i}{\partial x_j} + \frac{\partial \overline{u}_j}{\partial x_i}\right) \tag{2.39}$$

$$R_{ij} = -2\mu_{SGS}\overline{S}_{ij} + \frac{1}{3}\tau_{ii}\delta_{ij} \tag{2.40}$$

The right-hand term in equation (2.40) performs the same task as the second term in the Boussinesq hypothesis in equation (2.26): it ensures energy conservation between the normal SGS stresses and the kinetic energy of the SGS eddies.

Versteeg & *Malalasekera* (2007:110) noted that the LES model is not widely validated but with increasing computing resources the advantages of the LES approach will become predominantly more clear to the community.

2.7.1.10. Wall functions

Because high velocity gradients are present in the near wall region, excessive mesh refinement is required to realistically model flow in this regions (Chung, 2002:688). An alternative to computationally expensive mesh refinement is to use wall functions.

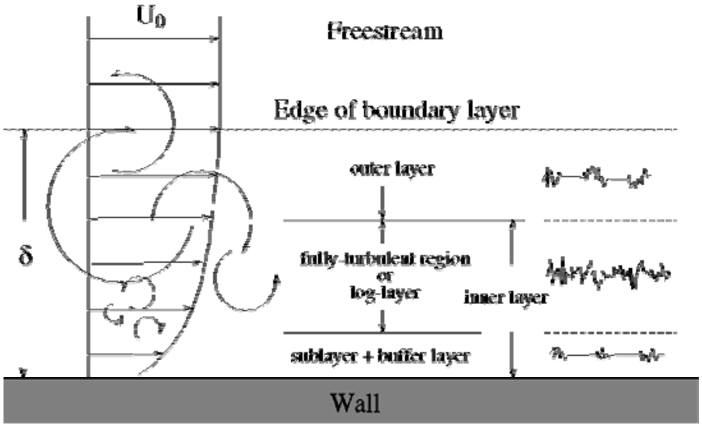

Figure 2.14: Structure of near-wall flow (Fluent User Service Centre, 2005).

By using wall functions, boundary conditions can be obtained through a set of mathematical models in order to satisfy the continuum equations. Wall functions used in wall treatment schemes use a set of assumptions for the distribution of scalar quantities when the viscous boundary layer is not resolved. Wall treatment can be applied throughout the viscous affected region depending on the near-wall mesh resolution in the inner layer (Figure 2.14). Wall treatment is necessary for κ-ε and

Reynolds stress models (RSM), since they are not valid in the near-wall region with high velocity gradients.

When using wall functions, the boundary conditions in the near-wall region for ε , κ and wall shear stress (τ_w), may be specified as (Chung, 2002):

$$\kappa = \frac{|\tau_w|}{\sqrt{c_\mu}} \tag{2.41}$$

$$\varepsilon = \frac{|\tau_w|}{a^\delta} \tag{2.42}$$

$$|\tau_w| = \frac{a|\nu^*|(c_\mu^{0.5}K)^{0.5}}{\ln(\varepsilon\delta^+)} \tag{2.43}$$

where K is the mean kinetic energy and a is a constant.

κ can be calculated iteratively at a non-dimensional distance δ^+ ≥ 12, $a = 0.419$, $\varepsilon = 9.793$ and

$$\delta^+ = \mathrm{Re}\,\delta(c_\mu^{0.5}K)^{0.5} \tag{2.44}$$

For $\delta < 12$, the laminar stress ($|\tau_w|$) and the viscosity ($|\nu^*|$) in the near-wall region is given by

$$|\tau_w| = \frac{|u_*|}{\mathrm{Re}\,\delta} \tag{2.45}$$

$$|\nu^*| = \mathrm{Re}\,\delta\frac{|\tau_w|}{|u_*|} \tag{2.46}$$

where u_* is the reference velocity derived from the turbulence model that is specified.

For wall-bound turbulent flow, the standard two-layer form of the law of the wall specifies that:

$$u^+ = \frac{1}{k}\ln y^+ + 5, \qquad \frac{\kappa}{u_*^2} = c_\mu^{-0.5}, \qquad \varepsilon = c_\mu^{0.5}\frac{\kappa^{\frac{3}{2}}}{\kappa y} \tag{2.47}$$

These conditions apply at the first grid point y from the wall if $y^+ \equiv yu_*/v \geq 11.6$ with $u^+ = \bar{u}/u_*$, but if $y^+ < 11.6$, then $\bar{u}$, κ and ε are interpolated to the wall values.

2.7.2. Contact point modelling

Creating computational meshes around contact points of sharp angled geometries can cause highly skewed fluid elements, meaning that some of the surfaces of the cells are much larger than other surfaces in the same cell (McLaughlin *et al.,* 2008).

These poor quality cells induce a skewness error that is caused by the convection term in the transport equation. The face value (*k)* between the cells P and N in Figure 2.15 is calculated along the line that connects the cell centres. Thus a skewness error is introduced when we assume *k'* represents the value at *k.* This error can be reduced by applying local grid refinement, as can be seen in Figure 2.15 (b), or by implementing an appropriate contact treatment that will reduce the need to represent the computational domain with sharp cells (Versteeg & *Malalasekera*, 2007).

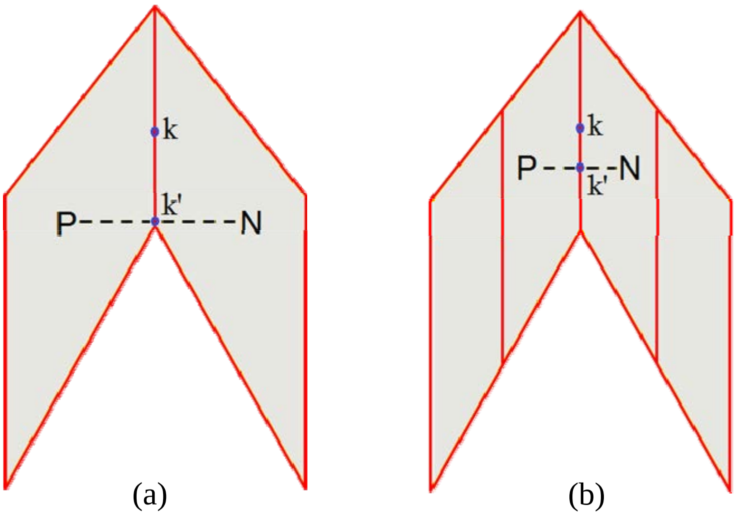

Figure 2.15: The error introduced by the convection term on highly skewed cells.

Logtenberg *et al.* (1999:2435), used contact points between their wall and sphere geometries, but had to manually manipulate the generated mesh around the contact points by adding additional circle lines to successfully solve the numerical model. This seemed to be the most realistic representation at the time, however Nijemeisland and Dixon (2001:236) discovered that using a common node at the contact point, caused the fluid elements in the region to become highly skewed. This did not seem to cause any concern for laminar solutions but when implementing a turbulent flow regime convergence could not be achieved. These highly skewed cells caused the flow velocity in the contact regions to increase dramatically which resulted in unrealistic solutions.

To avoid generating skew cells in the contact region, mesh refinement would have to be implemented. This is however not feasible since the mesh refinement needed to achieve this will dramatically increase the number of cells required to define the domain, as shown in Figure 2.16.

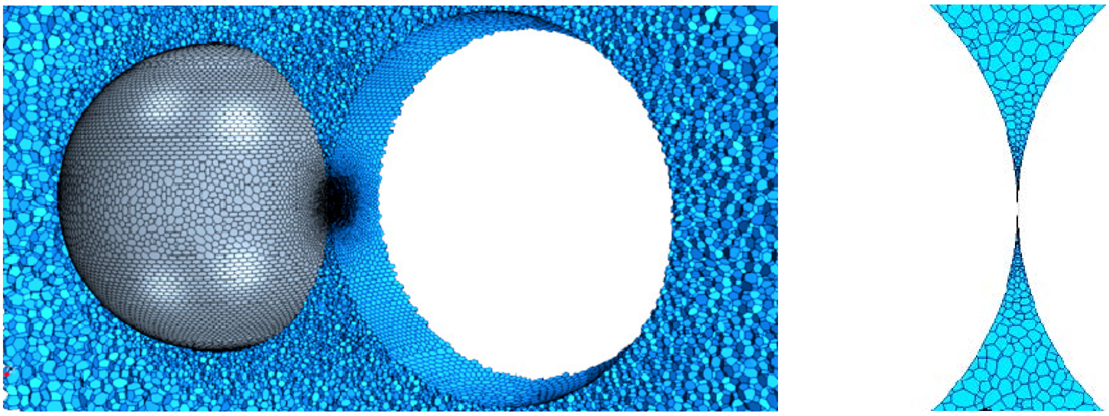

(a) 3D mesh representation ***(b) 2D mesh representation***

Figure 2.16: Mesh refinement in the contact area needed when using a contact point approach.

Nijemeisland and Dixon (2001:237) concluded that the only way to eliminate the skewed cells in the contact regions was by carefully designing a gap between the different entities. Their results showed that for a turbulence model to be solved, a maximum size of the original sphere should be reduced to 99.5% to create a gap large enough to obtain a sufficient quality mesh. Using this assumption of a gap between spheres would most definitely model the conduction heat transfer unrealistically since stagnant fluid areas exist around the contact point between spheres.

A different approach to contact treatment would be to remove the stagnant volumes from the fluid domain by connecting the spheres with a cylinder. Removing a cylinder of coolant from the fluid region enables a higher mesh quality and conserves resources because mesh refinement at the contact points is not needed to represent the sharp angled geometry. This approach was followed by McLaughlin *et al.* (2008:3) and Reyneke (2009).

Reyneke (2009), studied the effect of the cylinder contact treatment on the flow field by varying the circumference of the cylinder and analysing the flow fields and pressure drops over two horizontal spheres. He concluded that a cylinder with a diameter of 10 mm will not significantly influence the flow field. The results of the study are summarised in Table 2.9 and in Figure 2.17.

Table 2.9: Two sphere (TS) tests conducted by Reyneke (2009).

Case	***Description***	***Sphere dia. d_p (mm)***	***Pitch p (mm)***	***Contact dia. d_{cont} (mm)***	***Faces and cells generated on spheres faces /cells***
TS-1	Area contact	60	59.989	1.149	33762/17874
TS-2	5 mm Area contact	60	59.989	5	30342/16158
TS-3	10 mm Area contact	60	59.989	10	25294/12889

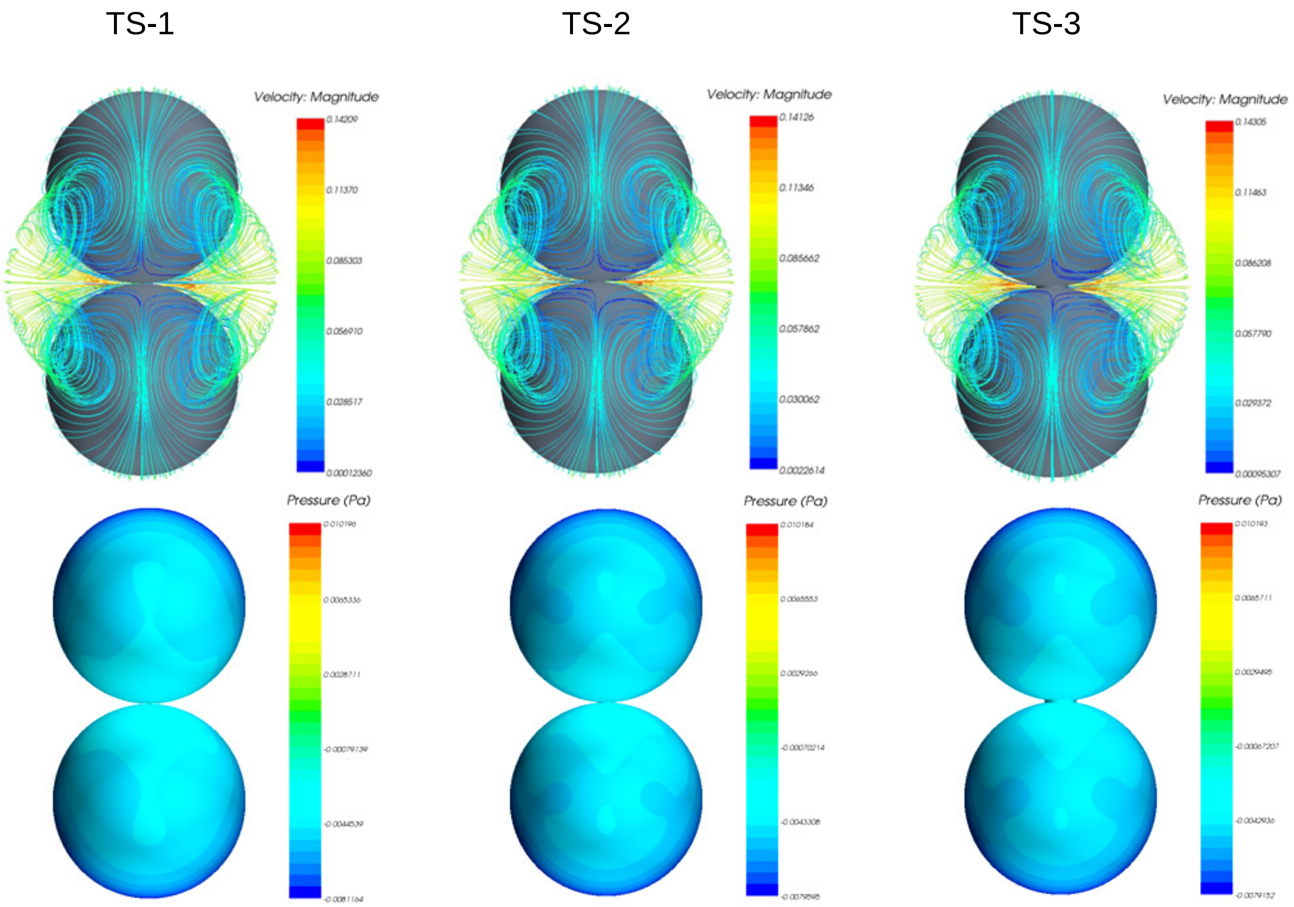

Figure 2.17: The TS results for the velocity distribution (above) and pressure distribution (below) (Reyneke, 2009).

Lee *et al.* (2007:2185) comprehensively studied different contact treatment techniques by conducting numerous simulations of two spheres (TS) in a flow stream to determine their effects on the local heat transfer and flow field. They used two horizontally aligned spheres that have the same diameter (60 mm) as that of the PBMR (pebble bed modular reactor) of 400 MWth. Four cases were simulated (summarised in Table 2.10) with TS-1 and TS-2 gap approximations and TS-3 and TS-4 pebble contacts.

Table 2.10: Description of test cases conducted by Lee et al. (2007:2185).

TS	***Description***	***Sphere Dia. d_p (mm)***	***Pitch p (mm)***	***Contact Dia. d_{cont} (mm)***	***Number of nodes and elements***
1	2 mm Gap	60	62	-	81,994/463,901
2	1 mm Gap	60	61	-	85,235/481339
3	Point Contact	60	60	0	141,318/805,772
4	Area Contact	60	59.967	2	141,320/805,604

Lee *et al.* (2007:2189) found that the different contact treatments significantly influence the flow regime around the spheres. Their results showed that the minimum pressure for TS-1 and TS-2 was at the point of maximum velocity which is in the centre between the two spheres while the minimum pressure for TS-3 and TS-4 was located at the outside parts of the two spheres because of the curvature and the blockage of the flow due to contact between the spheres. These results can be seen in Figure 2.18.

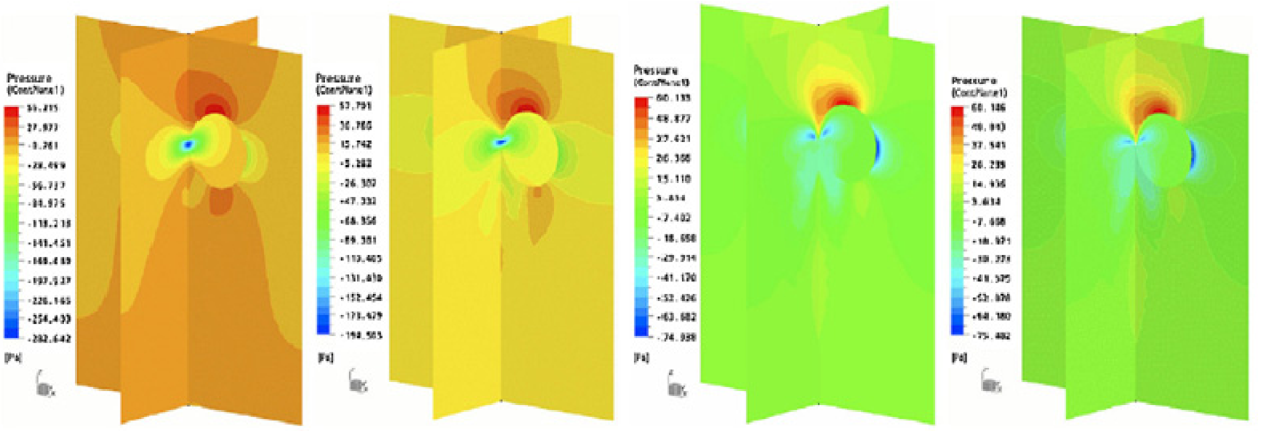

TS-1 TS-2 TS-3 TS-4

Figure 2.18: The results of the pressure distribution in the flow field conducted by Lee et al. (2007:2186).

Lee *et al.* (2007:2187) also noted large differences in the flow distribution between the different cases as can be seen in Figure 2.19 . Two detached flow currents (stream lines) are visible in both the contact cases, where as the gap approximation shows fused streamlines that tends to part with a smaller gap. Lee *et al.* (2007:2196) concluded that although the gap approximation between spheres has appealing advantages, it is evident that the simplification will generate inaccurate information of the flow field and should be avoided.

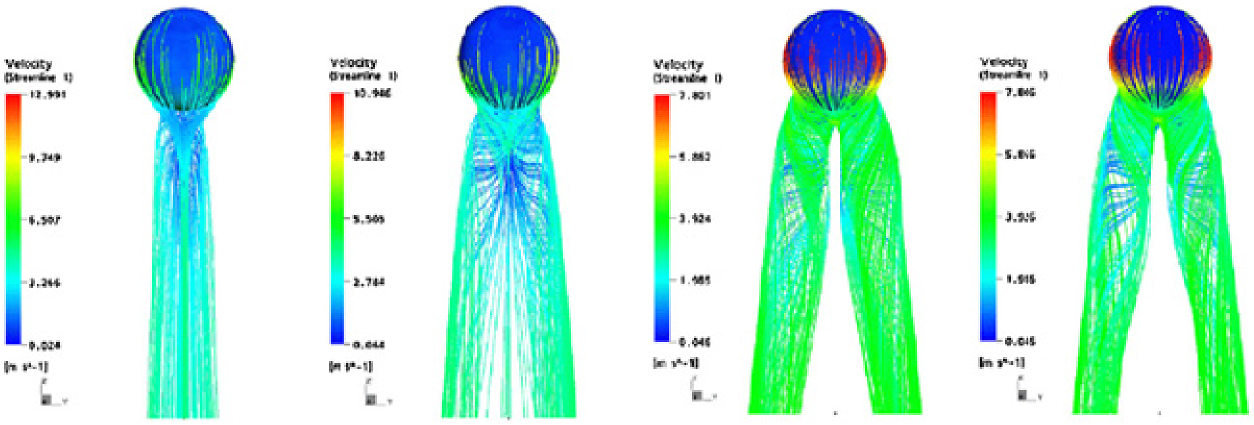

TS-1 TS-2 TS-3 TS-4

Figure 2.19: Streamlines between the different TS cases as conducted by Lee et al. (2007:2187).

Lee *et al.* (2007) only investigated a gap approximation between 2 mm and 1 mm, which is rather larger in terms of the minimum cell sizes traditionally used in these types of investigations, which leaves room for further investigation.

2.7.3. Previous mesh and turbulence approaches

Mesh generation is probably the most important part of any CFD setup, given that the volume mesh represents the mathematical description of the spaces and geometries in the flow domain, linking it directly to the accuracy of the solution. The density of the volume mesh not only has to be fine enough to satisfy the turbulence model that is used, it also has to adhere to the accuracy required to model the complexity of the flow in the domain.

Wu *et al*. (2010:1154) used a CFD code (FLUENT) to compare the advantages and shortcomings of explicit and implicit modelling. For their explicit approach they used 28 spheres with a diameter of 30 mm, arranged in a BCC structure with each sphere having its own heat source. Because they were modelling heat transfer and flow through the packed bed, it was thought necessary to use a fine mesh with over $2.01\text{x}10^6$ cells that consisted of structured and unstructured hexahedral and tetrahedral cells. They adopted the RSM and standard κ-ε model for their simulations (Wu *et al*., 2010:1153) with an inlet velocity of 0.648 m/s.

Reyneke (2009) used STAR-CCM+® (VERSION 6.02.011) to simulate flow over the bulk region of a randomly packed bed to validate his flow measurements. His bed consisted of 250 spheres that were discretised in a total of $4.56\text{x}10^6$ structured and unstructured cells. To achieve a reasonable fine mesh for the flow between the spheres, Reyneke (2009) specified maximum and minimum target pebble diameter-to-cell size (surface triangulation size) ratios of $d_p / d_c = 15$ and $d_p / d_c = 200$. Reyneke (2009) employed the Realizable κ-ε turbulence model throughout all of his explicit simulations with a particle Reynolds number of 438.

Reyneke (2009) based his mesh generation on the Wang-Kee In and Hassan (2008) combination of structured and unstructured mesh, where their structured cells consisted of 5 prism layers grown from the wall of the spheres, similar to the structured meshes of Calis *et al. (*2001:1716). Wang-Kee In and Hassan (2008:2) used unstructured meshes to locally refine the density of the cells at the contact points between the spheres. This was done to minimise the number of skewed cells in the contact area. They used unstructured polyhedral cells that had a target particle diameter-to-cell size ratio of $d_p / d_c = 20$ and a minimum of $d_p / d_c = 200$. The κ-ε, SST κ-ω and the Spalart-Allmaras turbulence models were employed to compare the results but no significant differences between the models were noted.

The research done by Calis *et al.* (2001) was one of the first attempts that explicitly modelled flow through a large packed bed of spheres. In their study they used 5 layers of structured prismatic cells adjacent to the sphere walls with unstructured tetrahedral cells following the prism layers into the fluid domain (Calis *et al.,* 2001:1716). The contact handling that was used assumed a gap between the spheres making it possible to generate high quality structured grids between the spheres. The resulting particle diameter-to-cell size used by Calis *et al.* (2001) corresponded to a ratio of $d_p / d_c = 12.7$. Calis *et al.,* (2001:1716) used the standard κ-ε and the RSM turbulence models to simulate single-phase flow through their packed beds with a commercial CFD code CFX for a particle Reynolds number ranging between $1 \times 10^{-2} < \mathrm{Re} > 5 \times 10^{4}$. The two turbulence models compared reasonably well, with the κ-ε model deviating 10% from the RSM's predicted pressure drop for the higher Reynolds numbers.

Guardo *et al.* (2005:1736) investigated the performance of the Spalart–Allmaras, κ-ε and the κ-ω turbulence models throughout the different turbulent flow regimes for Reynolds numbers between $130 < \mathrm{Re} > 912$. They concluded that the turbulence models lacked the ability to properly model the transition flow regime for low Reynolds numbers.

Tobis (2000:5364) studied the influence that different packed bed geometries have on the frictional resistance. In his study he numerically calculate the friction factors over six different types of beds. He used the same inlet velocity for all his simulations which related to a particle Reynolds number of 1800. Tobis (2000:5365) created unstructured tetrahedral meshes that had a particle diameter-to-cell size of $d_p / d_c = 19$ and used the $\kappa - \varepsilon$, RSM and Spalart-Allmaras turbulence models in his investigations. No significant differences between the turbulence models were noted.

The latest development in mesh type generation is the polyhedral mesh. It provides the most balanced solution for complex flow domains and is more efficient to generate and requires the same amount of surface preparation as a tetrahedral mesh (CD-ADAPCO, 2010). The biggest advantage of a polyhedral mesh over the tetrahedral mesh is that it generates five times less cells for the same surface mesh as can be seen in Figure 2.20.

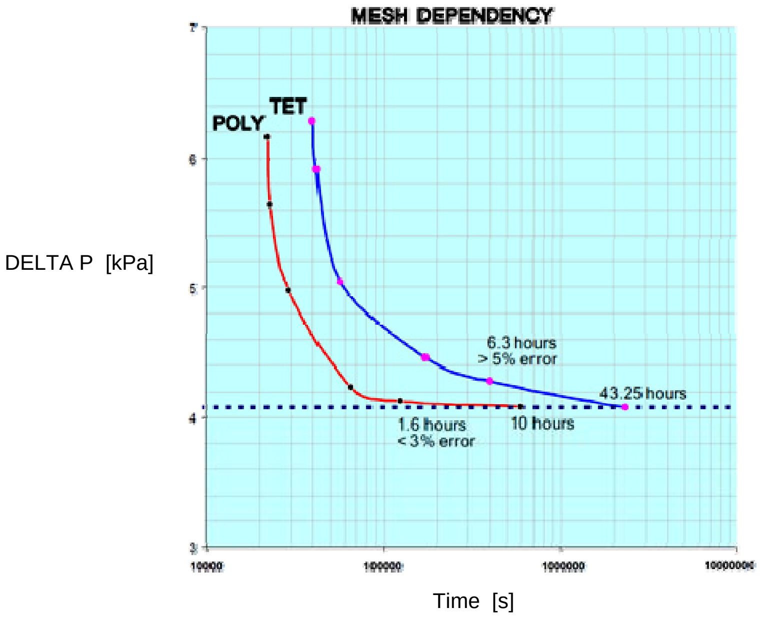

Figure 2.20: The comparison between the mesh efficiency of a polyhedral and tetrahedral mesh (Van Staden, 2009).

Creating a volume mesh is considered an art, and there is no set of rules that confines or focuses the implementation of a certain type of mesh. Only through the means of trial and error has experience led the development of a broad set of guidelines. One of the most important criteria in measuring the accuracy of the density of a mesh is by means of a mesh independency study. Unfortunately mesh independency studies are seldom shown in most CFD studies found in literature.

2.8. CONCLUSION

Van Antwerpen (2009) noted that although the different porosities in a randomly packed bed can be quantified by structured packings, the characterization of a porous structure using porosity on its own is inadequate. In order to expand our knowledge of the characterization of packed bed's, it is necessary to study the different flow phenomena inside structured and random packings. The first fundamental step towards a better understanding of the effect of a packed bed structure on flow is to study its mixing ability. This literature study identified tortuosity, TMD and the effective conductivity as important enhanced mixing parameters that will give valuable insight into the development of a generic geometrical description of a packed bed.

From the past literature it is evident that the broad set of guidelines for the simulation of packed beds can be further focussed and improved. It was noted that the velocity profile is dependent on the Reynolds number up to the point where the inertial forces are dominant. No recommendations were found from literature for the use of any specific turbulence model in the transitional flow regime.

Different contact handling (treatment) techniques were identified from literature. These techniques generally propose simplifications to solve numerous issues regarding skewed cells that form when the domain is meshed. It was noted that these simplifications would not be able to accurately simulate heat transfer through packed beds and that the computational resources required to model a packed bed without contact treatment is unrealistic.

It was also noted that the number of mesh generation and mesh independency studies from literature was somewhat limited, which is unfortunate.

Critical literature reviews are given throughout the literature study and will not necessarily be repeated in this conclusion.

3

MODELLING APPROACH

3.1. INTRODUCTION

This chapter investigates the numerical setup for simulating explicit packed beds. Important factors such as contact treatment, mesh density and turbulence modelling play a major role in the accuracy of the simulations. This chapter starts off by investigating different contact treatment techniques that can be used to improve the numerical representation of the sharp geometries in the contact regions between spheres. It is important to use the correct contact treatment for the type of simulation under investigation since the numerical representation of the contact region may influence the flow distribution around or downstream of the object (Lee *et al.,* 2007). The most suitable contact treatment was implemented in a mesh independency test that established the relationship between the mesh resolution and required accuracy when simulating flow through a packed bed of spheres. From the mesh independency test, the optimum mesh density was selected and implemented in a series of turbulence model tests that was used to determine the most suitable model for this study.

The CFD code that was used in this study to numerically model flow over packed beds, was STAR-CCM+® (VERSION 6.02.011).

. All of the meshing tools and solvers that were used are built into this one CFD code and no new numerical models or custom programming was added to aid any of the solutions or solvers.

3.2. CONTACT TREATMENT

Lee *et al.* (2007:2189) confirmed that the flow field downstream of spheres in contact are affected by the manner in which the contact points are modelled. Guardo *et al.* (2005: 1736) noted that pockets of stagnant flow exist between the contact points of the spheres. Thus when investigating flow through packed beds (with no heat transfer) it can be assumed that the flow in these pockets has a negligible influence on the flow field and may be removed (Reyneke, 2009). Lee *et al. (*2007) noted that when approximating the contact points with gaps, the resulting mesh was about half the size of the original mesh. Lee *et al.* (2007:2196) concluded that although the gap approximation between spheres has attractive advantages, it is apparent that the simplification will generate inaccurate information of the flow field and should be avoided.

The tests for this part of the study were conducted in two stages. The first stage focused on the development of a new contact treatment technique that is more realistic than the gap or cylinder techniques used by Lee *et al.* (2007) and Reyneke (2009), but does not compromise computing resources with elaborate mesh refinements. The second part of the tests compared the new contact treatment technique with some of the more established techniques.

3.2.1. Thin mesh contact treatment (TM tests)

STAR-CCM+$^{®}$ (VERSION 6.02.011) has a built in meshing tool that discretises the flow domain into a finite number of volumes. One of the meshes that STAR-CCM+$^{®}$ (VERSION 6.02.011) can generate is called a thin mesh. This thin meshing ability was developed to automatically generate prismatic cells in thin regions of a domain, which would generally be used between thin plate faces where heat transfer would take place, as shown in Figure 3.1.

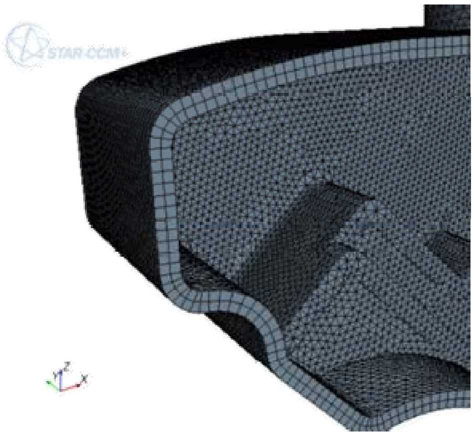

Figure 3.1: Thin mesher (CD-ADAPCO, 2010).

It was decided to implement the thin meshing capabilities of STAR-CCM+$^{®}$ (VERSION 6.02.011) together with a faster than normal cell growth rate, as a potential contact treatment technique. The numerical domain that was used for the TM tests consisted of a small volume, with two horizontally aligned spheres, as shown in Figure 3.2. The TM tests analysed the mesh density and skewness of the cells in this domain.

The sphere diameter (**d**) and the pitch (**P**) was 60 mm, thus assuming the worst case scenario of a point contact between the two spheres (sharing a single surface).

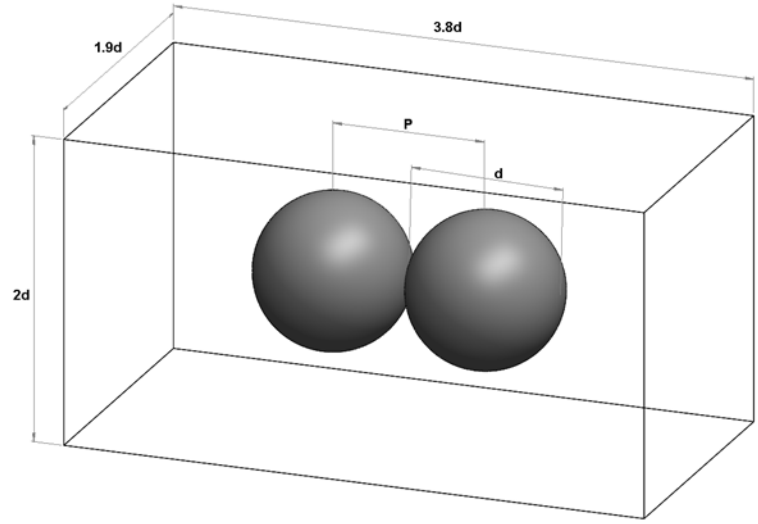

Figure 3.2: ***TM cases geometry.***

Mesh refinement and a very small minimum cell size is required to model contact points with a contact treatment and even more so without a contact treatment. This mesh refinement is necessary in the contact region to avoid creating a large number of skewed cells that may compromise the solution. Consequently the region with the most stagnant flow (contact region) has the most elaborate mesh density in the whole flow domain, as shown in Figure 3.3 (a) and Figure 2.16.

The thin meshing tool can automatically distinguish between thin and thick regions in a domain. This ability makes it very useful to restrict the mesh refinement to the contact regions, as shown in Figure 3.3 (b). The number of skewed cells that can be reduced by the thin mesher depends on the number of prism layers and the minimum cell size selected.

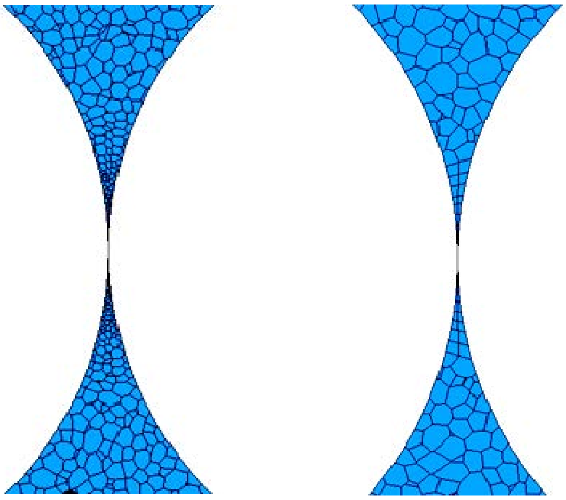

Figure 3.3: (a) Polyhedral mesh compared to (b) a prism mesh in contact region.

The setup of thin mesh contact treatment was examined by varying the minimum cell size and the number of prism layers between the contact points.

3.2.1.1. Mesh setup

The built-in mesh generator of STAR-CCM+$^{®}$ (VERSION 6.02.011) was used to create all the meshes in this study. This mesh generator is able to apply different minimum and target surface sizes for the boundaries and sphere surfaces. The boundaries in the domain consisted of the six planes (external boundaries) that surround the two spheres (internal boundaries). The target and minimum pebble diameter-to-cell size (surface triangulation size) ratios of $d_p / d_c = 15$ and $d_p / d_c = 30$ were specified for the external boundaries and a target ratio of $d_p / d_c = 28.57$ was chosen for the internal spherical boundaries. The minimum ratio for the internal boundaries was varied during the TM tests as can be seen in Table 3.1. A surface growth rate of 1.5 was specified rather than the default value of 1.3, since the only mesh refinement that occurs, is in the contact point regions were the velocity gradients are negligibly small. Unstructured polyhedral cells were grown from the internal and external boundaries with the exception of a few structured prism cells generated in the contact region. The number of prism layers between the contact points of the two spheres was also varied in order to determine the effect the layer concentration has on the mesh density and the number of skewed cells.

3.2.1.2. Results and discussion

A comparison of the results for the TM tests is shown in Table 3.1, where the delta cells column represents the difference in the number of cells created compared to the first TM test, where no prism layers were generated. The number of skew cells is measured in volume (mm^3), since the cell sizes change with a varying minimum surface size.

From the results it is evident that a decrease in the minimum surface size decreases the volume of skew cells but increases the total number of cells in the domain, while an increase in the number of prism layers seems to have the same effect.

Table 3.1: Geometrical variants for the TM cases.

Test	**Minimum surface size [mm]**	**Number of prism layers**									
		0		**2**		**3**		**4**		**6**	
		Skew cells [mm^3]	*Delta cells*	*Skew cells [mm^3]*	*Delta cells*	*Skew cells [mm^3]*	*Delta cells*	*Skew cells [mm^3]*	*Delta cells*	*Skew cells [mm^3]*	*Delta cells*
TM-1	1.5	0.56412	0	0.1428	21	0.1417	289	0.1978	284	0.1384	1045
TM-2	1	0.10443	200	0.09625	250	0.05839	691	0.03785	657	0.03741	1139
TM-3	0.75	0.04851	454	0.0107	185	0.0135	1456	0.01196	2420	0.0197	2362
TM-4	0.5	0.01110	1555	0.00377	1395	0.00675	1872	0.00488	3123	0.00378	3620
TM-5	0.35	0.00578	1513	0.00285	1937	0.00148	2883	0.00142	4196	0.00142	6372
TM-6	0.2	0.00066	5079	0.00022	3847	0.00021	5535	0.00018	8018	0.00019	11999

Van Antwerpen (2009) noted that for a random packed bed of spheres the average number of contact points per spheres is 5.62, which means that the number of cells required to model a single sphere in contact with its neighbouring spheres will dramatically increase from the results shown in Table 3.1.

Figure 3.4 compares the number of cells generated with the number of skewed cells formed for each of the prism layer cases. This indicates how efficiently an increase in the number of prism layers can reduce the number of skew cells without increasing the mesh size significantly. When constructing a linear trend line through the data points for each prism layer case, it is evident that two prism layers will deliver the best mesh efficiency, since it has the smallest number of cells-to-skew cell ratio for the whole range of meshing options.

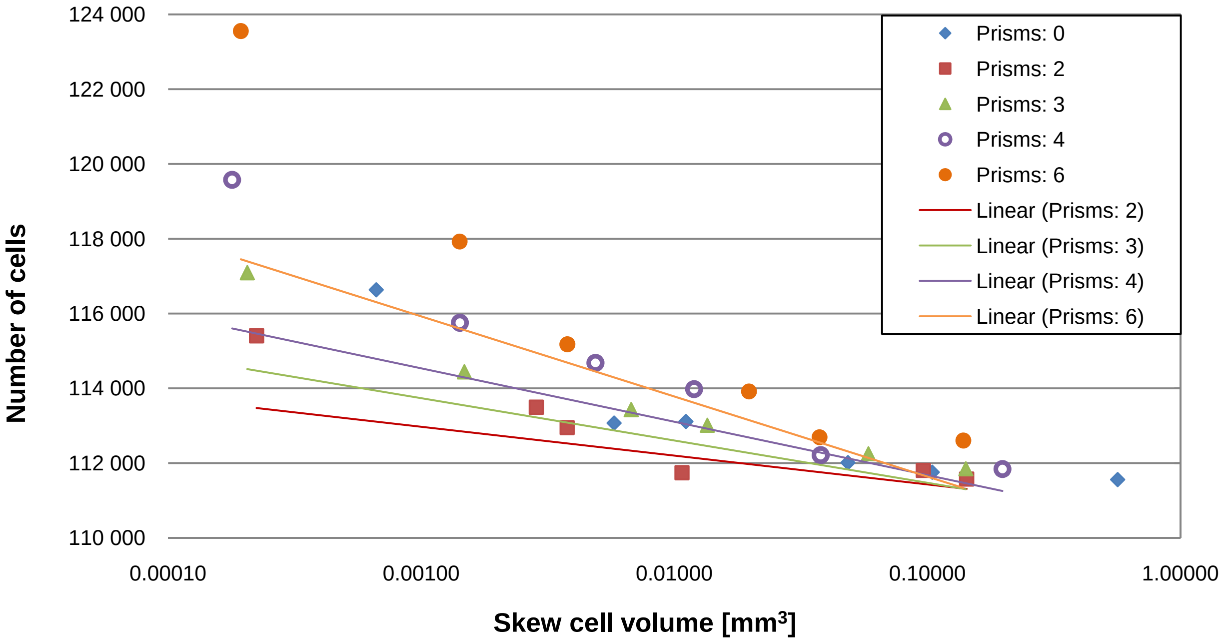

Figure 3.4: The volume of skew cells opposed to the size of the mesh generated.

It is also evident that the most balanced minimum surface size to use with two prism layers is 0.75 mm, since it does not compromise the mesh density and it is able to reduce the number of skew cells by 4.5 times compared to a normal polyhedral mesh. It was also noted that a normal polyhedral mesh would require 8.5 times more cells in the contact region to achieve the same volume of skew cells when compared to TM-3 with two prism layers. STAR-CCM+® (VERSION 6.02.011) has a built in cell quality remediation model that enable solutions to be obtained over bad cells, by modifying the gradients over these flagged cells.

The performance of this contact treatment will be evaluated in the next section of this chapter, which will give an indication of the ability of STAR-CCM+® (VERSION 6.02.011) to handle small numbers of skew cells.

3.2.2. The simulation of two spheres in contact (CT tests)

The intent of the CT simulations were to establish the performance and ability of the thin mesh contact treatment as a viable solution to the skew cell and mesh refinement problems associated with this type of simulations. Because microprocessor and dynamic RAM effective capacity doubles every 18 months (Schaller, 1997), it was felt necessary to re-evaluate the gap approximation, by narrowing the gap of 1 mm that was used by Lee *et al.* (2007:2185), to 0.4 mm. The new thin mesh and small gap approximation techniques will be compared to two other cases, one having an area contact and the other a single surface contact (point contact). The boundaries and constraints that were used to simulate the CT tests are shown in Figure 3.5 and the description is given in Table 3.2.

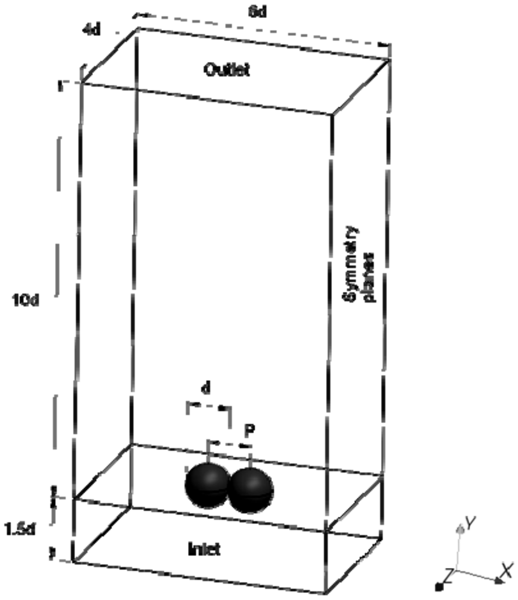

Figure 3.5: CT cases geometry.

In all the CT cases two horizontal spheres were used with a diameter of 60 mm, which is the same as that of the PBMR of 400 MWth. CT-1 was set up from the results of the previous section, which included a point contact approximation between the two spheres and the use of two prism layers in the contact region. CT-4 was modelled as the control with a target pebble diameter-to-cell size (surface triangulation size) ratio that is 1.8 times that of the other CT cases. The point contact approximations used in CT-1 and CT-4 were constructed by defining a single shared surface between the two spheres in contact. The area contact in CT-3 and the gap between the spheres in CT-2 were formed by adjusting the pitch between the spheres as shown in Table 3.2.

Table 3.2: CT case description.

Test	***Description***	***Contact dia. [mm]***	***Pitch [mm]***	d_p / d_c ***target***	d_p / d_c ***minimum***
CT-1	Thin mesh	-	60	50	80
CT-2	Gap approximation	-	60.4	50	80
CT-3	Area contact	2	59.967	50	80
CT-4	Control with surface contact	-	60	90	200

3.2.2.1. Boundary, mesh and solver setup

Since this dissertation originated from previous work done on the HTTU (High Temperature Test Unit) at the North-West University (Reyneke, 2009), in which nitrogen was used as primary fluid, the chosen fluid for this study was also nitrogen. The volume of the domain is 1.7 and 4.7 times larger than that used by Reyneke (2009) and Lee *et al.* (2007) respectively. The boundaries were specified as shown in Figure 3.5, with the velocity inlet and the pressure outlet specified at distances of 1.5 and 10 times the sphere diameter measured from the centre plane through the spheres. The four vertical planes were specified as symmetry planes, which mean that the shear stress at the boundary was zero and that the velocity and pressure face values were extrapolated from the adjacent cell's component that is parallel to these planes. The reference pressure was specified as standard atmospheric pressure which is 101.325 kPa. The relative pressure on the outlet was set at 0 kPa since the total pressure would be the sum of the reference and relative pressures. The velocity at the inlet was specified as 0.9 m/s with a corresponding particle Reynolds number of 3435 and a static temperature of 26.85°C.

The polyhedral volume mesh was grown from two different surface meshes, namely the external boundaries and the sphere surfaces. A conservative target and minimum surface size of 4 mm and 2 mm were specified for the inlet, outlet and symmetry planes (external boundaries) which correspond to surface sizes used on spheres from previous work done by Reyneke (2009), Calis *et al.* (2001) and Tobis (2000). For the CT-1, CT-2 and CT-3 the target and minimum surface sizes of 1.2 mm and 0.75 mm were chosen and is equivalent to a pebble diameter-to-cell size ratio of $d_p / d_c = 50$ and $d_p / d_c = 80$. This low minimum d_p / d_c ratio is in contrast to the ratios used by other researchers (Reyneke, 2009; *Calis et al.*, 2001; Tobis, 2000), but was selected in order to compare the solving ability and quality of the results that were produced by CT-2 and CT-3 with the results of CT-1, which was developed to use a low minimum d_p / d_c value as shown in the previous section. The thin mesh contact treatment was used in the CT-1 test, which generated two prism layers in the contact region. For the control simulation CT-4, a much finer mesh was generate by using a target and minimum pebble-to-cell size ratio of $d_p / d_c = 90$ and $d_p / d_c = 200$. The default growth rate of 1.3 was chosen for CT-2, 3 and 4, and a growth rate of 1.5 was chosen for CT-1 in accordance with the methodology of the contact treatment as developed in the previous section.

In this study the properties of nitrogen were assumed to be near to that of the ideal gas law and the steady state segregated type solver was used to solve temperature and flow over the cells. Since no significant differences were noted in the performance of different turbulence models and because no turbulence model analysis was conducted up to this stage, the Reynolds stress model

(RSM) was used in the CT simulations. The Reynolds stress equation model uses the exact Reynolds stress transport equation making it more accurate than the κ-ε model to account for the directional effect of the Reynolds stress field (Versteeg & *Malalasekera*, 2007:81). The *two-layer all y+ wall treatment* was used to solve the flow in the boundary layer, since excessive mesh refinement is required to realistically model flow in the boundary layer and no prism layers were generated over the spheres except for the contact regions.

Convergence of the simulations was measured by monitoring the change in continuity, momentum and energy over the boundaries per iteration. It is good practice to allow the simulation to converge its residuals to a value smaller than 0.001 for an accurate solution (CD-ADAPCO, 2010). The methodology that was used for solving the flow field was to first use a first-order differencing scheme, which only first-order accurate, based on the Taylor series truncation error, to develop the flow field and stabilize the solution. After a reasonable solution was obtained with the first-order convection equation, the differencing scheme was changed to a second-order differencing scheme to improve the accuracy of the results.

3.2.2.2. Results and discussion

Table 3.3 shows the resulting mesh sizes and the number of skew cells generated for each of the CT tests. The thin mesh, gap approximation and area contact techniques all delivered roughly the same mesh size, with the gap approximation having the least number of cells and the thin mesh the most, which is expected since CT-1 was modelled with a point contact between the two spheres. The volume of skew cells generated in CT-1 is less than was generated in the previous section and can be attributed to the reduction in the target cell sizes used with the same growth rate. Table 3.3 shows that although CT-4 used 2.5 times smaller cells in the contact area when compared to CT-1, it only managed to generate 0.0066 mm^3 less skew cells, while CT-1 was able to generate 0.041 mm^3 less skew cells with the same mesh specifications compared to CT-3. No skew cells were generated using the gap approximation.

Table 3.3: CT case mesh results.

Test	*Description*	d_p / d_c *target*	*Number of Cells/Faces [xE4]*	*Skew cells [mm^3]*
CT-1	Thin mesh	50	192.5/2.154	0.0078
CT-2	Gap approximation	50	191.6/2.168	0
CT-3	Area contact	50	192.3/2.149	0.048822
CT-4	Control: surface contact	90	418.7/7.692	0.001194

In the CT simulations, all but the energy residual converged to a value smaller than 0.001. This is because when pure flow is modelled with no heat or energy source, the energy residual tends to stay constant per iteration due to the minute changes in temperature over the domain. The energy residual was thus disabled in the rest of the pure flow simulations.

The stream line or flow profiles for all four cases are shown Figure 3.6. The colour contours represent the velocity magnitude over the same range of data for all the CT cases. In all four the CT cases the differences between the streamline profiles and the overlying velocity magnitudes are negligibly small. In the numerical simulations conducted by Lee *et al.* (2007:2187), large differences in the flow distribution between the 1 mm gap and both contact cases could be observed. The results of Lee *et al.* (2007:2187) showed two detached flow currents (stream lines) in the contact cases and somewhat fused streamlines in the gap approximation case as shown in Figure 2.19. The gap approximation (CT-2) of 0.4 mm used in this study show that if a small enough gap between the spheres is used, the resulting flow field and the stagnant flow region between the spheres will be the same as in the contact cases. Figure 3.7 shows the stagnant flow regions for the gap approximation and the control case.

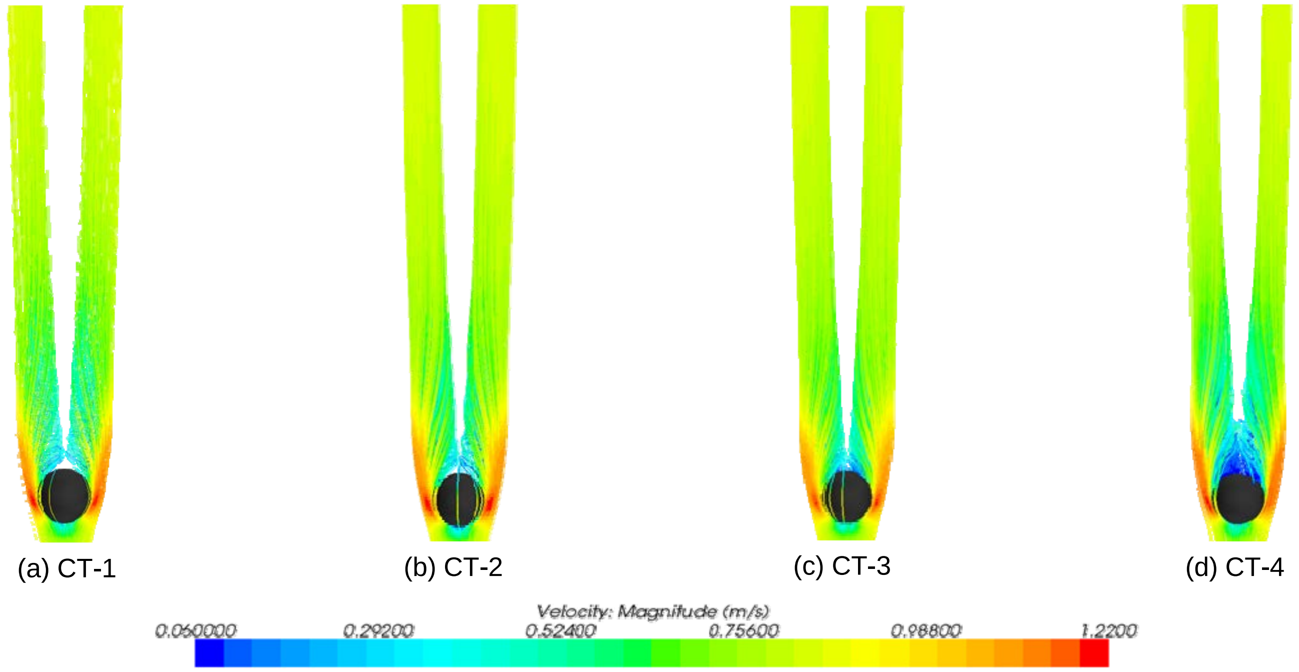
(a) CT-1 (b) CT-2 (c) CT-3 (d) CT-4

Figure 3.6: Streamline representation of the flow field and velocity magnitude downstream of the CT cases, in the (0,1,1) yz-plane

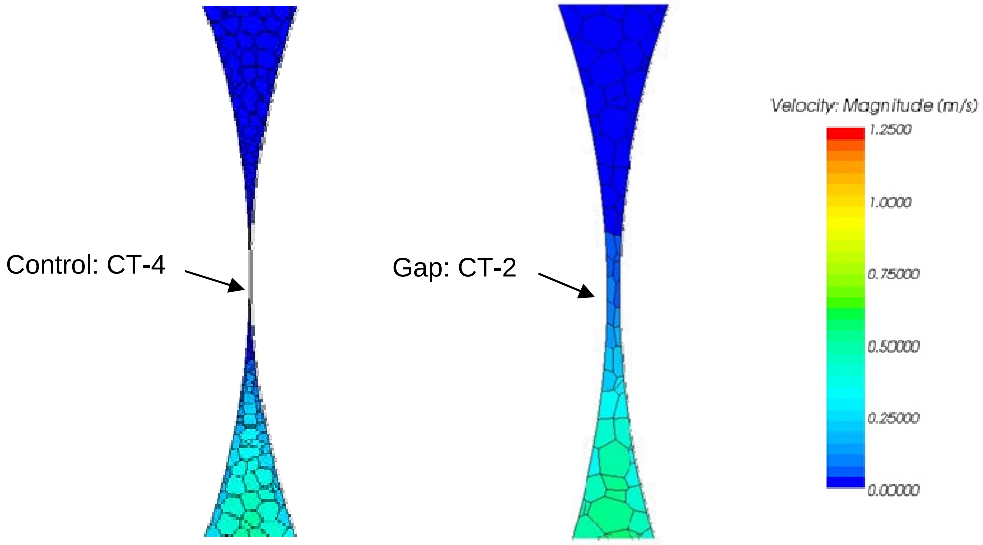

***Figure 3.7:* The stagnant flow region between contacting spheres (a) and the gap approximation (b).**

The pressure distribution over the spheres as well as the velocity contours of the flow field in the *xy-plane* are shown in Figure 3.8. The colour contours represent the pressure and velocity magnitudes over the same range of data for all the CT cases. In cases CT-1, CT-2 and CT-3 the pressure and velocity distributions are almost identical. The small differences that can be observed in CT-4 can only be attributed to the much finer mesh that was generated over the spheres that enabled the RSM turbulence model to accurately predict additional eddies downstream of the spheres as seen in Figure 3.9.

Although CT-4's contours differ slightly from the other CT cases, the results are nearly similar. The predicted maximum pressure drop values between the four CT cases is in good agreement with each other and the maximum difference of 0.63% resulted between CT-2 and CT-4. Similarly when comparing the maximum predicted velocity in the *xy-plane*, an even better comparison between the cases can be observed, with the maximum difference of 0.36% resulting between CT-1 and CT-4.

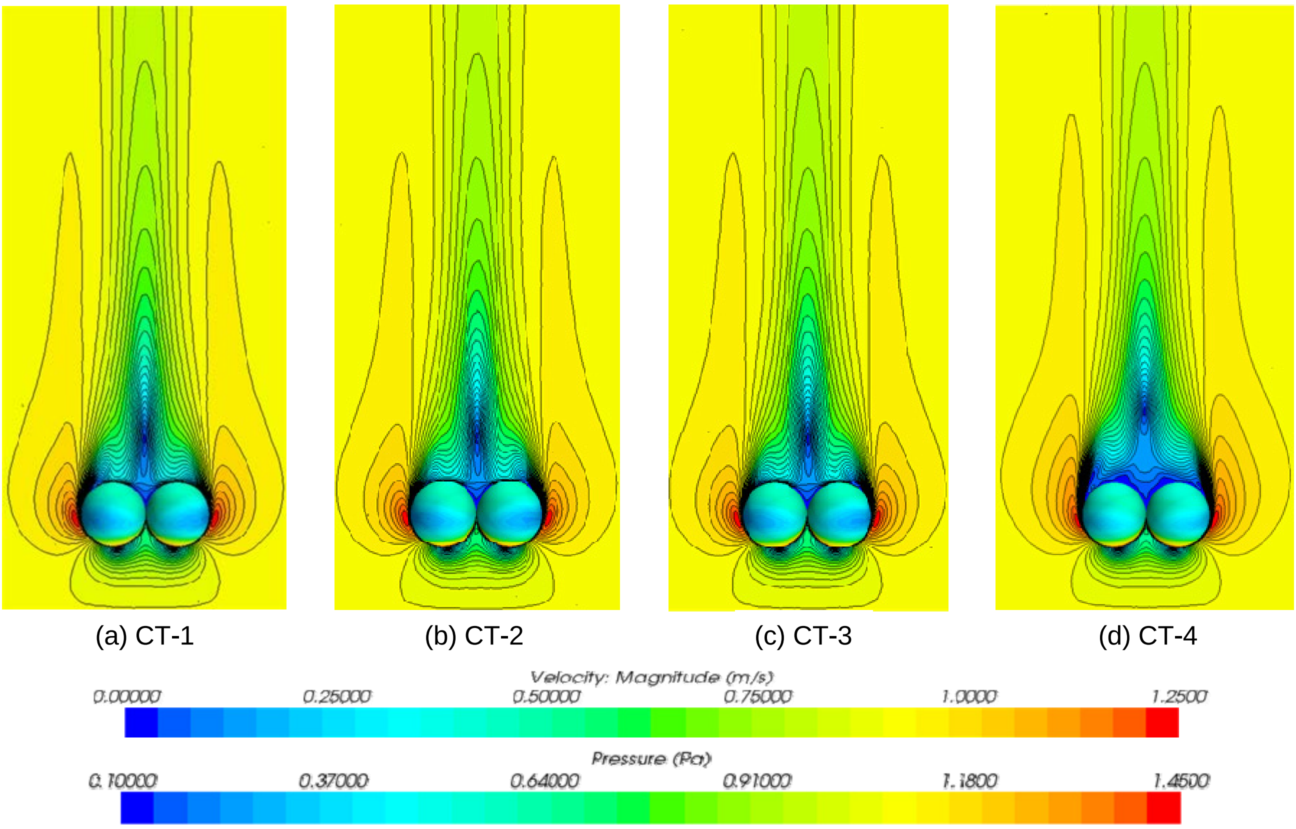
(a) CT-1 (b) CT-2 (c) CT-3 (d) CT-4

Figure 3.8: Scalar representation of the pressure distribution over the spheres and the velocity magnitude in the (1,1,0) xy-plane

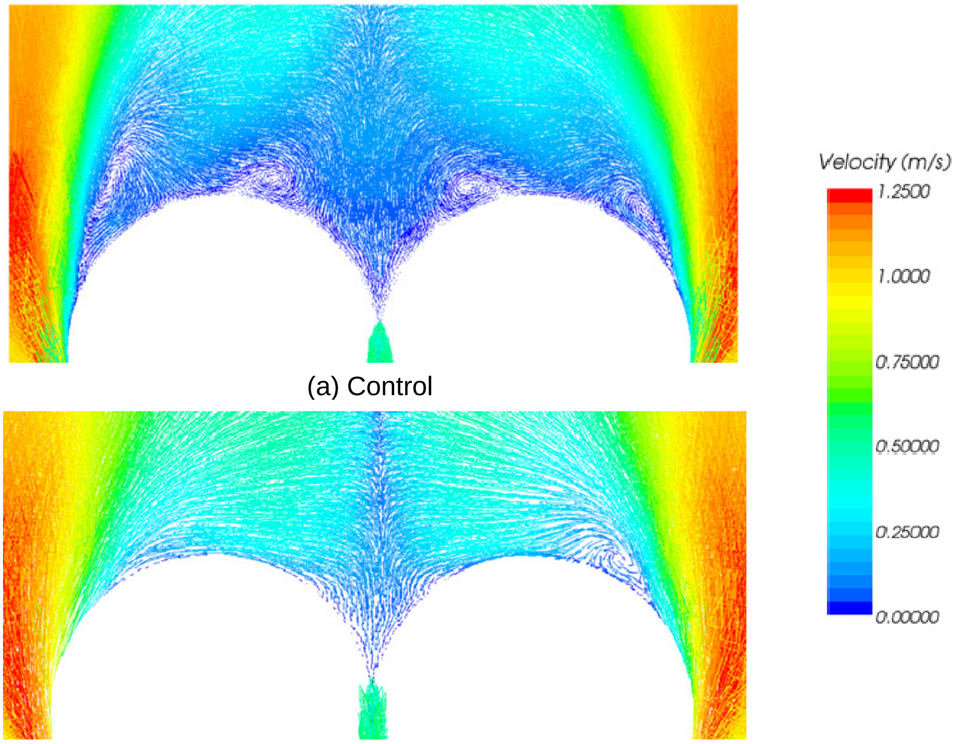
(a) Control

(b) Thin mesher

Figure 3.9: Velocity vector plot for (a) the control and (b) the thin mesher

From these results it can be concluded that STAR-CCM+® (VERSION 6.02.011) is able to solve the flow over spheres that contain a small number of skew cells in the contact region (up to a value of 0.049 mm^3) as tested in CT-3. It is also evident that flow (with no heat transfer) can be successfully modelled by using a gap approximation, provided that the gap is no more than 0.4 mm in size, as shown in CT-4. However, when a more realistic approach is needed that is able to take all aspects of the geometry into account, the thin mesh contact treatment seems to be superior.

3.3. MESH INDEPENDENCY AND VALIDATION TESTS (MD TESTS)

A simulation that is deemed to be mesh independent, will produce the same numerical answers when the mesh density is increased further. Therefore it is of great importance to establish to what values the simulation parameters will converge to when the numerical values are independent of the mesh size, in order to determine the accuracy and tolerances of the simulation results for a specific mesh size.

As mentioned in section 2.7.3, comprehensive mesh independence studies are lacking from literature for the simulation of turbulent flow over spheres. A detailed analysis of the mesh independency needed to accurately model turbulent flow over a packed bed of spheres, would enable future researchers to choose the most effective mesh density needed for the required accuracy of the specific problem under consideration.

Jafari *et al.* (2008:481) numerically analysed the overall flow behaviour through a large random packing of spheres, by conducting a small independency test consisting of three different mesh densities ranging between $5\times10^5 < Cells < 6\times10^6$. Jafari *et al.* (2008:482) recommended that a detail analysis of the mechanism of the turbulent generation in a packed bed be conducted.

This mesh independency study will serve as the ground work for turbulent flow simulations, which intends to model the flow through packed beds in great detail. This mesh independency study was thus conducted to establish the accuracy of the numerical solution obtained with the contact treatment selected in the previous section. An appropriate mesh density that was able to solve in a realistic time frame and accurately model different flow phenomena was chosen for the simulation conducted in the next section.

3.3.1. Description

Figure 3.10 shows the geometry and boundaries used in the mesh independency investigation. The randomly packed bed was created in Solid-Works® (2010) by using a macro and the coordinates of the numerical model developed for the HTTU's packed bed. This numerical representation of the HTTU's packed bed included the deformation of the spheres under load of the whole packing structure, which is represented as a small overlap in the CAD (computer aided design) geometry. The section extracted from the HTTU packed bed was at least five sphere diameters away from the walls, inlet or outlet regions, so that the section represent the bulk region of a randomly packed bed.

The fluid domain was once again constrained by six horizontal and vertical planes, with the bottom and top plane representing the velocity inlet and pressure outlet while the four vertical planes were specified as symmetry planes.

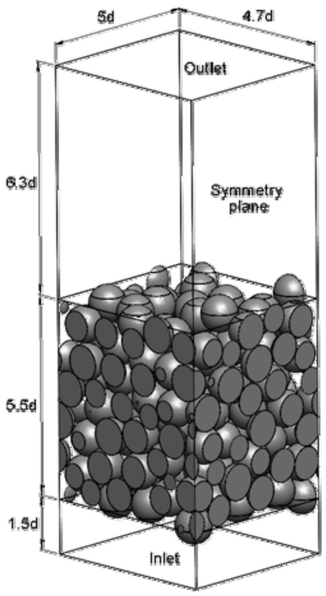

Figure 3.10: Random packed bed geometry of the mesh independency test.

The packed bed effectively consisted of 151.74 spheres, which were obtained by dividing the total volume of the solids by the volume of a single sphere. The solution was considered to be independent of the mesh when the pressure drop over a section of the packing for consecutive simulations converged to the same value.

The outlet plane of the test section was specified at 380 mm from the centre of the highest sphere of the packing while the inlet plane was specified to be 90 mm from the centre of the lowest sphere in the packing. It is important to set the outlet plane far enough from the last obstacle in the domain, because the eddies present in the outlet region will be treated as perpendicular flow to the outlet plane, which will have an impact on the flow further upstream in the domain. The outlet length was determined by incrementally increasing the distance between the last sphere and the outlet plane from 280 mm to 380 mm while monitoring the amount of reverse flow on the outlet. The reverse flow on the outlet subsided when the outlet length reached 340 mm.

The pressure drop over a section of the bed was used to validate the setup of the simulation as well as to determine when the solution was independent of the mesh density. The section over which the pressure drop was measured is shown in Figure 3.11. The pressure drop measuring region only consisted of a section of the bed that was 60 mm above the lowest and 90 mm below the highest points in the bed. This was done to allow the flow to develop inside the packed bed and to ensure that the porosity throughout the measuring region of the bed remained reasonably constant.

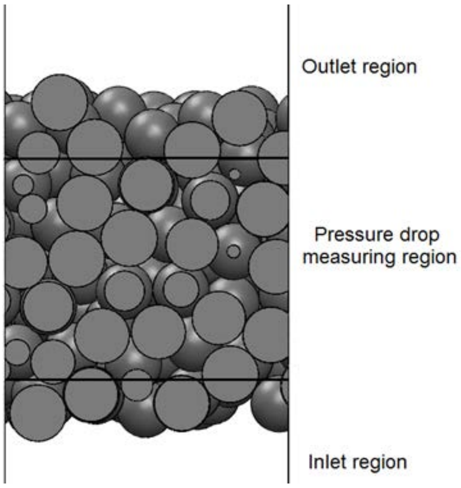

Figure 3.11: Valid pressure drop region.

The mesh density was incrementally increased by decreasing the surface cells of the spheres. These cells were decreased by changing the target surface cell size between 4.2 mm and 0.985 mm or $14.3 \leq d_p / d_c \leq 60.9$.

3.3.2. Boundary, mesh and solver setup

Nitrogen was once again the fluid used in the mesh independency test, and it was modelled as an ideal gas in steady state flow. A uniform velocity of 0.4487 m/s was specified for the velocity inlet which correlated to a mass flow of 2 kg/s through the empty annulus used in the HTTU. The same static temperature of 26.85°C (300 K) was used for the inlet and outlet boundary conditions. The pressure on the outlet plane was modelled relative to the reference pressure which was specified to be at standard atmospheric pressure, namely 101.325 kPa. All of the 151.74 spheres in the domain were treated as walls with the non-slip and smooth surface assumption. These wall assumptions allowed the model to accurately account for the shear stresses over the spheres.

The thin mesh contact treatment developed in section 3.2.2 was adopted in this mesh independency test. This contact treatment specified that a minimum particle diameter-to-cell surface size ratio of $d_p / d_c = 80$, a cell growth rate of 1.5 and two prism layers be used in the contact region between spheres. The surface meshes on the external (inlet, outlet and symmetry planes) and internal boundaries (spheres) were generated by using the target and minimum surface size ratios as shown in Table 3.4. The volume mesh was grown from the generated surface mesh by using unstructured polyhedral cells in the primary flow domain and structured prism cells in the stagnant contact regions between the spheres. A number of attempts were made to generate prism layers adjacent to the wall of the spheres, but the large number of contact points present around each sphere caused the prism layers to become irregular and to deform. Consequently it was decided to use structured meshes only as part of the contact treatment and to employ the *two-layer all y+ wall treatment* in the boundary layer.

Table 3.4: Mesh surface size description of the mesh independency tests.

Description	d_p / d_c	
	Target	***Minimum***
Inlet	15	30
Outlet	15	30
Symmetry planes	15	30
Spheres	14.3 - 60.9	80

The velocity used in the mesh independency tests correlated to $\mathrm{Re}_p = 2740$ which was assumed to be turbulent since Hlushkou and Tallarek's (2006:75) research showed that the flow through a packed bed will be inertially dominated when $\mathrm{Re}_p > 500$. Since the literature suggests that there are no significant differences in the performance between the different turbulence models and because no turbulence model analysis was conducted up to this point, the Realizable κ-ε model was used for all the mesh independency tests. The κ-ε turbulence model is the most validated model in industry and less computationally expensive than RSM. The κ-ε turbulence model was thus applied to obtain mesh independency in a reasonable time frame.

3.3.3. Results and discussion

In order to extract the pressure drop from the numerical solution it was necessary to determine the number of planes needed to give an accurate representation of the average pressure drop over the bed.

The packed bed was discretised into paired sections of planes as shown in Figure 3.12. The planes were spaced to fit into the valid pressure drop section, with a distance of 200 mm between each set of paired planes. The results from the converged solution of MD-5 (Table 3.5) were used to predict the average pressure drop over the planes.

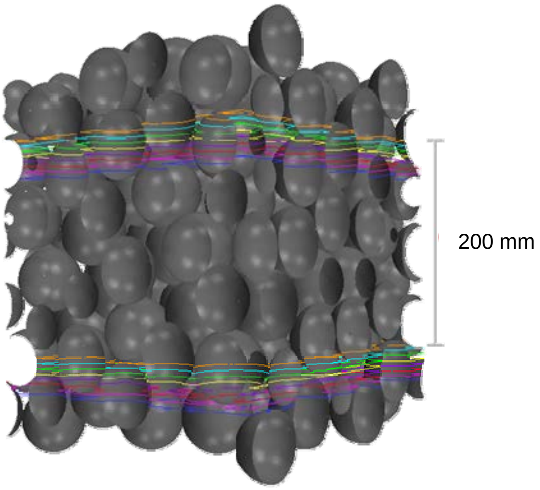

Figure 3.12: Pressure drop planes

Each of the planes had on average 39770 cells from which an average scalar can be obtained. To determine the effect that the number of paired planes had on the average pressure drop, the average pressure drop was calculated for different numbers of paired planes. Figure 3.13 shows the average pressure drop deviation obtained for different numbers of paired planes used. This deviation was calculated by comparing the average pressure drop obtained for an increasing number of paired planes to the previous number of paired planes. This method is best explained by the function shown in equation (3.1):

$$\begin{aligned} D_{(n)} &= \left(\frac{\sum_{n=1}^{(n-1)} \Delta P_{(n-1)}}{\sum_{n=1}^{(n)} \Delta P_{(n)}} \times \frac{n}{(n-1)} - 1 \right) \times 100 \quad \Bigg\} \; n>1;\ \Delta P_{(n)} > \Delta P_{(n-1)} \\ &= \left(1 - \frac{\sum_{n=1}^{(n-1)} \Delta P_{(n-1)}}{\sum_{n=1}^{(n)} \Delta P_{(n)}} \times \frac{n}{(n-1)} \right) \times 100 \quad \Bigg\} \; n>1;\ \Delta P_{(n)} < \Delta P_{(n-1)} \end{aligned} \tag{3.1}$$

where n is the number of paired planes used, $D_{(n)}$ is the deviation obtained and $\Delta P_{(n)}$ presents the pressure drop obtained by the nth paired planes.

The plane test shows that there was very little deviation between the number of paired planes used to obtain the average pressure drop over the 200 mm test section of the bed. Figure 3.13 shows that the deviation between the number of paired planes tends to level out after the 8th paired plane onwards. For completeness, 8 paired planes were used to determine the average pressure drop in the mesh independency tests.

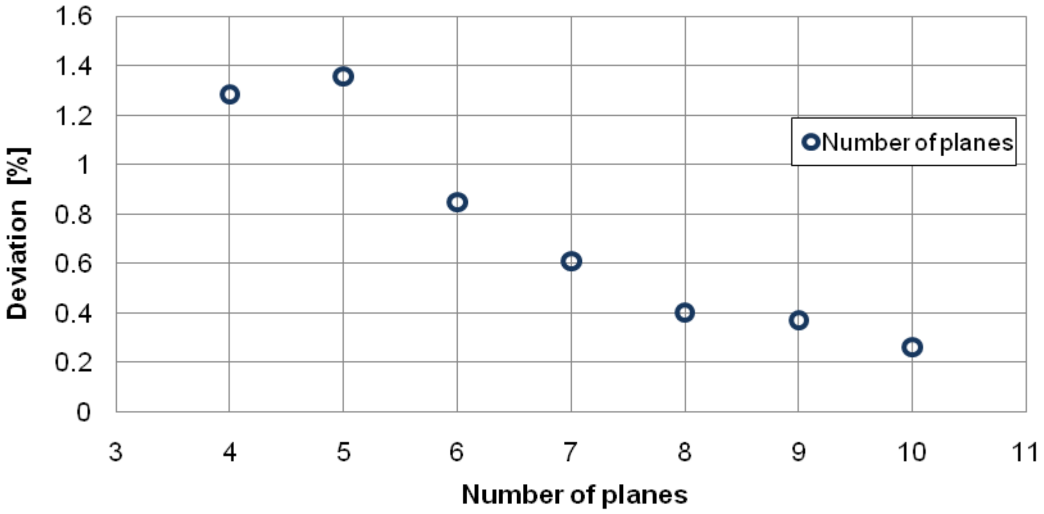

Figure 3.13: Moving average pressure drop deviation for an increased number of planes

The porosity of the random packing was calculated by excluding the top and bottom part of the packing. This was done to obtain a porosity that would represent the valid pressure drop region as shown in Figure 3.11. Two attempts were made to calculate the porosity, the first attempt excluded 60 mm from the top and bottom of the packing and the second attempt excluded 100 mm. Both attempts delivered a porosity of $\varepsilon = 0.3747$, which suggests that the porosity inside the packing was uniformly distributed.

The measured pressure drop that was taken from the valid pressure drop region will be compared with the theoretical values predicted by the pressure drop correlations of the KTA (1981) and that of Eisfeld and Schnitzlein (2001). The theoretical pressure drops were calculated using EES® (VERSION 8.874) which is an engineering equation solver, with the density and viscosity of nitrogen, at a temperature and pressure of 26.85°C and 101.325 kPa, resulting in $\rho = 1.138$ kg/m^3 and $\mu_f = 1.789 \times 10^{-5}$ kg/m-s.

Table 3.5 shows the pressure drop results obtained from the simulations as well as the deviation when compared with the theoretical pressure drop for each of the MD tests.

Table 3.5: The description and results of the MD tests.

Case	**Cell size [mm]**	**Number of cells [x10^6]**	**Pressure drop**	**Deviation [%]**	
				KTA	**Eisfeld and Schnitzlein**
MD-1	4.2	1.878	11.4668	10.87656	8.138464
MD-2	2.1	2.632	11.7734	8.493572	5.682264
MD-3	1.8	3.901	12.0909	6.025866	3.138744
MD-4	1.5	5.1695	12.358	3.949884	0.998983
MD-5	1.25	8.6466	12.6746	1.489173	1.537328
MD-6	1.1	9.655	12.7165	1.163514	1.872992
MD-7	1.03	12.7862	12.833	0.25804	2.806284
MD-8	0.985	15.41802	12.9123	0.358303	3.441563

The maximum mesh density that could be reached with the resources which were available at the time, was a total of 15.42 million cells generated with a target $d_p / d_c = 0.985$. Figure 3.14 shows the numerically calculated pressure drop plotted against the number of cells generated in the fluid domain. A fourth order polynomial fit was used to determine at which point the pressure drop would be independent of the mesh size. Using this function, a maximum pressure drop of 12.928 kPa at 16.75×10^6 cells was extrapolated. This is in excellent agreement with both the KTA (1981) and Eisfeld and Schnitzlein's (2001) pressure drop correlations, considering that extrapolated pressure drop only differs by 0.54% and 3.45% respectively.

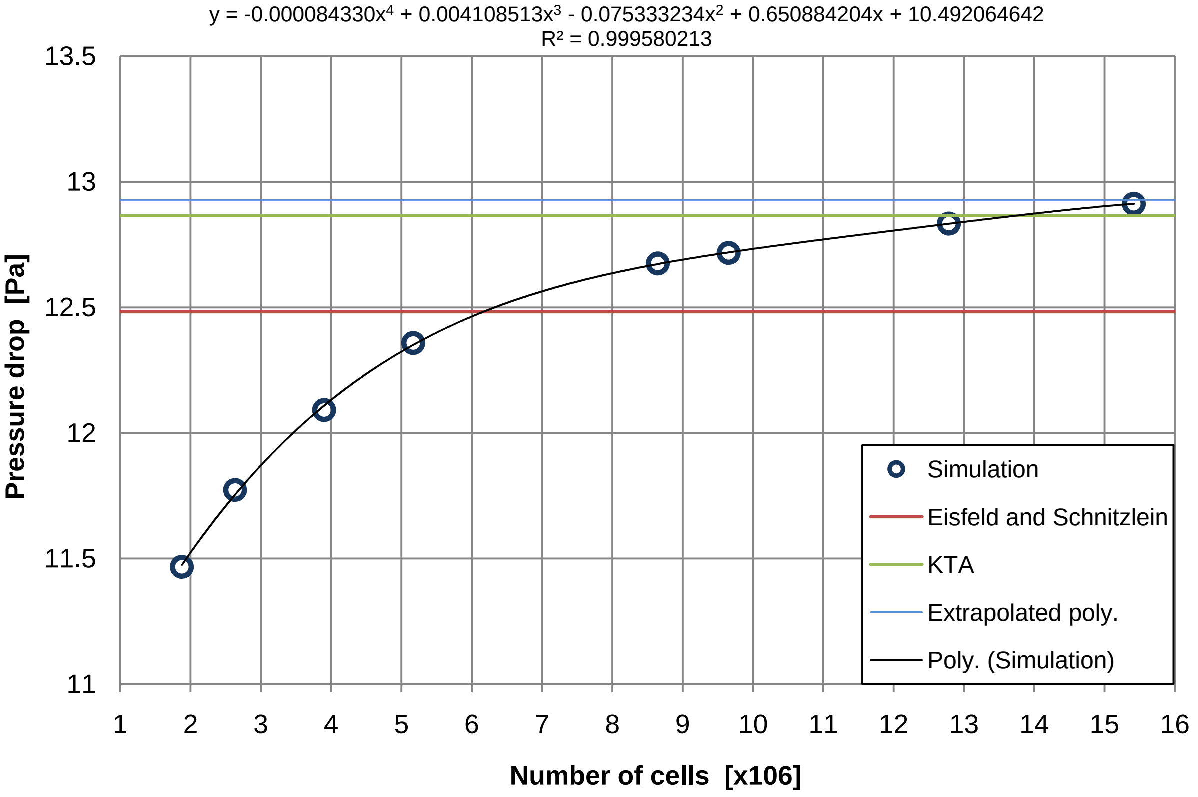

Figure 3.14: ***The simulated pressure drop over a randomly packed bed with an increasing mesh density compared to different pressure drop correlations.***

To test whether the mesh independency results were also valid for other turbulence models, the demanding LES model was also used with the same setup. The LES test used a target ratio of $d_p / d_c = 0.99$ which generated 14.0843 million cells. The pressure drop result obtained with the LES test compared to the fourth order polynomial function used to fit the κ-ε data, is shown in Figure 3.15. A deviation in pressure drop of 0.1% was measured between the two turbulence models, which clearly indicates that the mesh independency test is also valid for other turbulence models.

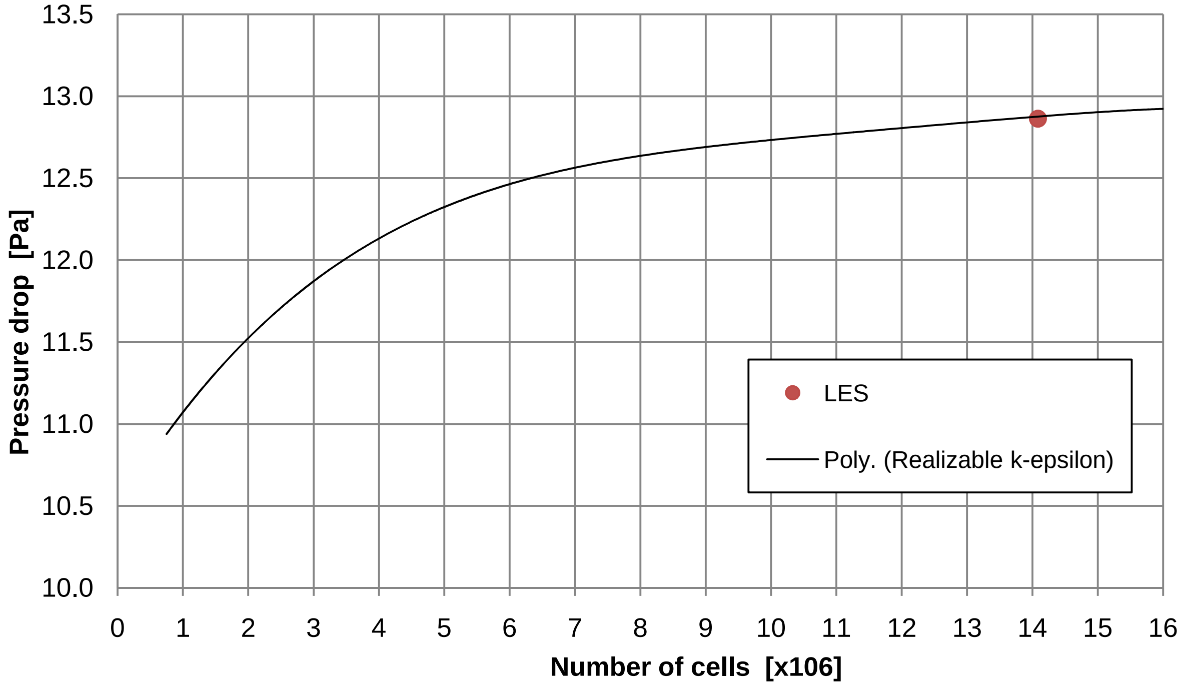

***Figure 3.15:* Pressure drop comparison between the LES and Realizable $\kappa - \varepsilon$ turbulence models.**

It was decided to use the KTA (1981) correlation to validate the remainder of the modelling that follows, since:

- both the KTA (1981) and Eisfeld and Schnitzlein (2001) correlations are in close agreement for a wide range of Reynolds numbers as mentioned in section 2.5;
- the KTA (1981) correlation was specifically developed for the licensing of modular nuclear reactors using perfectly spherical particles; and
- the pressure drop correlation would only be used for beds without wall constraints, thus the need to quantify the effects of the walls was unnecessary.

Figure 3.16 shows that the deviation between pressure drop predicted by the KTA (1981) correlation and the simulated value varies linearly with target surface cell size. This linear function was used to determine what target d_p / d_c value was needed for the accuracy required in the various simulations that followed in this study.

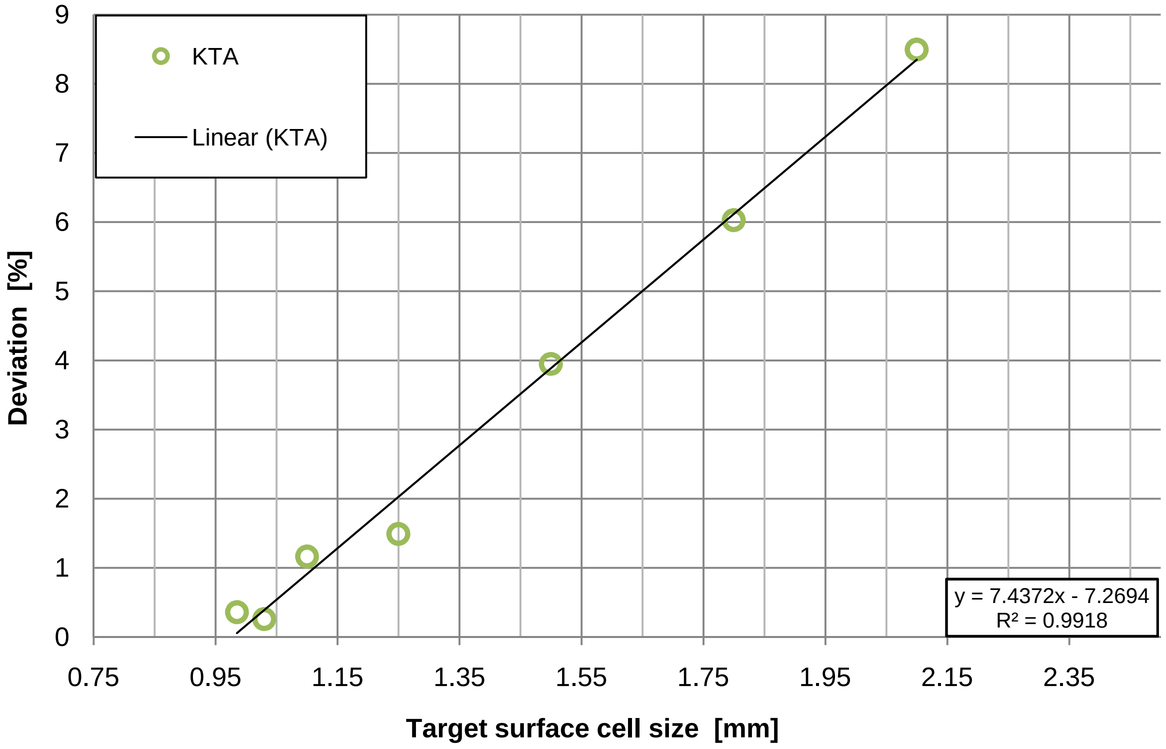

Figure 3.16: Percentage deviation for a given target surface cell size value, when compared to the KTA pressure drop correlation.

From the above results it is clear that the contact treatment, boundary, mesh and solver were properly setup to predict accurate and realistic results. Thus the methodology used to setup and solve all of the MD cases was also used in the sections that follow.

3.4. TURBULENCE MODEL AND VALIDATION TESTS

Each of the different turbulence models was developed for a specific problem or purpose, therefore having certain strengths for specific types of applications. In the numerical modelling of flow, the selection of the turbulence model will affect the accuracy and the amount of flow detail captured throughout the domain. Hassan (2008: 532) stated that the choice of turbulence model should be based on the type of flow, cost-to-time factor and the complexity of the geometry in the problem at hand.

In this section the performance of the κ-ω, Realizable κ-ε, RSM, Spalart-Allmaras and LES turbulence models (for flow through packed beds) will be reviewed and discussed. These turbulence models were evaluated by comparing the numerical results with the theoretical pressure drop as predicted by the KTA (1981) correlation, which then also served to validate and verify the numerical setup used this far in the study.

The TM tests were also conducted in two stages. The aim of the first stage tests was to compare the pressure drop of all the turbulence models with the KTA (1981) correlation for a single velocity inlet. These results were then used to filter out the most promising models which could then be used in second stage tests. The second stage served as a pressure drop and turbulence model validation test. The tests conducted in this stage used a wide range of Reynolds numbers that included viscous-inertial flow (30<Re<500) and inertial flow (Re>500).

3.4.1. Solution methodology

All the considered turbulence models use RANS modelling except for the LES model that constructs its equations by means of filtering rather than averaging as in the RANS equations.

The same solution methodology that was used for the CT tests (section 3.2.2) was also followed for all of the RANS modelling. This methodology entailed that a preliminary flow field should be calculated by using a first-order differencing scheme from which the final flow field was calculated using a second-order differencing scheme. This improved the accuracy of the results, the convergence and the time needed to obtain a solution.

The methodology used to solve the transient LES turbulence was more complex than the methodology used for the RANS models. Little information could be found in literature that describes the methodology for obtaining a transient solution or more specifically, literature that addresses the question of when a transient solution would represent a steady state solution. Thus after a few trial and error simulations it was found that because a steady state solution is required, some of the costly transient results could be avoided when the following steps were followed:

- Since we are not interested in the development of equilibrium conditions, the number of inner iterations for a single time step could be specified as one.

- Selecting a large time-step e.g. of one second, ensured that a flow field was quickly established between the inlet and outlet planes.

- After a preliminary flow field was developed, the size of the time-step was incrementally decreased while increasing the number of iterations between the time-steps. This ensured that the larger eddies were properly developed and the smaller eddies were accurately modelled for a steady state solution. This was found to deliver the quickest convergence.

- After the last time increment the number of inner iterations could be increased to ensure that the eddies were well represented.

It was found that the last step, as mentioned above, had no to very little effect on the flow parameter results.

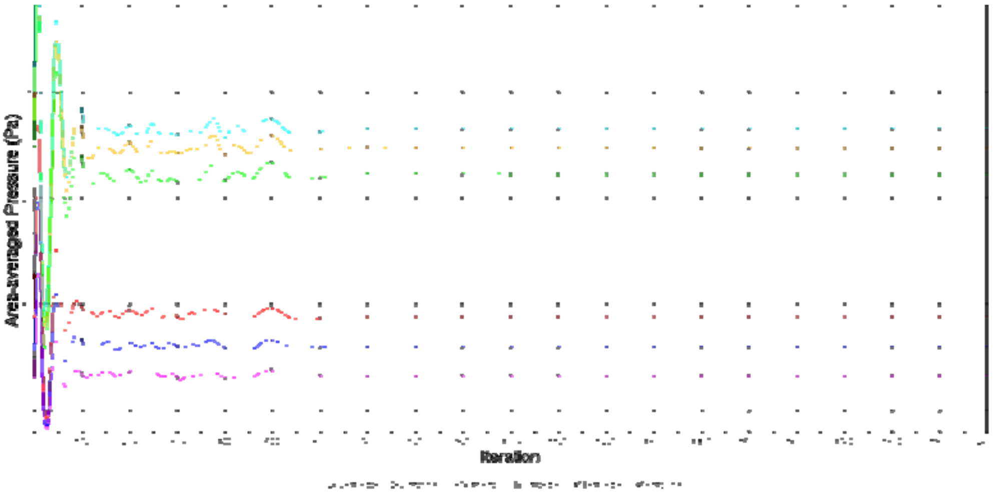

Figure 3.17: The average pressure calculated for several planes, using the LES turbulence model.

Figure 3.17 shows the average pressure drop calculated for several planes throughout a packed bed. An effective way of measuring whether a simulation has reached convergence is by monitoring a flow parameter e.g. pressure and the conservation parameters (mass, momentum and energy).

3.4.2. Single velocity simulation (SV tests)

As mentioned earlier, the aim of the first stage single velocity simulation tests (SV tests) was to compare the simulated pressure drop of all the turbulence models with the KTA (1981) correlation for a single velocity inlet. The turbulence models that delivered the best results in terms of accuracy and robustness would then be used in the next section, where they would be subjected to a wider range of Reynolds numbers.

The packed bed used in the SV cases was the exact same bed used in the mesh independency study and is shown in Figure 3.10. The physics and boundaries used in the mesh independency study was also used in the SV simulations, which included six horizontal and vertical planes, with the bottom and top plane representing the velocity inlet and pressure outlet while the four vertical planes were specified as symmetry planes. The outlet length of the test section was once again specified as 380 mm from the centre of the highest sphere in the packing structure, while the inlet was specified to be 90 mm from the centre of the lowest sphere in the packed bed.

The turbulence models that were tested included the standard κ-ω, Realizable κ-ε, RSM, Spalart-Allmaras and LES models. The mesh independency results showed that for a velocity of 0.4487 m/s, the Realizable κ-ε and LES models were able to predict the pressure drop through the packed bed with an accuracy of between 10.9 and 0.36% (depending on the mesh density) when compared with the KTA (1981) correlation. Thus it was decided to raise the complexity of the flow field by increasing the velocity for the SV cases to 0.8974 m/s ($\mathrm{Re}_p = 3426$) which correlated to a mass flow of 4 kg/s through the empty annulus as used in the HTTU.

The pressure drop over the bed was measured by discretising the bed into eight paired planes that were 200 mm apart in the valid pressure drop region as discussed in section 3.3.3 and shown in Figure 3.11.

3.4.2.1. Boundary, mesh and solver setup

Nitrogen was used as the fluid in all of the SV cases and was modelled as an ideal gas in steady state and transient flow. A static temperature of 26.85°C (300 K) was used for both the inlet and outlet boundaries. The pressure on the outlet plane was modelled at 101.325 kPa which was based on the reference pressure. The spheres in the domain were treated as walls with a non-slip and smooth surface assumption, to accurately account for the flow shear stresses over the spheres.

The thin mesh contact treatment was used in all of the SV cases, with a minimum particle diameter-to-cell surface size ratio of $d_p / d_c = 80$, a cell growth rate of 1.5 and two prism layers generated between the spheres. The surface meshes on the external (inlet, outlet and symmetry planes) and internal boundaries (spheres) were generated by using the target and minimum surface size ratios that were used in test MD-4. This case was chosen because it generated a reasonable number of cells that were able to predict the pressure drop within 1.49% when compared with the value predicted by the KTA (1981) correlation. Thus the target particle diameter-to-cell surface size ratios of $d_p / d_c = 15$ and $d_p / d_c = 48$ were used for the external (inlet, outlet and symmetry planes) and internal boundaries (spheres).

The same solution methodology that was discussed in section 3.4.1 was used to solve the flow with the relevant turbulence models.

3.4.2.2. Results and discussion

Table 3.6 shows the predicted pressure drops obtained using the different turbulence models and compares them with the value predicted by the KTA (1981) correlation.

Table 3.6: Different turbulence models' predicted pressure drop and deviation.

case	*Turbulence model*	*Pressure drop [Pa]*	*Deviation from KTA [%]*
1	***Realizable κ-ε***	44.2805	5.858254
2	***Standard κ-ω***	43.0962	8.376175
3	***Reynolds Stress model***	45.0964	4.12369
4	***Spalart-Allmaras model***	42.1183	10.45516
5	***Large Eddy Simulation***	46.3683	1.419529
6	***KTA Correlation***	47.0360	0

Note that according to KTA 3102.3 the uncertainty range for the KTA correlation is ±15% within scope of application with a confidence level of 95%.

The results show that the pressure drop predicted with the simulation based on the LES turbulence model came closest to the pressure drop predicted by the KTA (1981) correlation. The LES model obtained a pressure drop of 46.37 Pa, which is in excellent agreement with the KTA (1981) correlation, deviating by only 1.42 %. The Realizable κ-ε and the RSM turbulence models' results are also in good agreement with the KTA (1981) correlation, deviating by 5.86% and 4.12% respectively.

The standard κ-ω and the Spalart-Allmaras models were found to be the least robust of all the turbulence models tested. Both needed a few restarts with adjusted initial conditions to stabilize the solver's convergence. Even though the standard κ-ω and the Spalart-Allmaras model did not completely converge, their predicted pressure drops are also in reasonable agreement with the KTA (1981) correlation, deviating by 8.38% and 10.46% respectively.

The LES, RSM and Realizable κ-ε turbulence models were selected for the second stage of the turbulence model tests on ground of their robustness and accuracy achieved in the SV tests.

3.4.3. Multiple velocity simulations (MV tests)

The aim of the MV tests was to test the performance and robustness of different turbulence models and the simulation setup over a wide range of Reynolds numbers. The turbulence models under investigation in this section are LES, RSM and Realizable κ-ε. Six different inlet velocities were specified, with Reynolds numbers ranging between 428 and 3426, for each of the turbulence models.

The packed bed that was used for the multiple velocity simulations was less elaborate than the one used in the mesh independency study and the single velocity simulations. This MV packed bed effectively contains 91.7 spheres compared to the 151.7 spheres used in the packed beds of the previous two tests. This was done to ensure that the simulation results would be obtained in a reasonable time frame. The geometry of the packed used for the MV tests is shown in Figure 3.18.

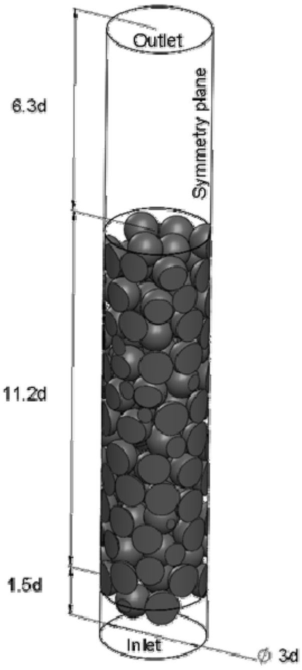

Figure 3.18: Random packed bed geometry used in the MV simulations.

This randomly packed bed representation was also extracted from the numerical model of the HTTU packing. The coordinates used to generate this bed were selected to be at least five sphere diameters away from any wall boundaries and in a different section of the numerical model than previously used. The bottom and top planes were modelled as a velocity inlet and pressure outlet, while the cylindrical section was specified as a symmetry plane. An outlet length of 380 mm was specified from the centre of the highest sphere in the packing while the inlet was specified to be 90 mm from the centre of the lowest sphere in the packing.

The KTA (1981) pressure drop correlation was once again employed as a benchmark that will be used to evaluate the performance of each of the turbulence models over a wide range of velocities, as shown in Table 3.7.

Table 3.7: MV cases description.

Test	**Inlet Velocity [m/s]**	Re_p
MV-1	**0.1122**	428.3
MV-2	**0.1383**	527.9
MV-3	**0.2723**	1039
MV-4	**0.4487**	1713
MV-5	**0.6652**	2539
MV-6	**0.89745**	3426

Guardo *et al.* (2005:1736) tested the performance of the Spalart–Allmaras, κ-ε and the κ-ω turbulence models for different flow regimes through a packed bed of packed spheres (FCC) and concluded that the turbulence models lack the ability to properly model the transition flow regime with low Reynolds numbers. To fully test and compare the turbulence models' abilities, the viscous-inertial flow regime was also included in MV tests 1 and 2.

It was necessary to filter out any inconsistencies that might occur locally due to changes in porosity and geometry. Consequently the pressure drop was measured using the technique developed in section 3.3.3, which suggests that the calculated pressure drop should consist of an average pressure drop that is measured between a series of paired planes that are equally spaced, as shown in Figure 3.19. Thus for the MV tests, the pressure drop was measured over a distance of 400 mm through the packed bed and repeated eight times and then averaged.

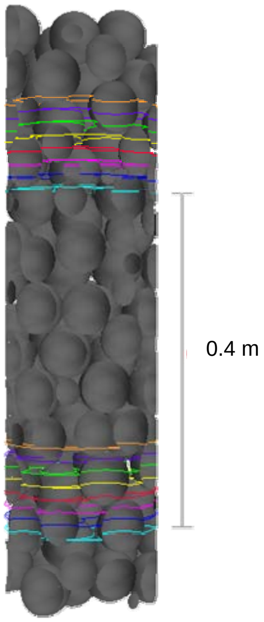

Figure 3.19: Paired pressure drop planes used in the MV cases.

Each of the sixteen planes had on average 9642 cells from which a pressure drop reading could be extracted. The porosity for this valid pressure drop region was calculated using Solid-Works® (2010) which gave a porosity of $\varepsilon_p = 0.395$.

3.4.3.1. Boundary, mesh and solver setup

Nitrogen was once again modelled as an ideal gas for steady state flow, with a static temperature of 26.85°C (300 K) specified over the inlet and outlet boundaries. The pressure on the outlet plane was kept at standard atmospheric pressure, which is 101.325 kPa, while the inlet plane modelled uniform flow for all the MV tests. The spheres were specified as walls with the non-slip and smooth surface assumption.

The mesh setup that was used in the MV tests was generated in the same manner as in the single velocity study. Accordingly target particle diameter-to-cell surface size ratios of $d_p / d_c = 48$ and $d_p / d_c = 15$ were used for the external (inlet, outlet and symmetry planes) and internal boundaries (spheres), and a minimum ratio of $d_p / d_c = 80$ was selected for the thin mesh contact treatment. The volume mesh was grown from the surface cells with a growth rate of 1.5, by using unstructured polyhedral cells in the primary flow domain and structured prism cells in the contact regions between the spheres. The volume representation consisted of a total of $4.90\text{x}10^6$ generated cells.

The solving methodology that was discussed in section 3.4.1 was used to solve the relevant turbulence models.

3.4.3.2. Results and discussions

The pressure drop for each case, as predicted by the theoretical and simulation models are shown in Table 3.8, while the deviation between the predicted pressure drop values for different turbulence models and the KTA (1981) correlation is shown in Figure 3.20.

Table 3.8: Pressure drop results and test description.

Test	***Velocity [m/s]***	Re_m	Re_p	***Simulated and theoretical pressure drop [Pa]***			
				κ-ε	***RSM***	***LES***	***KTA***
MV-1	***0.1122***	707.9	428.3	1.9890	2.051475	1.776794	1.6714
MV-2	***0.1383***	872.7	527.9	2.82704	2.999058	2.525987	2.4327
MV-3	***0.2723***	1717	1039	8.6023	8.592132	8.60888	8.381
MV-4	***0.4487***	2831	1713	20.8805	20.48599	20.78775	21.1672
MV-5	***0.6652***	4197	2539	41.9243	42.37193	43.08167	44.1912
MV-6	***0.89745***	5663	3426	72.1171	72.84812	73.87697	77.5306

As mentioned previously the uncertainty range for the KTA correlation is ±15% within scope of application with a confidence level of 95%. Re_m in Table 3.8 is the modified Reynolds number and was calculated as follows:

$$Re_m = \frac{Re_p}{1-\varepsilon} \tag{3.2}$$

$$10 \leq Re_m \leq 10^5 \tag{3.3}$$

Equation (3.3) shows the valid Re_m range of the KTA (1981) correlation, which confirms that the range investigated in this study is well within scope of the KTA (1981) equation.

From these results it is clear that the values predicted by the simulations based on the LES turbulence models are the most accurate for the velocity range tested. The Realizable κ-ε and the RSM models were not able to accurately predict the pressure drop between the non-linear laminar and turbulent flow regime as shown in Figure 3.20. The Realizable κ-ε and the RSM model were only able to predict a pressure drop within 19.0-16.2% and 23.3-22.7% compared to the KTA (1981) correlation for this transitional flow region. Since the KTA (1981) correlation's uncertainty range is ±15%, it can be concluded that the RSM and κ-ε model is inadequate to model the turbulence effect for transitional flow.

The findings of Guardo *et al.* (2005:1736) also confirm that RANS models lack the ability to accurately predict the pressure drop through a packed bed in this transition flow regime. In contrast to the RANS models, the LES model was able to accurately predict the pressure drop for low Reynolds numbers, deviating only between 6.3-3.8% when compared with the KTA (1981) correlation.

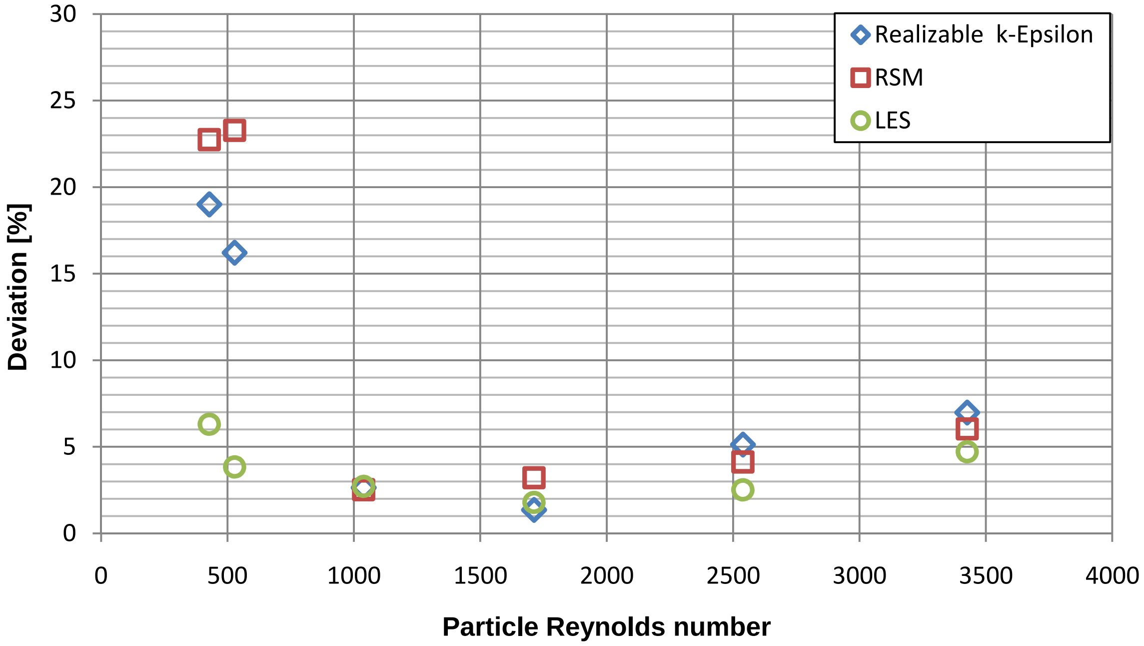

Figure 3.20: Simulated pressure drop deviation compared to the KTA correlation.

All three turbulence models predicted almost the exact same pressure drop of 8.6 Pa for $\mathrm{Re}_p = 1000$, which represents a low Reynolds number that is in the fully turbulent flow regime. The turbulence models start to deviate from each other and from the theoretical pressure drop for the higher velocities, with the Realizable κ-ε performing the worst and LES the best between $2540 < \mathrm{Re}_p < 3426$.

The results also serve as a comprehensive pressure drop validation test for a wide range of Reynolds numbers. Both RANS and LES models proved to be adequate to model turbulence for $\mathrm{Re}_p > 530$ and the LES model was also able to accurately model the turbulence present in the transitional flow regime for $\mathrm{Re}_p < 530$.

3.5. CONCLUSION

This chapter dealt with the fundamental question of how to accurately simulate flow through a packed bed of spheres. This question led to the revision of some established methodologies and the development of some new implementations. The main factors that were considered important to the accuracy of this type of simulations were contact treatment, mesh density and the turbulence modelling.

In the contact treatment study discussed in section 3.2.2, it was found that STAR-CCM+® (VERSION 6.02.011) is able to suppress the effect of a small number of skew cells on the numerical results. It is also evident that flow (with no heat transfer) can be successfully modelled by using a gap approximation, provided that the gap is no greater than 0.4 mm. However, when a more realistic approach is required, the thin mesh contact treatment is able to take all aspects of the contact geometry into account, without compromising computational resources.

The numerical setup was validated in the mesh independency study by comparing the simulated pressure drop with the value predicted by the KTA (1981) and Eisfeld and Schnitzlein's (2001) pressure drop correlations, over a wide range of mesh densities. It was found that the simulated results (extrapolated pressure drop) were in excellent agreement with values predicted by both the KTA (1981) and Eisfeld and Schnitzlein's (2001) pressure drop correlations, deviating between 0.54% and 3.45%. A linear function was also derived that can be used to determine what target d_p / d_c value is needed for the accuracy required in the different simulations that followed in this study.

The results from the turbulence model study showed that RANS and LES models were able to adequately model the effect of turbulence for $\mathrm{Re}_p > 530$. In contrast to the RANS models, the LES model was also able to accurately predict the pressure drop for low Reynolds numbers in the transition regime. This section also implemented a new approach to solving flow using the LES turbulence model which decreases the computational expense of this transient solver.

It can be concluded that by using the correct contact treatment, mesh density and turbulence model, highly accurate results can be achieved with moderate computational expenses.

4

ENHANCED MIXING

4.1. INTRODUCTION

Packed beds are generally used in industry due to their attractive contact to flow area ratio which gives them exceptional mixing abilities. To be able to fully characterise a packed bed structure, it is vital to understand the fluid mechanics involved. The first fundamental step towards a better understanding of flow through packed beds is to study its mixing ability. This chapter focuses on the development of explicit simulations and techniques necessary to extract and compare different mixing parameters. Van Antwerpen (2009) noted that by characterising a porous structure using porosity on its own is inadequate. His statement is also complemented by the fact that pressure drop correlations that exclusively use porosity as geometrical parameter, fail to accurately predict the pressure drop for most porosity ranges and structured packings.

Explicit simulations are not only able to give insight into the fluid mechanics of flow through packed beds, but can also be used to obtain different flow correlations. These flow correlations are of great importance since they influence the accuracy of more extensive implicit type simulations. It is evident that flow correlations lack the ability to characterise the packing structure by something else than porosity. Thus it is necessary to add additional geometrical parameters to these correlations to capture all of the different flow mechanics.

The mixing parameters that will be investigated in this chapter are tortuosity, TMD (thermal mixing degree) and effective conductivity due to the braiding effect.

4.2. TORTUOSITY

Tortuosity is arguably the most fundamental of all the mixing parameters mentioned. Lanfrey *et al.* (2010) defined tortuosity as the ratio of the length a solute travels through a porous medium to the length of the porous medium. From the definition it is clear that this mixing parameter can be used to characterize a porous structure, since it is directly linked to the complexity of the flow paths through a medium.

This section will discuss simulations that were performed for body-centred cubic (BCC), hexagonal close packing (HCP), cubic close packing (CCP) and random packed beds using explicit simulations to calculate the tortuosity.

4.2.1. Description

STAR-CCM+® (VERSION 6.02.011) has a built in streamline generator that uses velocity vectors to calculate tracer paths through a medium. The tortuosity of each of the packed beds can be determined by using these flow paths to obtain the ratio between the average lengths a solute travels through a bed, to the length of the bed.

Figure 4.1 shows the structured packed beds used in the tortuosity tests. The same random packed bed (unstructured) that was used in the mesh independency and single velocity tests, was also analysed in this section and can be seen in Figure 3.10. The structured packings were also created in Solid-Works® (2010) with the help of a programmed macro that uses different structured coordinates to generate each of the spheres. All of these coordinates were calculated in EES (VERSION 8.874). The random packing was generated as described in section 3.3.1.

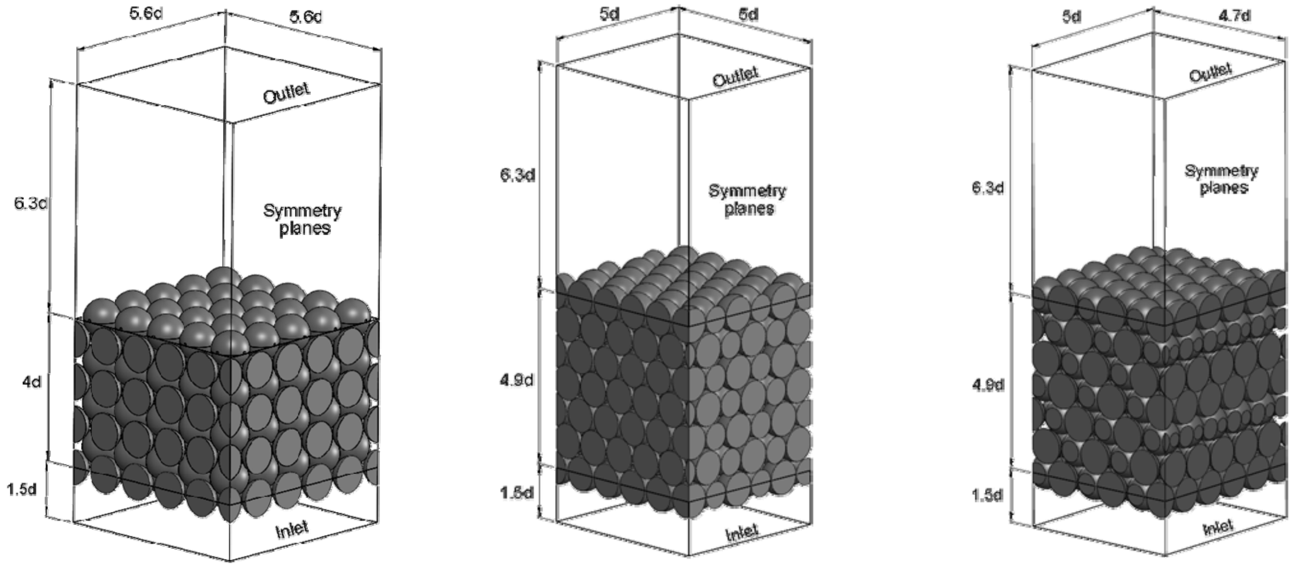

(a) (b) (c)

Figure 4.1: ***Geometrical description of the structure packed beds; (a) BCC, (b) HCP, (c) CCP.***

All of the structured packed beds were constructed using 60 mm spheres that slightly overlapped in the contact regions. An overlap of 0.06 mm was used between the spheres, which is in line with the average overlaps found in the random packed bed as explained in section 3.3.1. The packed beds' properties are shown in appendix A.

The fluid domain was constrained as shown in Figure 4.1, which is similar to the setup used in the mesh independency test. The streamlines were created by equally distributing the number of tracers in a 45 mm radius at the centre, 60 mm below the packed beds.

4.2.2. Boundary, mesh and solver setup

Since the numerical setup was validated in the previous chapter, the same setup will be used for the most of the simulations that follows. Table 4.1 summarizes the boundary conditions, the mesh generation parameters and the turbulence model that was used in the tortuosity tests. The internal and external descriptions refer to the sphere and plane boundaries, with L_{CT} and L_{CM} as their respective surface cell target and minimum sizes. The hybrid wall treatment that was specified relates to the *two-layer all y+ wall treatment*.

Table 4.1: Tortuosity tests: numerical setup

Description	Value
Mesh type	Polyhedral
Contact treatment	Thin mesh
Wall treatment	Hybrid
Wall friction: Spheres	Non-slip: smooth
Fluid used	Nitrogen
Turbulence model	LES
Velocity inlet [m/s]	0.44873
Reference pressure [kPa]	101.325
Static temperature [°C]	26.85
Internal L_{CT} [mm]	1.25
Internal L_{CM} [mm]	0.75
External L_{CT} [mm]	4
External L_{CM} [mm]	2
Cell growth rate	1.5

An inlet velocity of 0.4487 m/s was chosen for the tortuosity tests based on the results obtained in section 3.4.3 that showed that the LES turbulence model delivered the best results when compared to the KTA (1981) correlation at this velocity.

4.2.3. Data sorting technique

All of the packed beds' streamlines were generated in STAR-CCM+® (VERSION 6.02.011) and consisted of at least 50 different tracer elements. A tracer element refers to the path that a weightless particle would follow through a flow field. The number of tracer elements can be varied over a specified area, which allows the elements to follow different paths through the bed. A relatively large number of tracer elements ensure that a representative average of the bed's tortuosity will be obtained.

STAR-CCM+® (VERSION 6.02.011) is only able to present the data of the tracer paths in the form of non-sequential coordinates of all the cells that the tracer elements went through. Thus it was necessary to develop a sorting technique that isolated the different tracer paths and sorted the coordinates sequentially. Figure 4.2 shows the two dimensional (*y*-*z*) coordinates of the different paths that the tracer elements went through in the BCC packed bed.

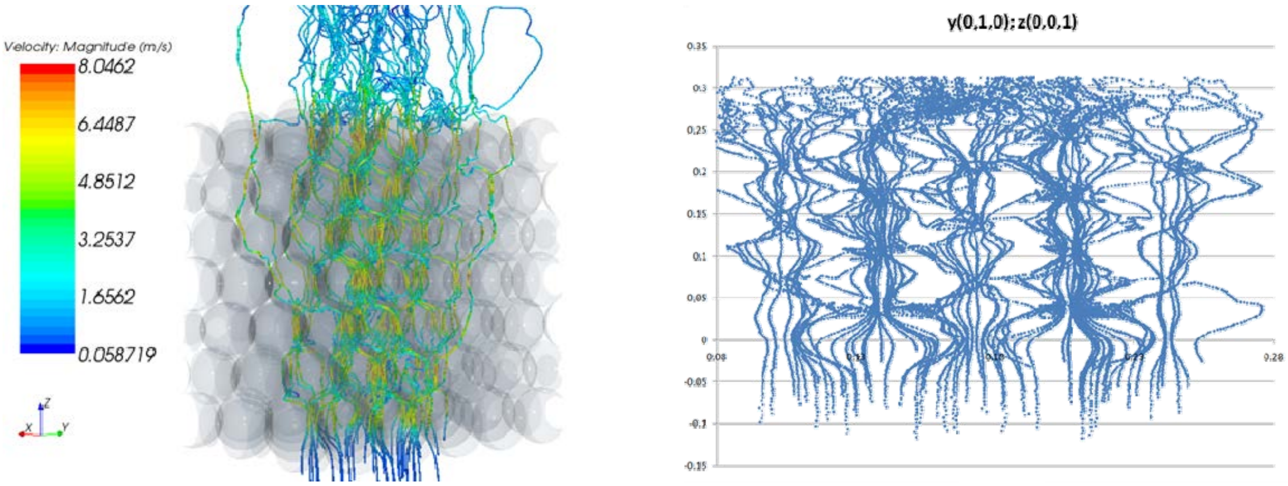

(a)

(b)

Figure 4.2: ***(a) Extracted simulation streamlines and (b) position coordinates of the BCC packed bed plotted in the y-z plane with the y-plane representing the axial direction and the z-plane the radial direction in meters.***

Figure 4.2 also shows that the flow is much more diffusive at the outlet (one sphere distance) than in the rest of the packed bed. Because of this increase in diffusion, the tortuosity calculations were limited to a region 60 mm from the inlet and outlet.

The sorting program was developed in Excel's VB (Visual Basic) code. This program sorted the data by arranging the coordinates axially (smallest to largest) and selecting the first coordinate from the un-sequential data as its first reference coordinate. The program then searched for the coordinate closest to the first reference point from the rest of the data, which would then be used as its next reference coordinate if found. This procedure was iterated until the first tracer path was sequentially sorted or certain criteria and tolerances were met. The program then reset and selected the first coordinate from the remaining data to begin the construction of the next streamline. This procedure would then iterate until all of the tracer path were sequentially sorted.

From Figure 4.2 it is evident that the paths overlap and that close proximities are shared in numerous regions. Because of this close proximity, the final number of sorted streamlines may differ from the original number specified in STAR-CCM+®. When the tracer paths overlap, the sorting algorithm might detect that a coordinate of the overlapping path is closer to its reference point and follow the new path instead. This phenomena is perhaps best explained by Figure 4.3.

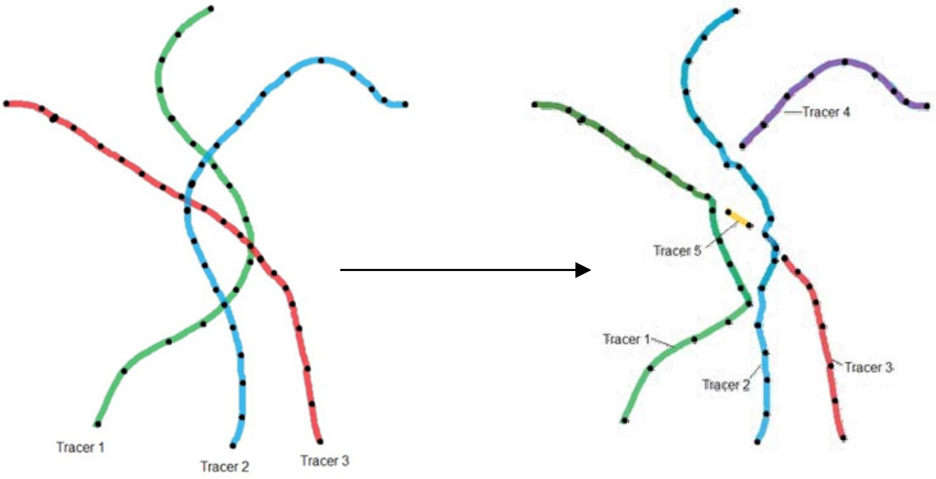

Figure 4.3: The effect overlapping tracer paths has on the number of streamlines.

Since a single tracer path consisted on average of 400 points over a length of 0.3 m, the effects these overlapping points had on the total length were negligible. The sorted data were visually inspected by comparing the raw data with sorted data in a three-dimensional scatter plot. Figure 4.4 shows reconstructed tracer paths of the flow through the BCC packed bed.

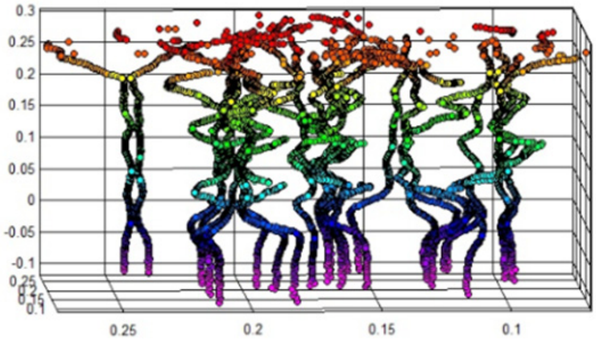

Figure 4.4: Reconstructed tracer paths from the sorted data

The tortuosity for each of the packed beds was obtained numerically by calculating the average resultant lengths of all the tracer paths and dividing them by the average axial lengths between all of the points as shown in Figure 4.5.

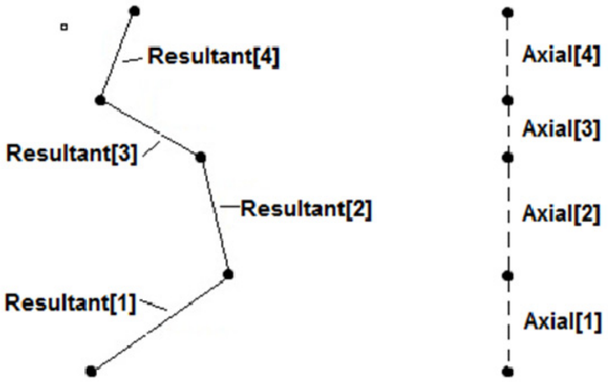

Figure 4.5: The axial and resultant lengths used to calculate the tortuosity of the packed beds.

4.2.4. Results and discussion

Table 4.2 shows the calculated tortuosity results and gives a description of all the tortuosity tests conducted. The RBP description refers to the random bulk packing.

Table 4.2: Tortuosity case description and results.

Test	***Description***	***Inlet velocity [m/s]***	***Pressure drop [Pa/m]***	***Porosity***	***Tortuosity***
T-1	***RBP***	0.2723	25.94	0.375	1.371
T-2	***RBP***	0.6652	65.10	0.375	1.370
T-3	***RBP***	0.4487	46.70	0.375	1.378
T-4	***BCC***	0.4487	50.21	0.320	1.248
T-5	***HCP***	0.4487	268.87	0.259	1.356
T-6	***CCP***	0.4487	322.81	0.259	1.400

The theoretical tortuosity model developed by Lanfrey *et al.* (2010: 1893) shows that tortuosity is independent of the Reynolds number. Tests T-1 to T-3 were conducted to confirm that the tortuosity calculation technique discussed in this section was also independent of the Reynolds number. The tortuosity values for the ***RBP*** tests differ only between 0.073% and 0.56%. These small differences in the tortuosity values can be ascribed to the statistical nature of the flow and the limited number of tracer elements used in the tests. The results of test T-1 to T-3 are thus in line with the findings of Lanfrey *et al.* (2010).

Kim and Chen (2006:129) investigated the diffusive tortuosity through different structures using a Pearsonian random walk simulation of solute tracers. Pure tortuosity can also be derived from their diffusive tortuosity results and is shown in Table 2.3. The BCC and FCC (HPC and CCP) tortuosity results obtained in this study is in good agreement with the results of Kim and Chen (2006:133) as shown in Table 4.3. The random packed bed used by Kim and Chen (2006) was considered to be a loose packing with an original porosity of 0.42. They compressed their random packing structure by allowing adjacent particles to overlap. This was done to obtain tortuosity results for lower porosity packed beds. The tortuosity values between the Pearsonian and the streamline calculations for the random packed beds are in reasonable agreement, deviating by 7.25%. The tortuosity value for Kim and Chen's (2006) random packing was obtained by fitting a fourth order polynomial function through their data and interpolating to a porosity of 0.375.

Table 4.3: Deviation in tortuosity results compared to Kim and Chen's (2006) results

Crystal structure	Deviation [%]
BCC	0.64
HCP	2.65
RBP	7.25

Since Kim and Chen (2006:129) varied their porosities by means of particle overlap, the interpolated tortuosity value cannot be seen as a valid benchmark test. The dynamics of the flow paths are altered when assuming large overlaps between particles and can be confirmed by the findings of Lee *et al.* (2007:2189), who concluded that different contact treatments can influence the flow regime around the spheres significantly.

In chapter 2 it was observed that the theoretical model of Lanfrey *et al.* (2010) tends to over predict the tortuosity values for denser packings since its proportionality constant (k_p) was scaled for an SC unit cell. This proportionality constant was rescaled empirically to the results obtained in this study and is shown in Table 4.4.

Table 4.4: Empirically derived proportionality constant for different porous structures.

Crystal structure	***Proportionality constant [k_p]***
HCP	0.36
BCC	0.46
RBP	0.66

The tortuosity results obtained in this study and those of Kim and Chen (2006:129) are in good agreement even though different simulation techniques were used. This suggests that explicit simulations can be used to obtain the tortuosity values for different porous structures. The streamline technique discussed in this section is less computationally expensive than the Pearsonian random walk simulations used by Kim and Chen (2006) and would thus be recommended.

Further work is needed to validate the empirical proportionality constants shown in Table 4.4, by conducting similar tortuosity tests over a wide range of Reynolds numbers.

4.3. TEMPERATURE MIXING DEGREE (TMD)

The main transport mechanism for mass or thermal dispersion through a packed bed is convection (Van Antwerpen, 2007). Dispersion through a packed bed can be obtained by measuring a concentration or a temperature gradient over a porous medium. Yao *et al.* (2002:236) studied the effect of thermal mixing by defining a dimensionless temperature mixing degree (TMD) which is a unique criterion for characterising a temperature mixing process. They used temperature difference to characterize the degree of mixing efficiency in a hot gas chamber.

The work discussed in this section was conducted to develop the techniques required to study the mixing efficiency of packed beds using the TMD criterion.

4.3.1. Description

The TMD tests calculated the mixing efficiency for BCC, HCP, CCP and RBP packed beds (without wall constraints) for a single velocity. In order to calculate the mixing of a fluid, it is necessary to define or characterise a gradient entity that will be present in one of the two inlet streams. From equation (2.12) it is clear that the TMD equation can also be adopted to calculate the mixing efficiency using any measureable concentration gradient e.g. gas or particles. The TMD tests conducted in this study used a temperature gradient to satisfy equation (2.12) which is in line with the originally proposed function of Yao *et al*. (2002).

The same structured and unstructured packed beds used in the tortuosity tests (section 4.2) were also used in this part of the study. To simulate thermal diffusion through packed beds it was necessary to introduce a temperature gradient at the inlet region. This was done by dividing the inlet region into a hot and cold section. All of the packed beds were fitted with this additional inlet region as shown in Figure 4.6. The ratio between the hot inlet and cold inlet is in line with the ratio used by Kgame (2011) to obtain his braiding temperature profile.

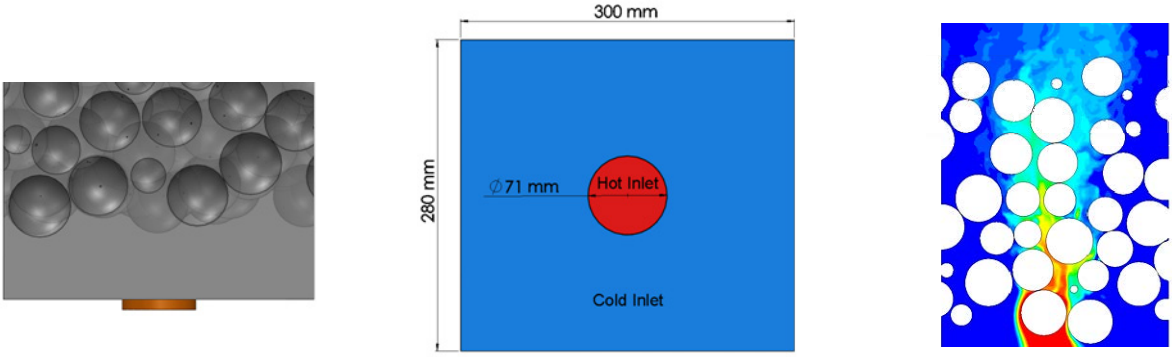

(a) Side view ***(b) Bottom view*** ***(c) Dispersion***

Figure 4.6: (a-b) Fluid inlet regions of the RBP packing as used in the TMD tests, (c) thermal dispersion through the RBP packing.

The TMD measures the mixing efficiency of a structure by comparing the maximum temperature downstream of the fluid stream with the maximum temperature at the inlet. The maximum temperatures were monitored throughout the packed beds by extracting the temperatures from scalar planes, as shown in Figure 4.7. The maximum temperature for each of these sections was calculated by averaging the top 0.02% highest temperatures in the scalar planes. The 0.02% was calculated by dividing the obtained temperature distribution into sections that differs by 0.01°C and calculating the average number of cells within these sections. This was done to ensure statistical stability from unrealistic maximum temperatures that may occur due to skew cells.

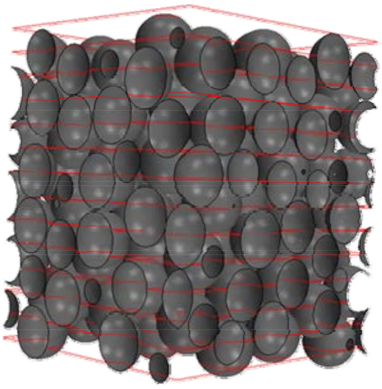

Figure 4.7: ***Scalar plane section used in the TMD tests.***

When this normalized TMD values were compared with the original TMD, it was found that the average deviation between all of the beds was only 0.065%. This indicates that all of the packed beds have high quality meshes. For the rest of this study the TMD was calculated by normalizing the maximum temperature values, as it is considered to be good numerical practice.

4.3.2. Boundary, mesh and solver setup

The numerical setup used for the TMD tests is summarized in Table 4.5. The wall of the cold inlets was specified to be non-slip. This was done to ensure that the cold and hot inlet streams entered the mixing region at the same velocity. An arbitrary temperature difference of 60°C was used between the two inlets streams, since the TMD uses a dimensionless temperature difference to calculate the mixing efficiency.

Table 4.5: Numerical setup for the TMD tests.

Description	Value
Mesh type	Polyhedral
Contact treatment	Thin mesh
Wall treatment	Hybrid
Wall friction: Spheres	Non-slip: smooth
Wall friction: Hot inlet	Slip
Fluid used	Nitrogen
Turbulence model	LES
Velocity inlet: Cold [m/s]	0.44873
Velocity inlet : Hot [m/s]	0.44873
Reference pressure [kPa]	101.325
Static temperature [°C]	26.85
Inlet temperature: Cold [°C]	26.85
Inlet temperature: Hot [°C]	86.85
Internal L_{CT} [mm]	1.25
Internal L_{CM} [mm]	0.75
External L_{CT} [mm]	4
External L_{CM} [mm]	2
Cell growth rate	1.5

A Reynolds independency test was also conducted and will be discussed in the next section. These multi-velocity TMD tests were conducted for 0.1572 m/s, 0.4487 m/s and 0.8975 m/s.

4.3.3. Results and discussion

Figure 4.8 shows the TMD values obtained for the structured and unstructured packed beds. From this data it is evident that the mixing ability of the structured packed beds follows the same type of trend. The results shows that the CCP packing has the best overall mixing ability of the structured beds followed by the BCC and HCP packings. The results show that there appears to be no explicit link between the porosity and mixing abilities of the packed beds tested.

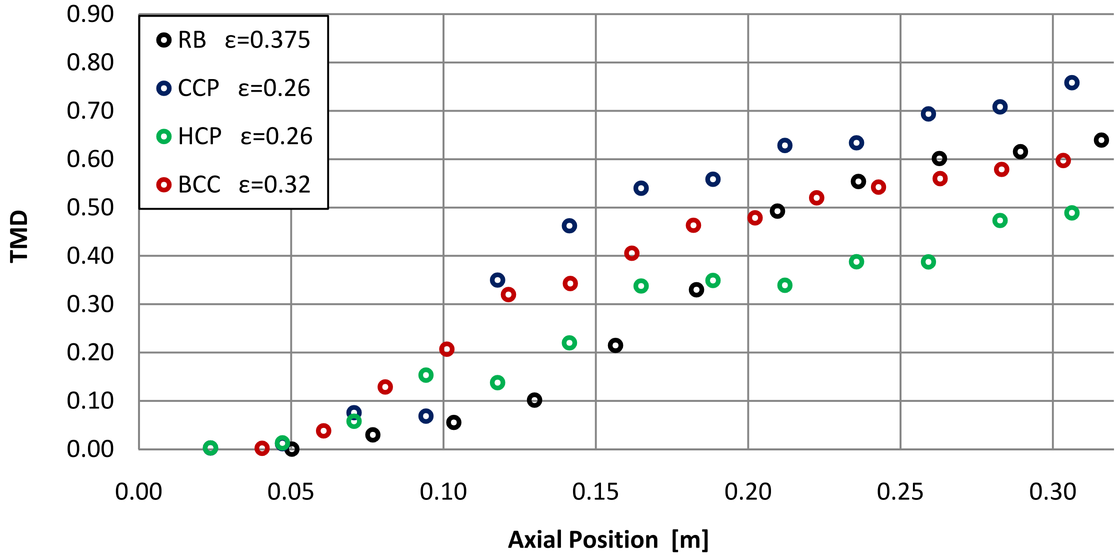

Figure 4.8: ***Axial TMD distribution through the structured and unstructured packed beds.***

The BCC packing, which has a porosity of 0.32 compared to 0.26 of the FCC packings (CCP and HCP), mixes the fluid better than the HCP packing. The RBP packing shows a delayed mixing trend in the inlet region, but rapidly increases after two sphere diameters from the inlet. This is mainly caused by the low porosity at the inlet region of the RBP packing. This low porosity is caused by the coordinate selection in the bulk region of the numerical HTTU packing, which can be seen in Figure 4.6 (a). This inlet mixing of the RBP can thus be considered to be unrealistic.

Figure 4.9 shows the TMD distribution for different Reynolds numbers over the RBP packed bed. The Reynolds numbers that were used in the multi-velocity TMD test were between 600 - 3426. The results appear to be independent of the Reynolds numbers tested, having a maximum deviation of 3.19 % after 0.37 m and maximum average deviation of 4.36% for the whole axial length.

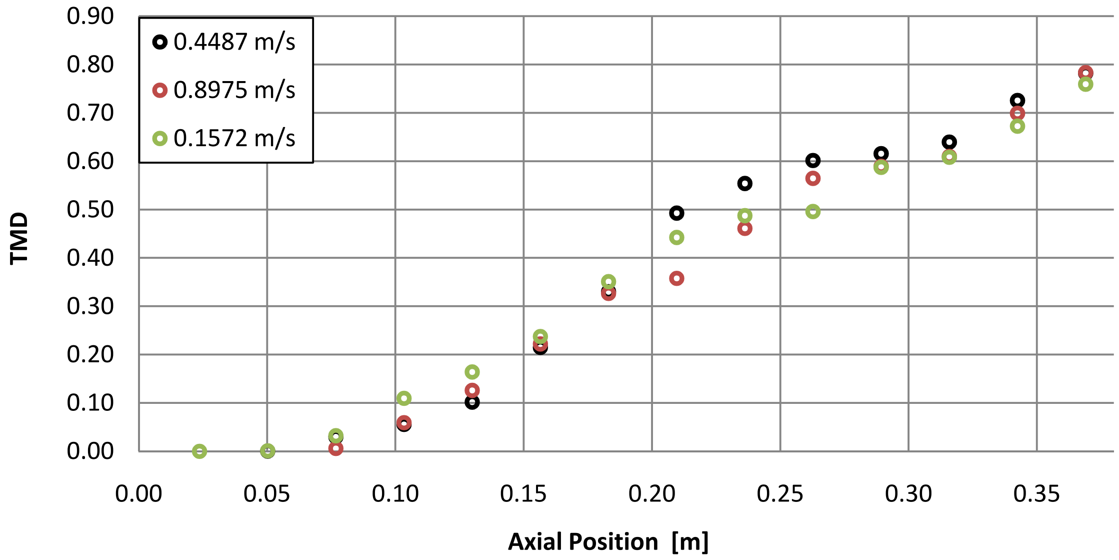

***Figure 4.9:* TMD distribution for the RBP for different Reynolds numbers.**

The relatively small variances in the TMD distribution can be attributed to the dynamic nature of the turbulence model employed (being LES), since it uses transient equations to solve the flow field. Small eddies that exist in the voids of the pebbles have the ability to delay or accelerate small pockets of warm or cold fluid in high temperature gradient regions, as can be seen in Figure 4.10.

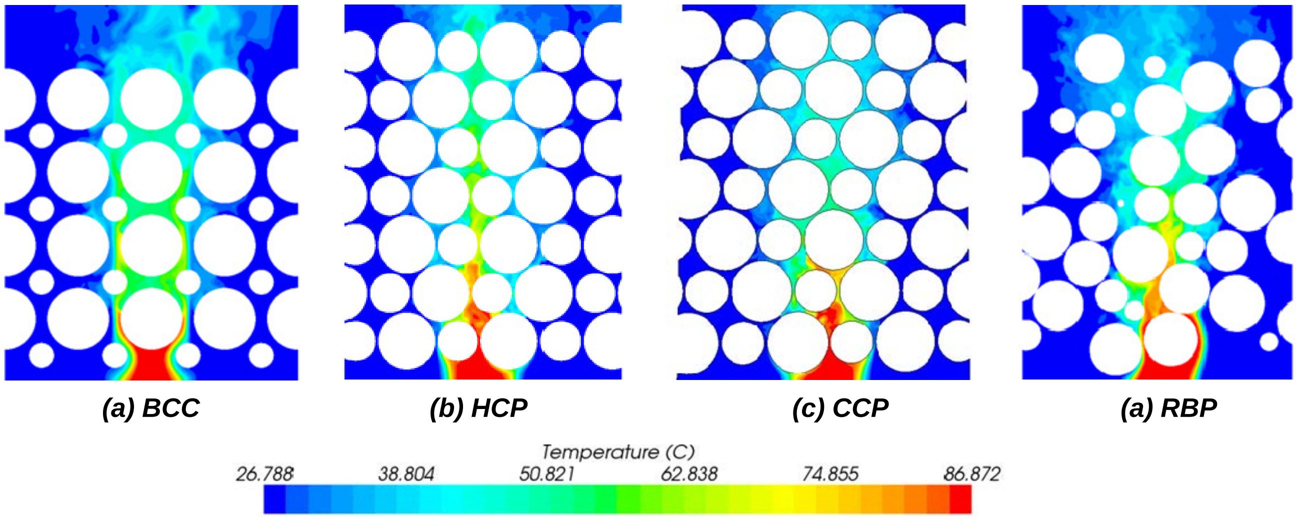

***Figure 4.10:* Temperature distribution through the packed beds used in the TMD tests .**

Both the BCC and HCP packings have flow channels that go straight through the packings as shown in Figure 4.11. This is also one of the reasons why the HCP packing has a lower mixing ability than the rest of the packings which is also evident in Figure 4.10 (b). Since one of the flow paths in the HCP packings is directly in line with the hot inlet, the heat dispersion through that channel is less than observed through the BCC channels.

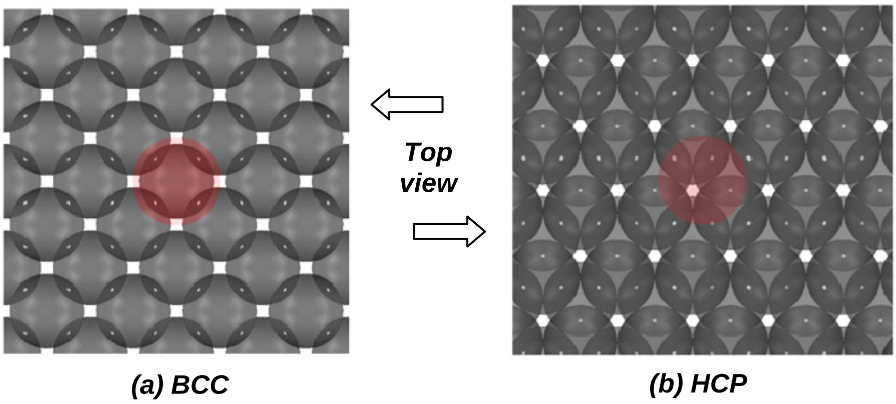

Figure 4.11: The flow channels and hot inlet regions of the (a) BCC and the (b) HCP packed beds, as viewed from above.

From the flow path phenomena and TMD results, it evident that this type of TMD test simulations of structured packed beds should use larger hot inlet regions and longer packed beds in order to draw comprehensive conclusions concerning the mixing abilities of packed beds. Since this study focused more on the methodology and execution of explicit simulations, any further structure and flow analysis was deemed beyond the scope of the study.

Since the computing resources for this study were limited, it is recommended that larger and more extensive explicit packed beds should be used in future studies, to derive concrete conclusions or correlations.

4.4. THE BRAIDING EFFECT

The term 'braiding effect' represents the thermal diffusion enhancement caused by turbulent mixing inside packed pebble beds (Kgame, 2011). This mechanically enhanced diffusion can be accounted for by increasing the effective conductivity of the fluid (Van Antwerpen, 2007). Kgame (2011) calculated this effective radial thermal conductivity coefficient (k_{er}) in a BCC structured packed bed by measuring braiding temperature profiles at the bottom and top of the packing. He then used this experimental data to calculate the k_{er} with CFD simulations as discussed in section 2.6.1.

This section discusses the development and validation of the explicit BETS (braiding effect test section) simulation, as well as the calculation of the effective thermal conductivity caused by the braiding effect for different structured packed beds.

4.4.1. Explicit BETS simulation

The aim of this section is to discuss a simulation similar to the BETS experiment that was performed by Kgame (2011). The BETS experimental setup was discussed in section 2.6.1. The quality of the simulation and the results were determined by comparing the temperature profile obtained in the simulation with the temperature profile measured in the BETS experiment.

The BETS experiment used a BCC packed structure that is different to the BCC packing used thus far in this study. The BCC packings used in the tortuosity and TMD simulations consisted of the conventional structure as shown in Figure 4.1 and Figure 4.11, whereas the BCC structure used in the BETS experiment was orientated on the diagonal plane compared to the conventional structure. This diagonal BCC structure is shown in Figure 4.12 (a) with the red spheres representing the diagonal plane. The main difference between these two types of BCC packings is that the diagonal orientation blocks the flow channels that were able to go straight through in the conventional packing as shown in Figure 4.11 (a) and Figure 4.12 (b).

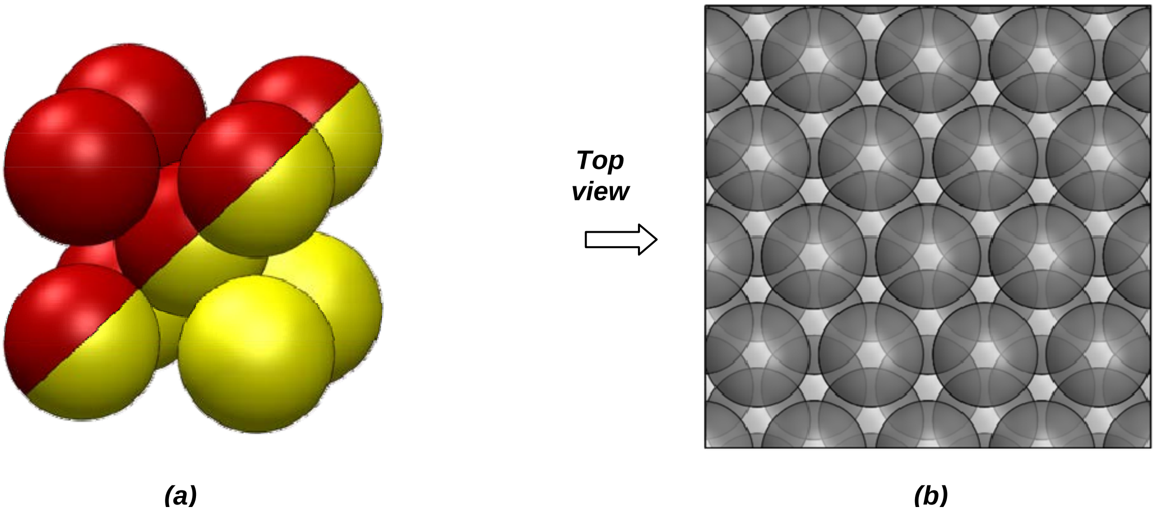

(a) (b)

Figure 4.12: BETS diagonal BCC crystal structure

Figure 4.13 (b) shows the geometry and boundaries used in the BETS simulation. This test section representation of the BETS experiment was also created in Solid-Works® (2010) using macros and coordinates. Due to computational constraints, the simulation only represented 24% of the actual BETS experimental area, as shown in Figure 4.13 (a). The packed bed consisted of 431 spheres (effective) with a pebble diameter of d = 28.58 mm. The fluid domain was constrained by the planes shown in Figure 4.13 (b), with the right vertical plane modelled as a wall and the rest of the vertical planes symmetry boundary conditions.

The sphere structure in the BETS experiment was held together with strings and had a small gap of 2.34 mm between adjacent spheres (Kgame, 2011). This caused the BETS bed to have a porosity value higher than that of the theoretical BCC packed bed ($\varepsilon = 0.352$). The BETS simulation used the same spacing between the spheres but did not include the strings in the geometry.

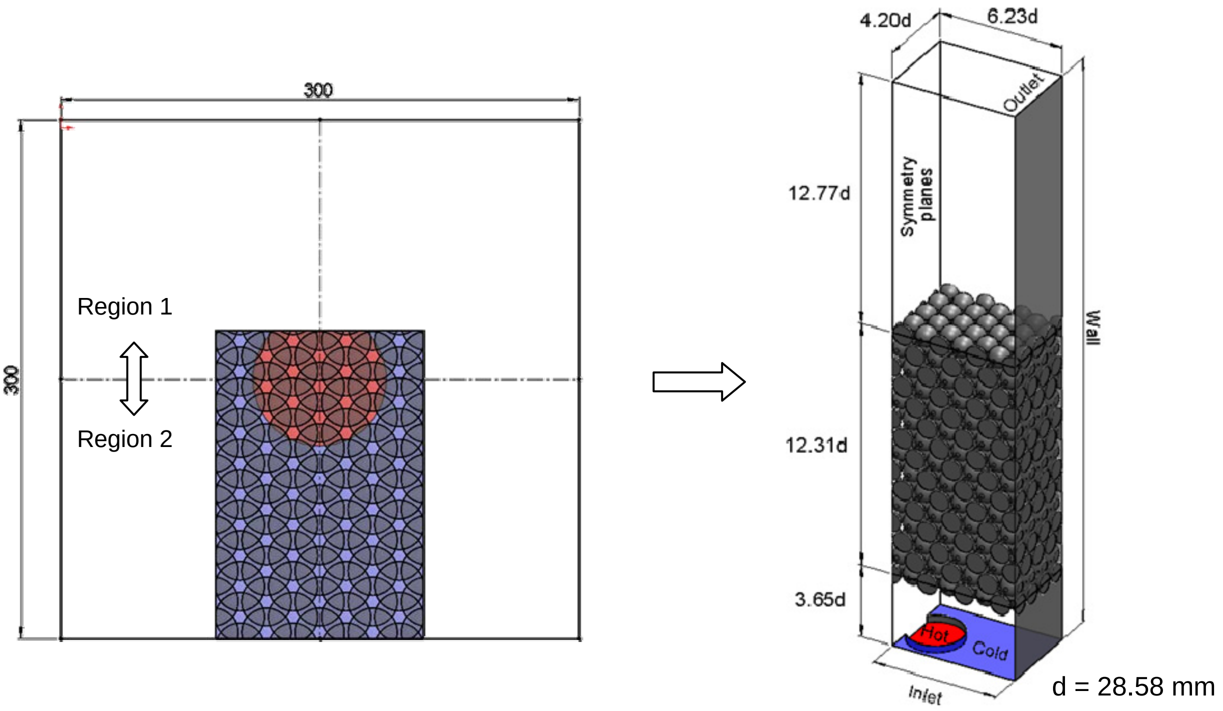

(a) (b)

Figure 4.13: (a) Simulation representation compared to the BETS experiment viewed from the top and the (b) geometrical description of the BETS explicit simulation test

The fluid domain used in this simulation overlaps the centre of the experiment, as can be seen in Figure 4.13 (a). This was done to avoid the effect that the symmetry plane assumptions have on the temperatures at the centre of the packing, since radial sorting technique (that will be discussed below) is very sensitive for the first small increments at the centre.

The BETS simulation only modelled half of the actual length that was used in the experiment. Therefore only the bottom braiding temperature profile was of interest which was situated 4.67d from the top of the packing, as shown in Figure 4.14. This large outlet region was used to avoid

Karman vortex type effects due to the transient nature of the LES turbulence model, which was used to simulate the turbulence present in the BETS experiment.

Kgame (2011) documented the uncertainty values for the BETS tests and noted that the tolerance for the thermocouple installation was 5 mm. For this reason it was decided that the braiding temperature profile would be extracted using plane sections 5 mm above and below the specified height and averaged for the length between the centre and the wall as can be seen in Figure 4.14.

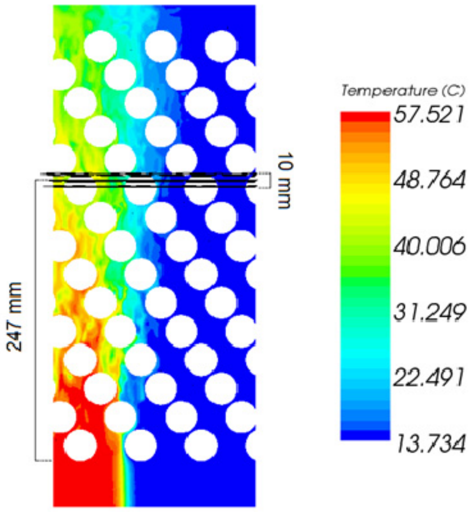

Figure 4.14: Braiding temperature profile planes.

The braiding temperature profile was obtained from the simulation by writing a sorting program in Visual Basic in Excel (Microsoft office 2007). The sorting (averaging) technique used, divided the domain (all the planes extracted) into 1 mm radial sections, as shown in Figure 4.15. The temperatures in these cross sections were averaged and allocated to a radial position between the centre of the bed and the wall.

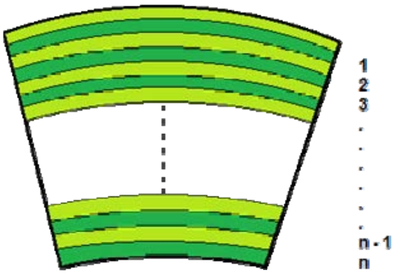

Figure 4.15: Averaging sections used to extract the braiding temperature profile.

Although the pressure drop stays constant when using a transient solver it was noted in the TMD tests that the temperature profiles experienced small changes over time. Thus it was decided to time-average the braiding temperature profiles over four different time steps by extracting the temperature data in one-second intervals. The effect that this time-averaging had on the temperature was not calculated due to the manner in which the data were extracted. It is recommended that further work be done to determine this transient effect the LES turbulence model has on this type of temperature profiles.

4.4.1.1. Boundary, mesh and solver setup

The numerical setup used for the BETS simulation is summarized in Table 4.6. The wall of the cold inlets was specified to be non-slip, to ensure that the cold and hot inlet enter the mixing region at the same velocity.

The same temperature, pressure and velocity inlet conditions used by Kgame (2011) were implemented as boundary conditions for the BETS simulation.

No contact treatment was specified between the spheres, since the gap of 2.34 mm was larger than the minimum cell sizes specified for the internal and external boundaries.

Table 4.6: Numerical setup for the BETS tests

Description	Value
Mesh type	Polyhedral
Wall treatment	Hybrid
Wall friction: Spheres	Non-slip: smooth
Wall friction: Wall	Non-slip: smooth
Wall friction: Hot inlet	Slip
Fluid used	Nitrogen
Turbulence model	LES
Velocity inlet: Cold [m/s]	0.5207
Velocity inlet : Hot [m/s]	0.5207
Reynolds number	3000
Reference pressure [kPa]	300.86
Static temperature [°C]	13.83
Inlet temperature: Cold [°C]	13.83
Inlet temperature: Hot [°C]	57.52
Internal L_{CT} [mm]	0.8
Internal L_{CM} [mm]	0.6
External L_{CT} [mm]	4
External L_{CM} [mm]	2
Cell growth rate	1.5

To accommodate the large number of spheres used in the BETS simulation, it was decided to use a target $d_p / d_c = 35.73$ and a minimum value of $d_p / d_c = 47.63$. This target and minimum pebble-to-cell size ratio deviated by 4.77% from the values determined in the mesh independency study in section 3.3.3 and was deemed to be suitable for these type of simulations.

4.4.1.2. Results and discussion

Figure 4.16 shows the thermocouple installation used in one of the BETS experiments. The simulation conducted in this section correlates to this specific test.

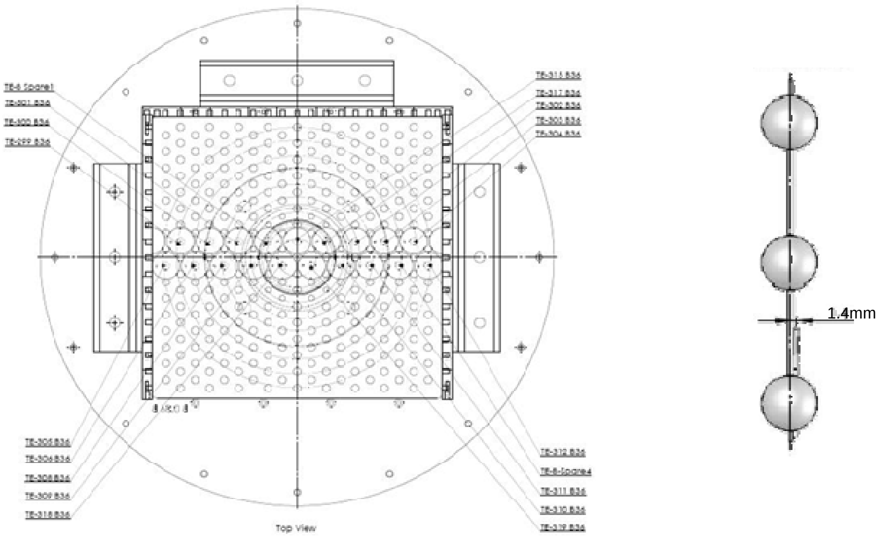

Figure 4.16: BETS Bottom Layer thermocouple installation positions, (Kgame, 2011).

Figure 4.17 shows the braiding temperature profiles obtained experimentally and through the numerical calculations. This figure also shows the polynomial fits of the sixth order through the simulated and experimental data. The experimental data is characterized into two regions as specified in Figure 4.13 (a).

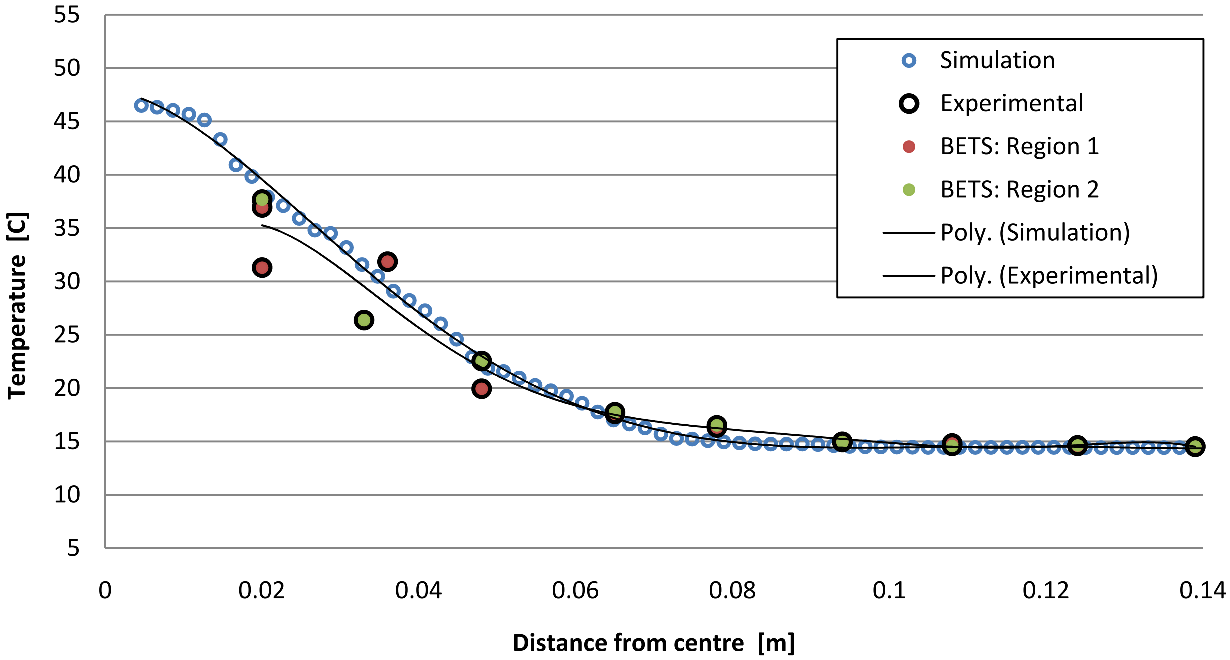

Figure 4.17: The BETS experimental and simulated braiding temperature profiles.

Equation (4.1) and (4.2) shows the polynomial fit and the RSQ value for the simulation data where y represents the braiding temperature and x the distance from the centre of the bed and similarly equation (4.3) and (4.4) represents the experimental data fit and RSQ value.

$$\begin{aligned} y = {} & -19\,156\,375.2246x^6 + 15\,348\,896.0625x^5 - 4\,361\,603.3151x^4 + \\ & 550\,987.9767x^3 - 27\,762.1923x^2 - 50.2940x + 47.9106 \end{aligned} \tag{4.1}$$

$$RSQ = 0.9987 \tag{4.2}$$

$$\begin{aligned} y = {} & -324\,482\,726.9668x^6 + 163\,841\,892.7780x^5 - 32\,734\,883.0908x^4 + \\ & 3\,252\,360.9675x^3 - 162\,382.8900x^2 + 3\,337.1749x + 12.1805 \end{aligned} \tag{4.3}$$

$$RSQ = 0.9528 \tag{4.4}$$

From the experimental results it can be said that the temperature values near the centre were greatly influenced by an unknown factor, since Kgame (2011) calculated the maximum thermocouple deviation as 0.6°C and the maximum temperature difference measured were 6.4°C. This temperature difference phenomenon reaches a maximum deviation at a distance of 20 mm from the centre and is negligible after 65 mm as shown in Figure 4.17. The same phenomenon was observed for a wide range of Reynolds numbers tested in the BETS experiment. Due to this large deviation in the centre region, the RSQ value of the polynomial fit in equation (4.4) is in rather poor agreement with the data.

From equation (4.2) and Figure 4.17 it is evident that the polynomial fit is in good agreement with the averaged simulation data and will thus be used to compare the simulation and experimental results. A maximum deviation of 5.44% and an average deviation of 2.29% were obtained when comparing the simulated and experimental braiding temperature fits. These deviations verify that the simulated and experimental results are in reasonable agreement and further validate the setup and methodologies used.

Figure 4.18 shows the high temperature gradients present in numerous regions due to the structure of the packed bed. The voids or pockets where the thermocouples were installed, were directly above spheres which caused the hot and cold fluid to split over the surface and channel the hot and cold fluid into these pockets, creating a high temperature gradient region.

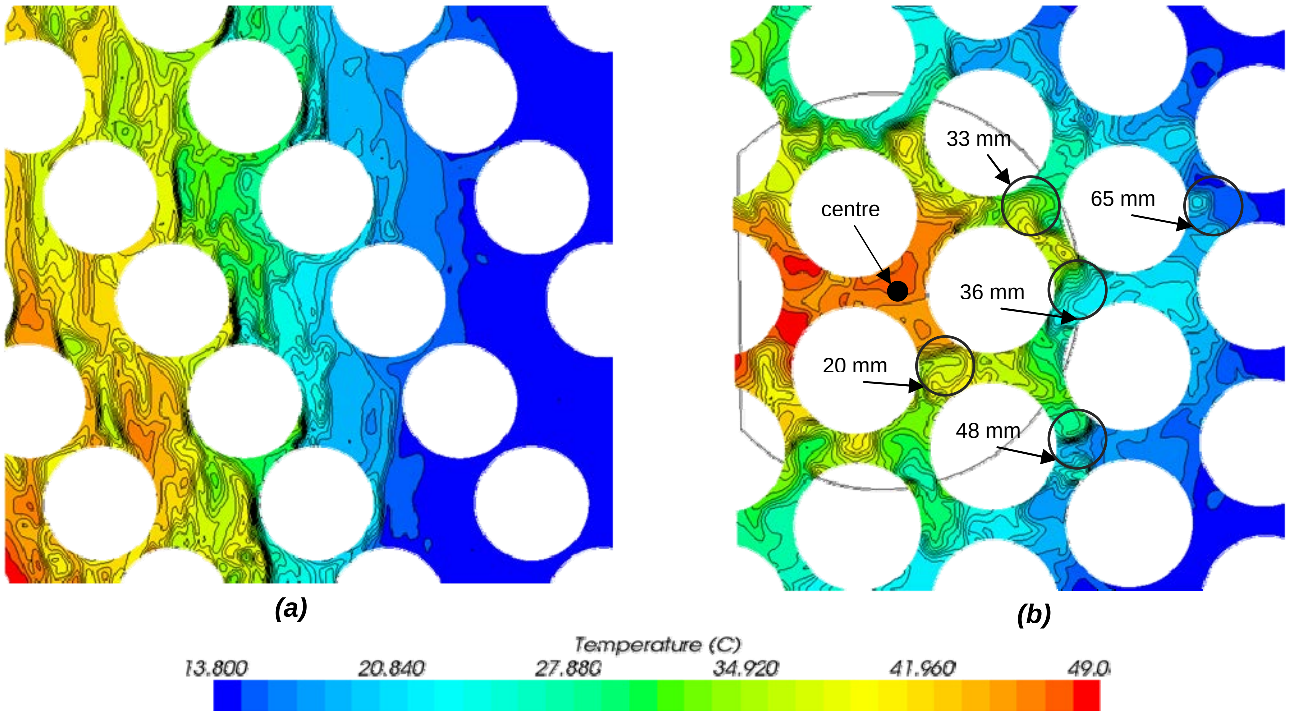

***Figure 4.18:* Temperature gradients in the thermocouple pockets, with (a) viewed in the axially direction and (b) in the radial.**

Figure 4.18 (b) shows some of the different regions where the thermocouples were installed in the BETS experiment in radial distance from the centre. From this numerical result it appears that the high temperature differences measured in the BETS experiment might be caused by the BCC structure and not by human or instrumentation errors.

To investigate this phenomenon further the minimum and maximum temperatures were extracted from the thermocouple regions. This was done with a presentation probe which was set to the tolerances of the thermocouple installation. Figure 4.19 shows the minimum and maximum results obtained in these regions. The same type of high and low trend that were observed in the BETS experiment can also be seen in the simulation results. This demonstrates the ability of numerical calculations to solve complex problems and present solutions which would have been very difficult to obtain experimentally. The simulated maximum values seem to over-predict the experimental temperatures which is expected since the thermocouples did not necessarily measure the maximum temperature over these region. The minimum values are in good agreement with the lower experimental values. Since the experimental temperature profile was derived by averaging the measured temperatures over four different runs, the temperature values were normalized. The simulation results presented in Figure 4.19 were only calculated for a single run. More detailed calculations were deemed outside the scope of this study.

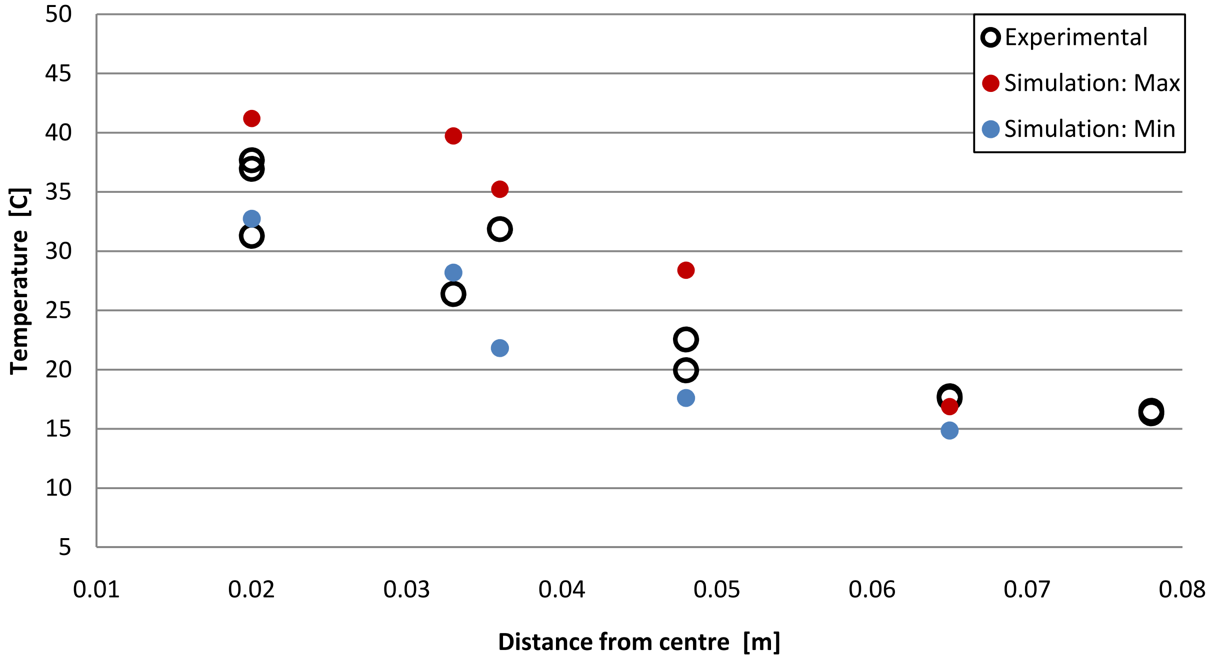

Figure 4.19:* *Minimum and maximum simulation temperatures obtained in thermocouple pockets

From these results it can be concluded that the numerical results validate the simulation setup and that the simulation was able to give valuable insights into the experimental irregularities.

4.4.2. Effective thermal conductivity

Van Antwerpen (2007) noted that the "enhanced" thermal dispersion caused by a porous structure in a fluid can be modelled by increasing the thermal conductivity coefficient of the fluid. Kgame (2011) used this methodology to calculate the effective thermal conductivity of the BETS structure by comparing the experimental radial temperature profile with an implicit BETS simulation's temperature profile and continuously adjusting the fluid's thermal conductivity to obtain the best fit.

As explained in chapter 2, Kgame (2011) already demonstrated how the effective thermal conductivity can be obtained by means of a CFD simulation and an experimentally measured temperature profile. This same procedure was used to expand on Kgame's study for random, BCC, HCP and CCP packed beds. In order to develop a robust methodology for the explicit simulation of thermal dispersion through packed beds, it was necessary to validate the boundary conditions, physics model and the mesh conditions for the different simulation models. This validation was done by comparing the BETS experimental temperature profiles with the temperature profiles obtained by the simulation model.

The boundary conditions were set up to represent the BETS test section without the explicit or implicit presence of the spheres. This was done with the intention that the molecular and turbulent thermal conductivity solely accounted for the enhanced (extra/turbulent) mixing.

Although Kgame (2011) simulated an eighth of the BETS test section implicitly, this study simulated the whole BETS test section. This was done due to preliminary results that showed that the symmetry planes had indeed had an effect on the temperature profile through the bed as shown in Figure 4.20.

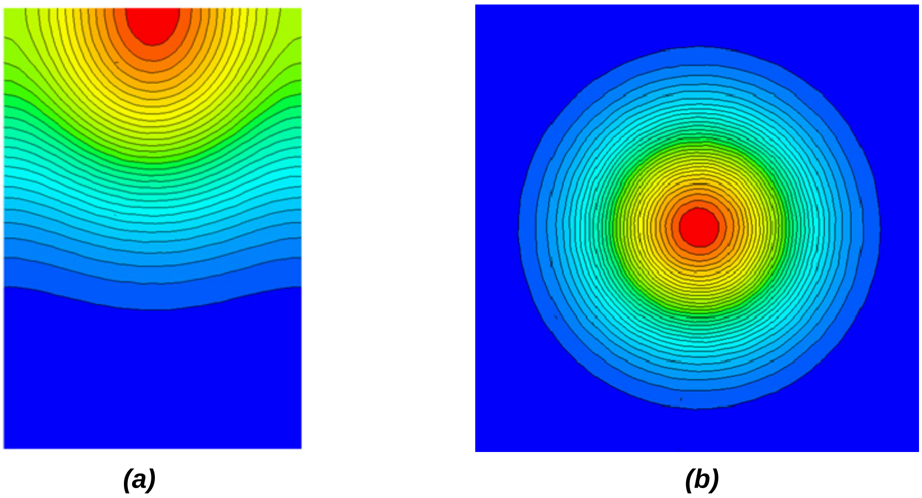

***Figure 4.20:* The effects of the symmetry planes have on the temperature profile with (a) the sectioned and (b) the total BETS section.**

The symmetry planes use the parallel components of velocity and temperature from the adjacent cells and reconstructed gradient to calculate the face values (the shear stress and heat flux is zero at the boundary). Because the temperature distribution is cylindrical, the non-cylindrical symmetry constraints cause irregularities at the boundaries as the planes only extrapolated the parallel components.

The effective thermal conductivity was calculated by iteratively guessing a value for the molecular thermal conductivity of the fluid. This was done in order to fit the simulation temperature profile to the experimental temperature profile. Kgame (2011) used the square of the Pearson product moment correlation coefficient (RSQ) as his fitting criteria. As mentioned in section 2.6.1, The RSQ parameter can lead to inaccurate answers with uneducated initial guess values. This is because the RSQ correlation coefficient does not take the residuals between the simulated and experimental temperature profiles into account. Therefore it was decided to combine the RSQ parameter with the root mean square deviation coefficient (RMSD). This combined coefficient (CC) is defined as:

$$CC = RMSD \times (1 - RSQ) \times 100 \tag{4.5}$$

This CC parameter was used to calculate the optimal fit between the simulated and experimental temperature profiles. Figure 4.21 shows the convergence of CC parameter for different k_{er} values. A third order interpolation technique was used to calculate the lowest CC value between the guess values.

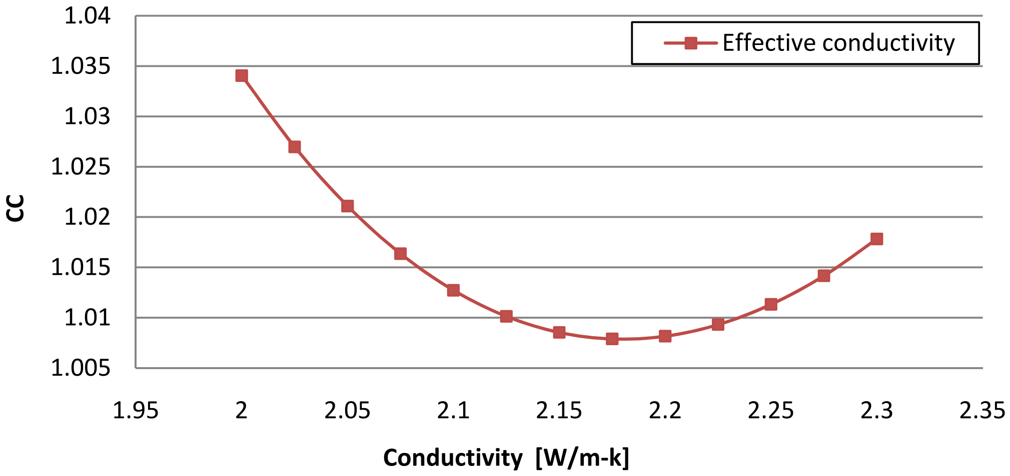

Figure 4.21: Combined coefficient convergence for the BETS test.

Two different geometries were used in this section. Figure 4.22 (a) and (b) shows the geometry and boundaries used to calculate k_{er} for the BETS and different bulk packings. The packed beds simulated in the TMD test were used to derive the different braiding temperature profiles needed to calculate k_{er} in the implicit simulation shown in Figure 4.22 (b). Consequently the hot inlet wall constraints differ from the BETS implicit simulation in (a).

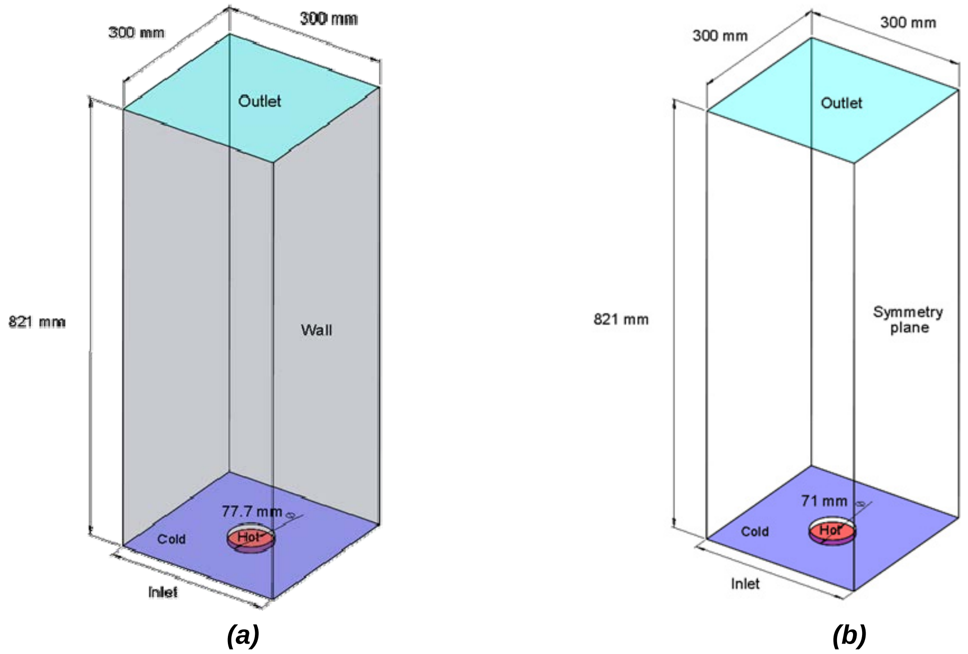

***Figure 4.22:** Implicit BETS simulation geometry with wall constraints (a) and implicit geometry with symmetry planes (b).*

The braiding temperature profiles were extracted by employing the same technique used in section 4.4.1. For the bulk tests, the temperature profile was extracted at a height of 265 mm from the bottom of the packing as shown in Figure 4.23 (a).

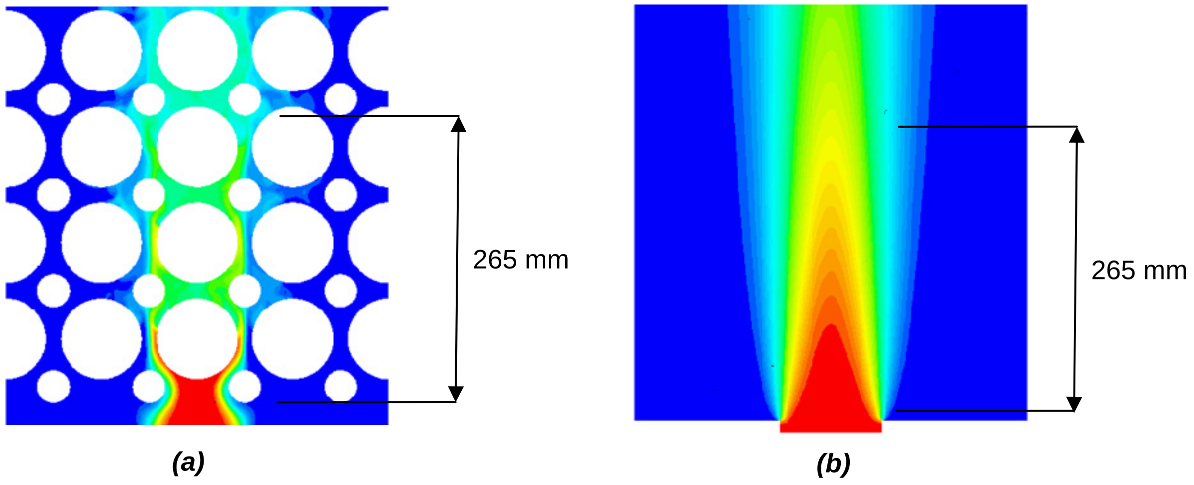

***Figure 4.23:** Implicit simulation temperature distribution and temperature extraction regions.*

The implicit simulations modelled the diffusion of the packed beds from the inlet regions, therefore the height of the extracted temperature profiles were measured from the cold inlet region as shown in Figure 4.23 (b). It was thus assumed that the short inlet region of the explicit simulation, that is needed for flow development, has a negligible small thermal diffusion effect due to the relatively small molecular conductivity coefficient in this region.

4.4.2.1. Boundary, mesh and solver setup

The numerical setup used for the BETS implicit simulation is summarized in Table 4.7. The "bulk" column represents the setup used for the different bulk structures.

Table 4.7: Numerical setup for the effective conductivity tests

Description	BETS	Bulk
Mesh type	Polyhedral	Polyhedral
Wall treatment	Hybrid	Hybrid
Wall friction	Non-slip: smooth	-
Wall friction: Hot inlet	slip	slip
Fluid used	Nitrogen	Nitrogen
Turbulence model	LES	LES
Velocity inlet: Cold [m/s]	0.5207	0.4487
Velocity inlet : Hot [m/s]	0.5207	0.4487
Reynolds number	3000	1713
Reference pressure [kPa]	300.86	101.33
Static temperature [°C]	13.83	26.85
Inlet temperature: Cold [°C]	13.83	26.85
Inlet temperature: Hot [°C]	57.52	86.85
Internal L_{CT} [mm]	3	3
Internal L_{CM} [mm]	1	1
External L_{CT} [mm]	3	3
External L_{CM} [mm]	1	1
Cell growth rate	1.3	1.3

To verify that the target cell size was sufficient to model the thermal diffusion through a fluid column, a brief mesh independency test was conducted and the results are shown in Figure 4.24. This test used a high effective thermal conductivity or fluid (nitrogen) thermal conductivity coefficient of 3 W/m-k for both cases.

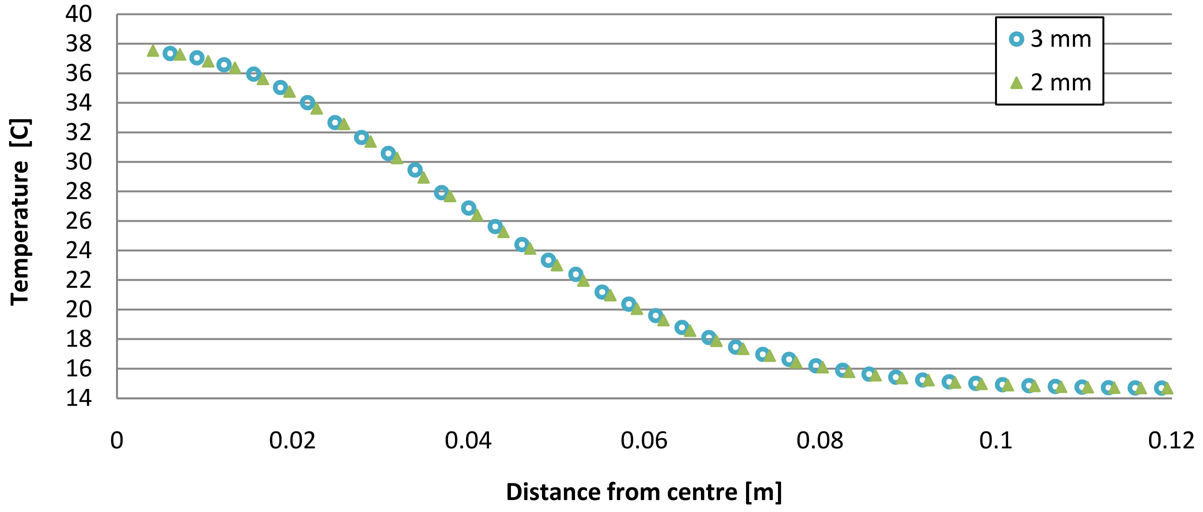

Figure 4.24: Implicit mesh independency study.

The results show that the temperature profiles obtained from these implicit simulations are identical. Thus it can be concluded that the results are mesh independent for both these cases and that it a target cell size of 3 mm was sufficient.

4.4.2.2. Results and discussion

Kgame (2011) calculated the effective thermal conductivity of the BETS beds by using the RSQ parameter, as shown in Table 4.8. His simulations were only able to converge to an RSQ value of 0.973 which gave a conductivity of $k_{er} = 3.01$ W/m-K. Table 4.8 also shows the three tests conducted with the data obtained in this study, with k-1 and k-2 using the RSQ parameter approach and k-3 the CC parameter approach. From this results it is evident that k_{er} is very sensitive to different RSQ values. Table 4.8 shows that k-1 has the same RSQ value as the value obtained by Kgame (2011) and produced a similar effective conductivity value of $k_{er} = 3.16$ W/m-K, deviating by 5.1% from that of Kgame (2011).

This study was able to obtain much higher RSQ values than Kgame (2011) and resulted in a very different effective conductivity result as reflected in k-2. These high RSQ values were greatly improved with the total BETS implicit simulations when compared with the sectioned BETS simulations (as used by Kgame (2011)) due to the symmetry phenomena as shown in Figure 4.20.

Table 4.8: Effective conductivity comparison.

Test	RSQ	RMSD	CC	k_{er}
Kgame (2011)	0.973	-	-	3.01
k-1	0.973			3.16
k-2	0.9941	-	-	1.57
k-3	0.9928	1.397	1.008	2.18

Figure 4.25 shows the implicit temperature profiles obtained from the BETS test section, with different gas conductivity coefficients. The conductivity guesses ranged between 3 and 2 W/m-k and converged to a value of $k_{er} = 2.18$ W/m-k when using the CC parameter.

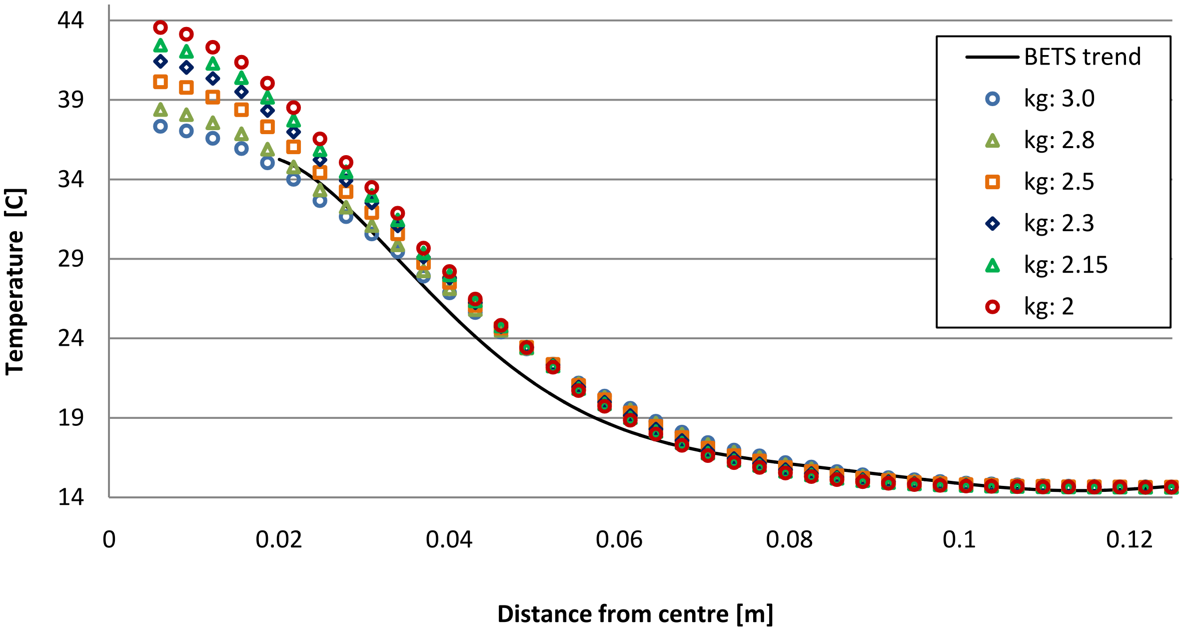

Figure 4.25: Implicit temperature profiles with different gas conductivities and the BETS normalized experimental temperature profile.

Appendix B shows the braiding temperature profiles and implicit temperature profiles obtained for the different packed beds tested in this section.

Table 4.9 shows the results obtained for all of the effective conductivity tests conducted. Results EC-3 to EC-6 represents the bulk region tests and was calculated in the same manner used to calculate the BETS effective conductivity value. From the bulk tests it is evident that much larger deviations can be observed between the different packing structures than those observed in the tortuosity and TMD results. The same beds that were used in the TMD tests were also used for the effective conductivity tests (EC-3 to EC-6), therefore the same inadequacies will apply to them. The RBP bed has the highest thermal diffusion coefficient followed by the CCP, BCC and HCP beds, which is similar to the results obtained in the TMD tests. It can also be observed that the effective thermal conductivities obtained for the bulk BCC and the BETS BCC beds differ by 35.3%. This large deviation can be linked to the different BCC orientation, different porosities, wall constraints, difference in the temperature extraction height, different velocities used, different temperature differences between the hot and cold inlets as well as the different bed sizes.

Table 4.9: Effective conductivity tests description and results.

Test	*Description*	k_{er} *[W/m-K]*
EC-1	***BETS-1***	2.18
EC-2	***BETS-2***	2.04
EC-3	***RBP***	1.28
EC-4	***CCP***	1.05
EC-5	***BCC***	0.77
EC-6	***HCP***	0.48

Tests EC-1 and EC-2 show the effective thermal conductivity obtained by fitting the implicit results to the experimental and simulated temperature profiles. A deviation of 6.90% can be observed between these two tests, which is a reasonable result since the BETS experiment only used nineteen thermocouples and lacked detail in its temperature profiles.

It can be concluded that the BETS results obtained in this study are in good agreement with the results of Kgame (2011) when the same fitting techniques were used, which validates the numerical setup used for these tests. The results also show that this fitting technique is highly sensitive for values of the RSQ parameter and that the exclusion of the symmetry planes and the introduction of the CC parameter improved the stability of the solutions.

4.5. CONCLUSION

Packed beds are generally used in industry due to their attractive contact-to-flow area ratio which gives them exceptional mixing abilities. To be able to do a detail characterization of a packing structure, it is vital to understand the fluid mechanics through a packed bed. The first fundamental step towards a better understanding of the effect a packed bed structure has on flow is to study its mixing ability. This chapter showed that explicit simulation is able to accurately model enhanced thermal diffusion due to turbulent mixing, through packed beds. Various enhanced mixing tests were developed and conducted in this section. These mixing tests were not only used to gain valuable insights into the flow through packed beds, but were also used to validate the numerical methodology and setup.

In the tortuosity study discussed in section 4.2, it was found that the tortuosity calculations are independent of the Reynolds number, which is also confirmed by Lanfrey *et al.* (2010). The tortuosity results obtained for the BCC and HCP packed beds were in good agreement with the results of Kim and Chen (2006:133), deviating 0.64% and 2.65%, which validated the sorting technique developed and used in this section. The results of their random packing were discarded since it was not directly applicable to the structure used in this study. It was also observed that the theoretical model of Lanfrey *et al.* (2010) tends to over-predict the tortuosity values for denser packings which can be ascribed to the proportionality constant (k) that was scaled for an SC unit cell in their model.

The results from the TMD tests showed that there appears to be no specific link between the porosity and mixing abilities of the packed beds tested, but this could be attributed to the relatively small beds used and the positioning and size of the warm outlet used. It was also observed that the RBP showed a delayed mixing trend in the inlet region, which was attributed to the low porosity in this region which is unrealistic. A multi-velocity TMD test for the RBP was conducted for Reynolds numbers between 600 - 3426. The results showed the TMD criteria to be independent of the Reynolds numbers tested. It was concluded that the results indicated that more elaborate packed beds are needed to derive concrete conclusions from this type of mixing tests.

The same type of high and low temperature trend that were observed in the BETS experiment could also be seen in the simulation results and was attributed to the thermocouples' positioning in high temperature gradient areas within the BCC structure. A maximum deviation of 5.44% and an average deviation of 2.29% were obtained between the simulated and experimental braiding temperature fits. These relatively small deviations verify the setup and methodologies used.

In the effective thermal conductivity section it was noticed that the symmetry planes used in the implicit simulation caused irregular braiding temperature profiles. This was ascribed to the symmetry planes that only extracted the parallel component from a cylindrical temperature distribution to reconstruct the different gradients at the perpendicular boundaries. Thus it was decided to model the whole BETS test section. It was concluded that the BETS results obtained in effective thermal conductivity study were in good agreement with the results of Kgame (2011) when the same fitting techniques were used, which validates the numerical setup used for these tests. The results also show that this fitting technique is highly sensitive for values of the RSQ parameter and that the exclusion of the symmetry planes and the introduction of the CC parameter improved the stability of the solutions.

5

SUMMARY AND CONCLUSION

5.1. EXECUTIVE SUMMARY

This study addressed the numerical modelling of flow and diffusion in packed beds of mono-sized spheres.

Chapter 1 showed the need for the development of a numerical modelling methodology for packed beds which is crucial to obtain highly accurate explicit simulation results. Attention was given to the numerical approach needed to address the treatment of the contact between spheres, the resolution of the computational mesh and the modelling of turbulence. Emphasis was placed on the development of explicit simulations and techniques necessary to extract and compare different mixing parameters. The numerical methodology was to be validated by comparing the simulated results with different pressure drop correlations and by comparing the mixing parameters obtained in this study with those from previous work. The aim of this study was not to derive correlations or to implement correlations into any form of implicit simulation.

Chapter 2 identified different enhanced mixing parameters that could provide valuable insights into the flow phenomena inside packed beds. It was noted that the broad set of guidelines for the simulation of packed beds can be further focussed and improved e.g. the numerical approach needed to address the treatment of the contact between spheres, the resolution of the computational mesh, and the modelling of turbulence. The contact treatment techniques in literature generally propose simplifications which cannot be used to simulate heat transfer between spheres. No recommendations were found in the literature for the use of any specific turbulence model in the transitional flow regime, since all previous attempts proved to be inaccurate. It was also noted that the mesh generation and mesh independency studies were somewhat limited, which is unfortunate.

Chapter 3 addressed a number of numerical issues in the development of an appropriate modelling approach. The results presented a sound modelling methodology, capable of producing accurate numerical results. The main factors that were considered important to the accuracy of this type of simulations were contact treatment, mesh density and the turbulence model. The contact treatment study concluded that flow can be successfully modelled with a small gap approximation but in order to realistically model all the aspects of the contact geometry without compromising computational resources, the newly developed thin mesh contact treatment would be recommended. The numerical setup was validated in the mesh independency study by comparing the simulated pressure drop with the pressure drop predicted by the KTA (1981) and Eisfeld and Schnitzlein (2001) pressure drop correlations, which were in excellent agreement. This section also showed for the first time that the LES turbulence model was the only model capable of accurately predicting the pressure drop for low Reynolds numbers in the transition regime. This section also implemented a new technique to solving the LES turbulence model which decreases the computational expense of this transient solver.

Chapter 4 showed that explicit simulations are able to accurately model enhanced thermal diffusion due to turbulent mixing through packed beds. These mixing tests were not only used to gain valuable insights into the flow through packed beds, but were also used to validate the numerical methodology and setup. In the tortuosity study it was found that the tortuosity calculations were independent of the Reynolds number, and that the newly developed tortuosity tests were in good agreement with previous techniques used. The results from the TMD tests showed that there appears to be no specific link between the porosity and mixing abilities of the packed beds tested, but could be attributed to relatively small bed sizes used and the positioning and size of the warm inlet. A multi-velocity test showed that the TMD criterion is independent of the Reynolds number. It was concluded that the results from the TMD tests indicated that more elaborate packed beds were needed to derive applicable conclusions from this type of mixing tests. The explicit BETS simulation results confirmed the high and low temperature trends that were observed in the experimental data and was attributed to the thermocouples being placed in high temperature gradient areas. Relatively small deviations between the simulation and experimental data also verified the setup and methodologies used. It was concluded that the BETS results obtained in the effective thermal conductivity study were in good agreement with the results of Kgame (2011) when the same fitting techniques were used. The results also showed that this fitting technique is highly sensitive for values of the RSQ parameter and that the exclusion of the symmetry planes improved the RSQ results. It was concluded that the introduction of the new CC parameter is more suited for this fitting technique than using only the RSQ parameter.

5.2. CONCLUSION

It can thus be concluded that all the outcomes defined in Section 1.3 were met. Comprehensive research was conducted in order to implement various numerical constraints into explicit and implicit simulations of flow through packed beds of uniform spheres. New modelling approaches and methodologies were developed and thoroughly validated using five different criteria from previous work. In addition to the validations done, numerous modelling implementations of experiments were conducted for different packed beds that gave interesting insights into the fluid mechanics of flow through packed beds. The explicit simulations were not only able to accurately predict the spatial distribution of different flow parameters, but also to give valuable insights into some irregularities found in experimental measurements. However, some additional research should be done on expanding the size of the packed beds before concrete conclusions or implicit correlations can be derived from this type of simulations.

5.3. RECOMMENDATIONS FOR FURTHER RESEARCH

Although the methodology of explicitly modelling flow through packed beds was comprehensively validated, the following recommendations regarding the expansions and applicability of the packed beds can be made:

- The mesh independency tests were only conducted for a single Reynolds number and need to be expanded to an array of higher Reynolds numbers to be able to determine the numerical reach of different mesh sizes at elevated velocities.

- Although a wider range of Reynolds numbers were tested for the turbulence models, it is still unclear how the LES turbulence model will perform with very high Reynolds numbers.

- Further work is needed to validate the empirical proportionality constants shown in Table 4.4, by conducting similar tortuosity tests over a wide range of Reynolds numbers.

- In the TMD tests it was noticed that the size of the hot inlet to particle size influenced the mixing through the beds, especially in the structured packings. The effect of this ratio should be further investigated in order to improve the TMD and the secondary braiding effect test results.

- The RBP packing that was used to represent the bulk region of a random packed bed had a low porosity inlet region since the partially generated spheres were excluded from this inlet geometry. This resulted in an unrealistic TMD distribution which should be re-evaluated using a randomly packed bed that includes a realistic inlet region.

- Computing resources was the limiting factor to the size of the packed beds that could be accurately modelled. It is recommended that future studies implement more elaborate beds to determine the effect of some parameter constraints on the results obtained in this study.

BIBLIOGRAPHY

ASHBY, M.F. & JONES, D.R.H. 2002. Engineering materials 1: an introduction to their properties and applications. 2nd ed. London: MFG Books Ltd. p 45-57.

BEY, O. & EIGENBERGER, G. 1996. Fluid flow through catalyst filled tubes. *Chemical engineering science*, 52(8):1365-1376, Nov.

CALIS, H.P.A., NIJENHUIS, J., PAIKERT, B.C., DAUTZENBERG, F.M. & VAN DEN BLEEK, C.M. 2001. CFD modelling and experimental validation of pressure drop and flow profile in a novel structured catalytic reactor packing. *Chemical engineering science*, 56(4):1713-1720, Feb.

CD-ADAPCO. 2010. User's Manual to Star-CCM+® VERSION 6.02.011, New York, US.

CHUNG, T.J. 2002. Computational fluid dynamics. 1st ed. Cambridge: Cambridge University Press. p. 679-710.

DE KLERK, A. 2003. Voidage variation in packed beds at small column to particle diameter ratio. *Advances in chemical engineering*, 49:2022–2029.

DU TOIT, C.G., VAN DER WALT, A.J.K. & VAN DER MERWE, J. Using effective viscosity to account for the effect of the walls on the pressure drop through an annular packed bed. (*In* Proceedings HTR2008: 4th International Topical Meeting on High Temperature Reactor Technology, September 28 – October 1, 2008, Washington DC, USA.)

DU TOIT, C.G. 2008. Radial variation in porosity in annular packed beds. *Nuclear engineering and design*, 238(11): 3037-3079, Nov

EISFELD, B. & SCHNITZLEIN, K. 2001. The influence of confining walls on the pressure drop in packed beds. *Chemical engineering science*, 56(2001):4321-4329, Nov.

ERGUN, S. 1952. Fluid flow through packed columns. *Chemical engineering progress,* 48(2):89-94, Feb.

FLUENT USER SERVICE CENTRE. 2005. Introductory Fluent notes V6.4. http://my.fit.edu/itresources/manuals/fluent6.3/help/html/ug/node511.htm Date of access: March 2005.

GIESE, M., ROTTSCHÄFER, K. & VORTMEYER, D. 1998. Measured and modelled superficial flow profiles in packed bed with liquid flow. *The American institute of chemical engineers journal*, 44(2):484-490, Feb.

GUARDO, A., COUSSIRAT, M., LARRAYOZ, M.A., RECASENS, F. & EGUSQUIZA, E. 2005. Influence of the turbulence model in CFD modelling of wall-to-fluid heat transfer in packed beds. *Chemical engineering science*, 60(6):1733-1742, March.

HASSAN, Y.A. 2008. Large eddy simulation in pebble bed gas cooled core reactor. *Nuclear engineering and design,* 238:530–537.

HLUSHKOU, D. & TALLAREK, U. 2006. Transition from creeping via viscous-inertial to turbulent flow in fixed beds. *Journal of chromatography A,* 1126:70-85, Jun.

JAFARI, A., ZAMANKHAN, P., MOUSAVI, S.M. & PIETRARINEN, K. 2008. Modelling and CFD simulation of flow behaviour and dispersivity through randomly packed bed reactors. *Chemical engineering journal,* 144:476-482.

KGAME, T.L. 2011. Evaluation of the enhanced thermal fluid conductivity for gas flow through structured packed pebble beds. Potchefstroom: North-West University. (Dissertation - M.Eng.)

KIM, A.S. & CHEN, H. 2006. Diffusive tortuosity factor of solid and soft cake layers: a random walk simulation approach. *Journal of membrane science,* 279(2006):129-139.

KTA (KERN TECHNISCHES AUSSCHUSS NUCLEAR SAFETY STANDARDS COMMISSION). 1981. Reactor core design of high-temperature gas-cooled reactor, part 3: loss of pressure through friction in pebble bed cores. Safety Standards, KTA 3102.3, Issue 3/81.

LANFREY, P.Y., KUZELJEVIC, Z.V. & DUDUKOVIC, M.P. 2010. Tortuosity model for fixed beds randomly packed with identical particles. *Chemical engineering science,* 65(2010):1891–1896.

LAUNDER, B.E. & SPALDING, B. 1974. The numerical computation of turbulent flows. *Computer methods in applied mechanics and engineering,* 3(2):269-289, March.

LEE, J.,PARK, G., KIM, K. & LEE, W. 2007. Numerical treatment of pebble contact in the flow and heat transfer analysis of a pebble bed reactor core. *Nuclear engineering and design*, 237(22):2183-2196, Nov.

LIU, F.L., ZHANG, Z.P. & YU, A.B. 1999. Dynamic simulation of the centripetal packing of mono-sized spheres. *Physica A*, 268:433–453.

LOGTENBERG, S.A., NIJEMEISLAND, M. & DIXON, A.G. 1999. Computational fluid dynamics simulations of fluid flow and heat transfer at the wall-particle contact points in a fixed-bed reactor. *Chemical engineering science,* 54:2433-2439.

MCLAUGHLIN, B., STAINSBY, R., DENNIER, A., MACINTOSH, S., WORSLEY, M., GRIEF, A. & VAN HEERDEN, E. 2008. Development of local heat transfer and pressure drop models for pebble bed high temperature gas-cooled reactor cores. (*In* Proceedings HTR2008: 4th International Topical Meeting on High Temperature Reactor Technology, Sept. 28 – Oct. 1, 2008, Washington DC, USA.)

MENTER, F.R. 1994. Two-equation eddy-viscosity turbulence modelling for engineering applications. *AIAA journal,* 32(8):1598-1605

MORALES, M., SPINN, C.W. & SMITH, J.M. 1951. Velocities and effective thermal conductivities in packed beds. *Industrial engineering and chemistry,* 43(6):226-232

NIJEMEISLAND, M. & DIXON, A.G. 2001. Comparison of CFD simulation to experiment for convective heat transfer in a gas-solid fixed bed. Chemical Engineering Science, 84(1-3):231-246, March.

PRICE, J. 1968. The distribution of fluid velocities for randomly packed beds of spheres. *Mechanical & chemical engineering transactions,* 1(7):7-14, May.

REICHELT, W. 1972. Zur Berechung des Druckverlustes einphasig durchströmter Kugel - und Zylinderschüttungen. *Chemie Ingenieur Technik*, 44(18):1068-1071.

REYNEKE, H.J. 2009. Investigation into the velocity distribution through an annular packed bed. Potchefstroom: North-West University. (Dissertation: M.Eng.)

RODI, W. 1991. Experience with two-layer models combining the k-e model with a one-equation model near the wall. (*In* 29th Aerospace Sciences Meeting, January 7-10, Reno, NV, AIAA 91-0216.)

SCHALLER, R.R. 1997. Moore's law: past, present and future. *IEEE spectrum.* George Mason University, June.

SCHWARTZ, C.E. & SMITH, J.M. 1953. Flow distribution in packed beds. *Industrial and chemical engineering*, 45(6):1209-1218, Mar.

SHIH, T.H., LIOU, W.W., SHABBIR, A., YANG, Z. & ZHU, J. 1994. A new *k*- ε eddy viscosity model for high Reynolds number turbulent flows. *Computers fluids,* 24(3): 227-238.

SMAGORINSKY, J. 1963. General circulation experiments with the primitive equations. *The basic experiment, Mon. weather,* 91(3):99-164.

SPALART, P.R. & ALLMARAS, S.R. 1992. A one-equation turbulence model for aerodynamic flows. AIAA-92-0439.

SUBAGYO, STANDISH, N. & BROOKS, G.A. 1997. A new model of velocity distribution of single-phase fluid flowing in packed beds. *Chemical engineering science, 53(7):1375-1385, Dec.*

TOBIS, J. 2000. Influence of bed geometry on its frictional resistance under turbulent flow conditions. *Chemical engineering science*, 55(22):5359-5366, Nov.

VAN ANTWERPEN, H.J. 2007. Modelling a pebble bed high temperature gas-cooled reactor using a system-CFD approach. Potchefstroom: North-West University. (Dissertation: M.Eng.)

VAN ANTWERPEN, W. 2009. Modelling the effective thermal conductivity in the near-wall region of a packed pebble bed. Potchefstroom: North-West University (Thesis: PhD)

VAN DER WALT, A.J.K. & DU TOIT, C.G. Pressure drop through annular packed beds. (*In* Proceedings SACAM06. Fifth South-African Conference on Computational and Applied Mechanics. Jan. 17-18, 2006, Cape Town, South Africa.)

VERSTEEG, H.K. & MALALASEKERA, W. 2007. An introduction to computational fluid dynamics, the finite volume method. 2nd ed. London: Pearson Education Limited. p. 64-342.

WANG-KEE IN, W.J. & HASSAN, Y.A. 2008. CFD simulation of a coolant flow and heat transfer in a pebble bed reactor. (*In* Proceedings HTR2008: 4th International Topical Meeting on High Temperature Reactor Technology, Sept. 28 – Oct. 1, 2008, Washington DC, USA.)

WILCOX, D.C. 1998. Turbulence modelling for CFD. 2nd edition. California: DCW Industries Inc.

WU, C.Y., FERNG, Y.M. & LIU, C.C. 2010. Investigating the advantages and disadvantages of realistic approach and porous approach for closely packed pebbles in CFD simulation. *Nuclear engineering and design.* 240:1151–1159

YAO, M.S., HUANG, Z.Y., MA, C.W. & XU, Y.H. 2002. Simulating test for thermal mixing in the hot gas chamber of the HTR-10. *Nuclear engineering and design,* 218:233–240.

ZOU, R.P. & YU, A.B. 1995. The packing of spheres in a cylindrical container: the thickness effect. *Chemical engineering science*, 50:1504-1507.

APPENDIX A: Properties of packed beds used

This appendix provides a description of the packed beds used in this study. The volume properties refer to the volume of the space occupied by the spheres and the height property represents the height of the packed bed and not the flow domain.

A-1 Two spheres in contact: short

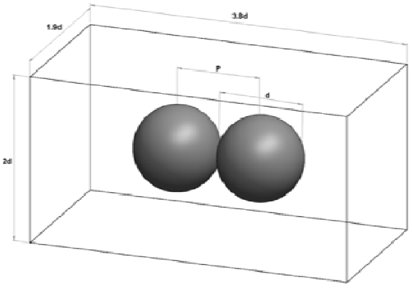

Figure A-1: Two spheres in contact: short

Table A-1: Description of Two spheres in contact: short

Description	***Value***
Volume [m^3]	0.000226
Flow area [m^2]	0.02599
Height [m]	0.0600
Sphere dia. [m]	0.0600
Effective number of spheres	2

A-2 Two spheres in contact: long

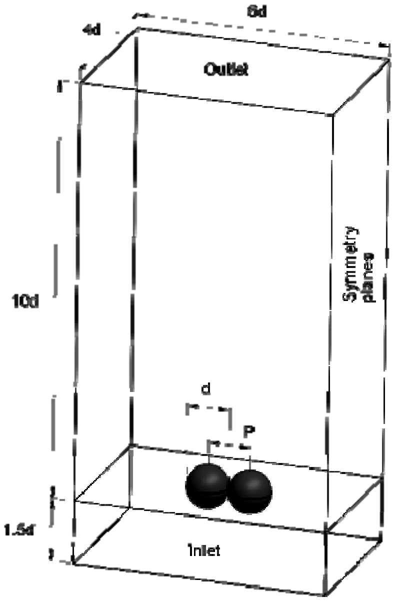

Figure A-2: Two spheres in contact: Long

Table A-2: Description of Two spheres in contact: long

Description	***Value***
Volume [m^3]	0.000226
Flow area [m^2]	0.0864
Height [m]	0.0600
Sphere dia. [m]	0.0600
Effective number of spheres	2

A-3 Long cylindrical random packed bed

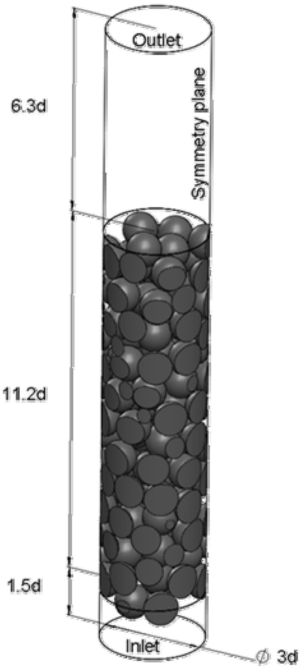

Figure A-3: Long cylindrical random packed bed

Table A-3: Description of long cylindrical random packed bed

Description	***Value***
Volume [m^3]	0.0104
Flow area [m^2]	0.0255
Height [m]	0.7321
Radius [m]	0.09
Sphere dia. [m]	0.06
Effective number of spheres	91.7

A-4 Random bulk packed bed

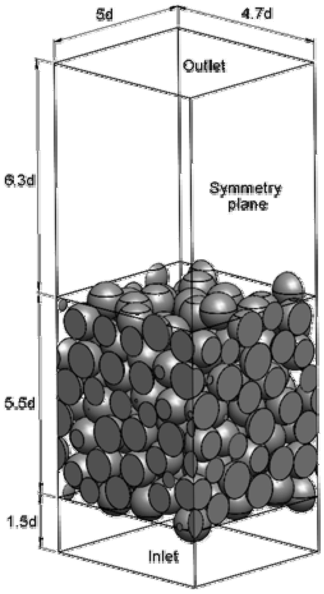

Figure A-4: Random bulk packed bed

Table A-4: Description of long cylindrical random packed bed

Description	***Value***
Volume [m^3]	0.0172
Flow area [m^2]	0.0846
Height [m]	0.3900
Sphere dia. [m]	0.06
Effective number of spheres	151.7

A-5 BCC packed bed

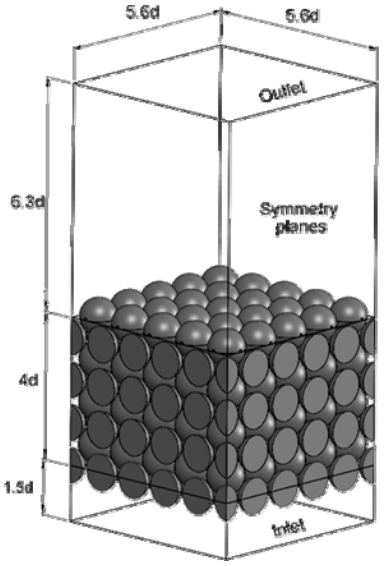

Figure A-5: BCC packed bed

Table A-5: Description of BCC packed bed

Description	*Value*
Volume [m^3]	0.0216
Flow area [m^2]	0.1134
Height [m]	0.3000
Sphere dia. [m]	0.06
Effective number of spheres	191.2

A-6 HCP packed bed

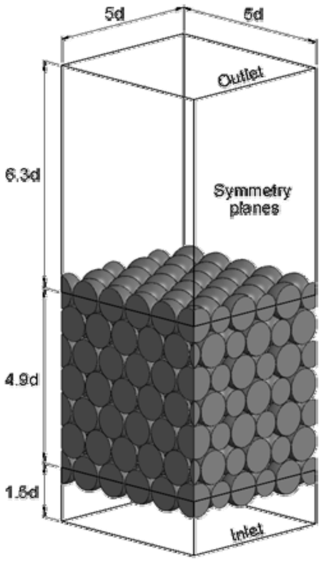

Figure A-6: HCP packed bed

Table A-6: Description of HCP packed bed

Description	*Value*
Volume [m^3]	0.0218
Flow area [m^2]	0.0900
Height [m]	0.3540
Sphere dia. [m]	0.06
Effective number of spheres	192.6

A-7 HCP packed bed

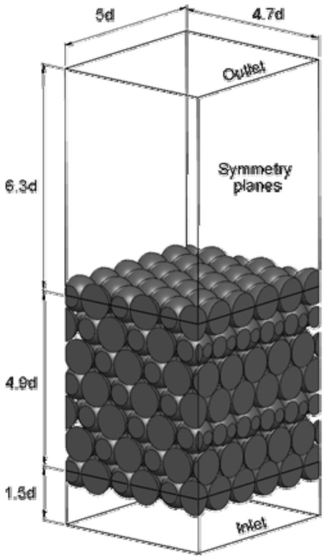

Figure A-7: HCP packed bed

Table A-7: Description of HCP packed bed

Description	*Value*
Volume [m^3]	0.0217
Flow area [m^2]	0.0846
Height [m]	0.3540
Sphere dia. [m]	0.06
Effective number of spheres	191.8

A-8 Diagonally packed BCC bed

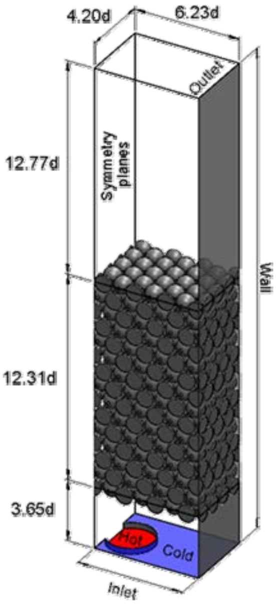

Figure A-8: Diagonally packed BCC bed

Table A-8: Description of diagonally packed BCC bed

Description	*Value*
Volume [m^3]	0.00813
Flow area [m^2]	0.0214
Height [m]	0.3804
Sphere dia. [m]	0.0285
Effective number of spheres	492.2

APPENDIX B: Braiding temperature profiles and effective conductivity fits

This appendix provides the braiding temperature profiles and implicit fits obtained in the effective conductivity tests. The temperatures near the centre seem irregular due to the hot gas diffusing off-centre due to the different structures and packings. This temperature profiles were obtained over four different time steps and averaged due to the transient turbulence model (LES) used.

(4.6)

B-1 Braiding temperature profile: BCC packed bed

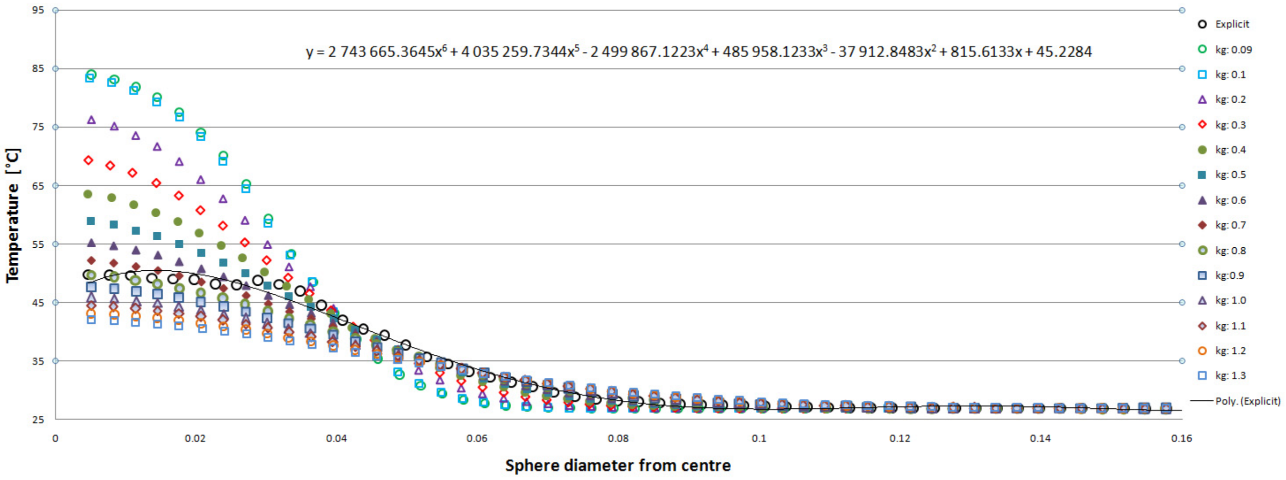

Figure B-1: Braiding temperature profile for the explicit and implicit simulations of the BCC packed bed with different gas conductivity coefficients

B-2 Braiding temperature profile: HCP packed bed

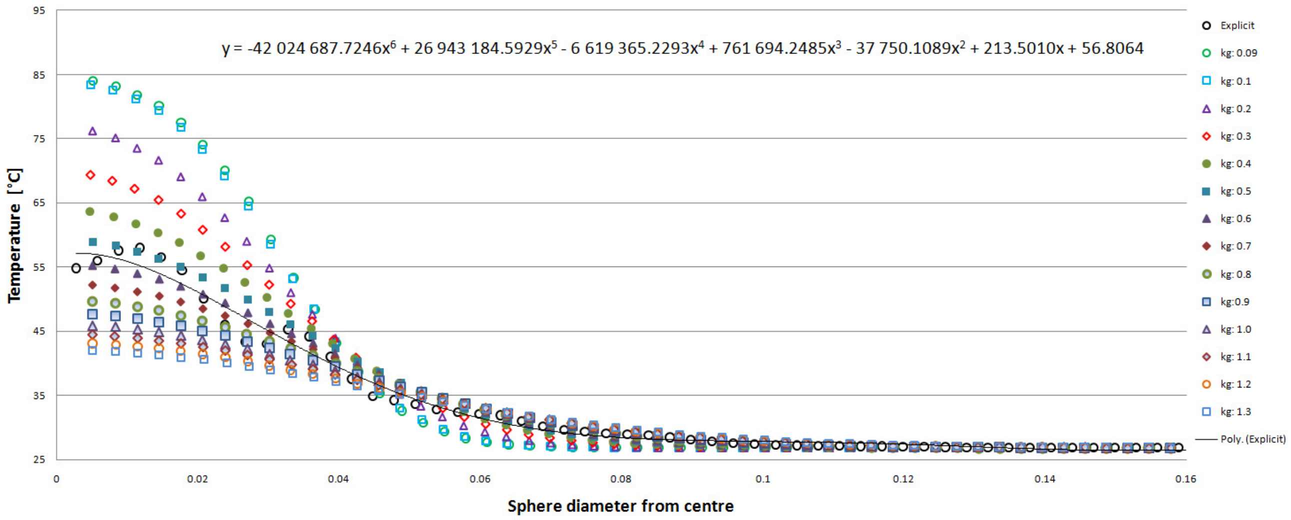

Figure B-2: Braiding temperature profile for the explicit and implicit simulations of the HCP packed bed with different gas conductivity coefficients

B-3 Braiding temperature profile: CCP packed bed

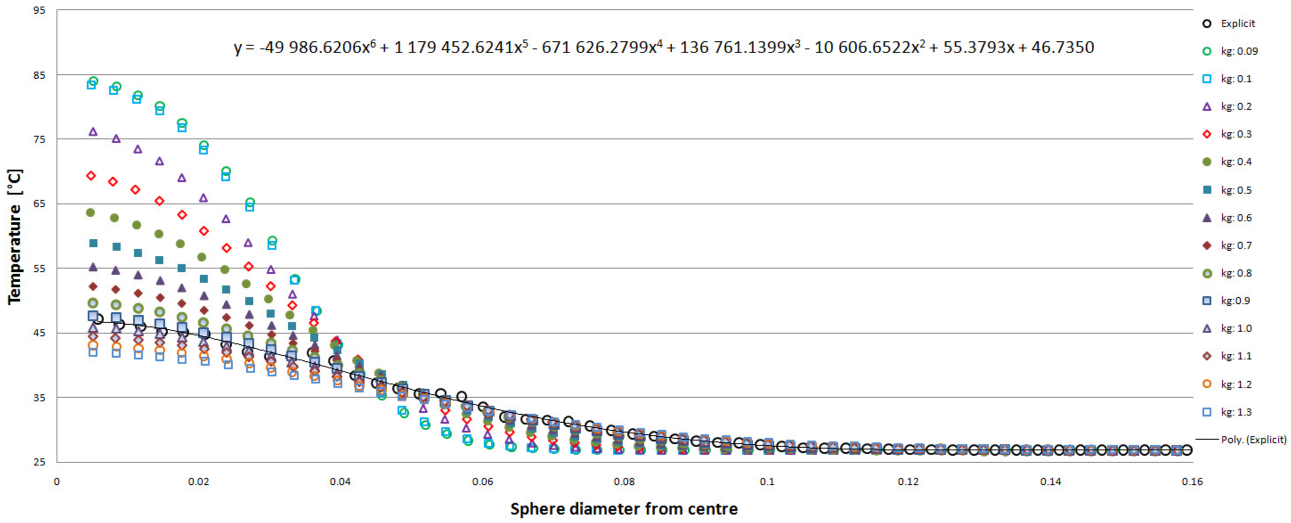

Figure B-3: Braiding temperature profile for the explicit and implicit simulations of the CCP packed bed with different gas conductivity coefficients

B-4 Braiding temperature profile: Random packed bed

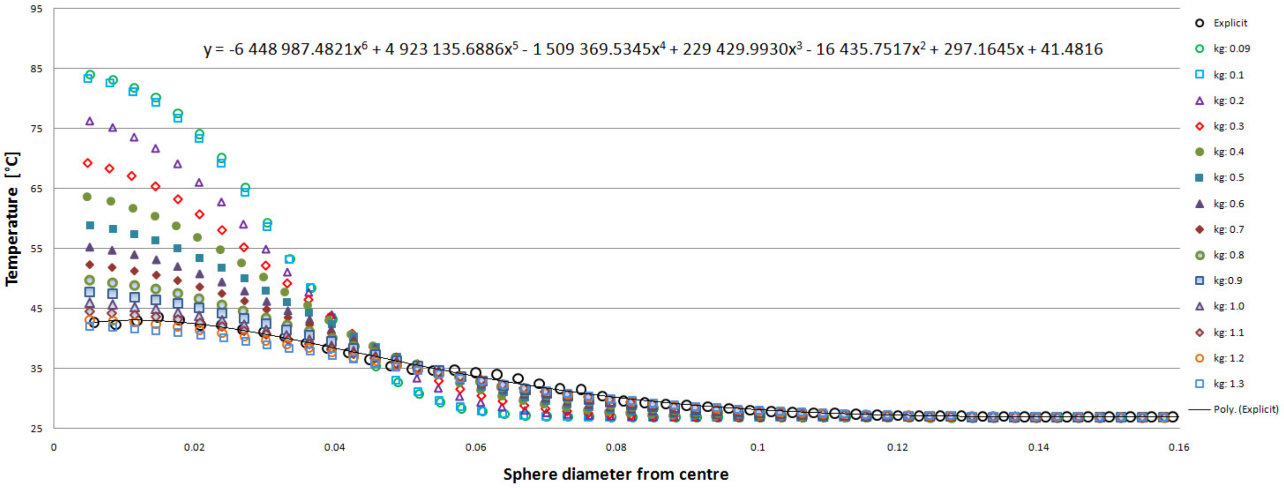

Figure B-4: Braiding temperature profile for the explicit and implicit simulations of the Random packed bed with different gas conductivity coefficients